Investigation of the Role of the X-Linked Opitz Syndrome Gene, *MID1*, in Craniofacial Development

By

Saidi Jaafar
BSc.Ed (Hons) (Malaya), MSc (Malaya)

A thesis submitted in total fulfilment of the requirements of the degree of Doctor of Philosophy (PhD)

Dental School
Faculty of Health Sciences

&

School of Molecular & Biomedical Science
Faculty of Sciences
The University of Adelaide
Adelaide 5005
Australia

July, 2005

DECLARATION

The work contained in this thesis contains no material that has been accepted for the award of any other degree or diploma in any university or other tertiary institution and, to the best of my knowledge and belief, contains no material previously published or written by another person, except where due reference has been made.

I give consent to this copy of my thesis, when deposited in the University Library, being available for loan and photocopying.

Saidi Jaafar

14. 7. 2005

ACKNOWLEDGEMENTS

There are many people whom I would like to thank, not only for their help and co-operation, but for their great influence on me throughout the entirety of this PhD project. The most grateful appreciation goes to my supervisor, Dr Timothy Cox, for all his guidance, help, understanding and endless support throughout my time in the Cox Lab. I am also appreciative of the support and encouragement of my co-supervisors, Professor Grant Townsend and Dr Tracey Winning. All three of you have always been there whenever I have needed advice on this project.

I would also like to acknowledge the past and present members of the Cox Lab throughout my PhD, Liza Cox, Belinda Washbourne, Kieran Short, Dr Yi Zou, Dr Joerg Drenckhahn, Dr Quenten Schwarz, Dr Blair Hopwood, Dr Annette Alcasabas and Sonia Donati. All of you have made a huge contribution to my PhD life and I also thank you all immensely for providing an enjoyable working atmosphere.

I am also very grateful for the assistance given by John Mackrill and Chris Cursaro, School of Molecular and Biomedical Science, Sandy MacIntyre and Alan Bishop, Hanson Institute, Institute of Medical and Veterinary Science (IMVS), and Hans Schoppe, Department of Pathology, Medical School. The contributions of the members of School of Molecular & Biomedical Science, Dental School and Laboratory Animal Services were also greatly appreciated.

A very special word of gratitude belongs to my 'Aussie Parents', Lee and Keith Jurgs, for opening their home to me and for their continuous support, encouragement and assistance in all things. I have felt so much at home in Australia because of you.

Finally, but most importantly, I gratefully and lovingly acknowledge my family especially my Mum and Dad, and my sisters and brothers for their loving support, care and understanding. I love and miss you all so very much!

THESIS SUMMARY

Normal formation of the vertebrate face requires appropriate growth, contact and fusion of craniofacial primordia in the ventral midline. Perturbations in these steps in facial development can result in an array of facial defects, the most common of which are cleft lip with or without cleft palate (CLP). Mutations in the *MID1* gene result in the X-linked form of Opitz GBBB syndrome (OS) in which CLP is a prominent feature. In fact, *MID1* represents one of only a few genes causally linked to CLP. The human *MID1* gene encodes a 667 amino acid microtubule-associated RING finger (RBCC) protein that functions as part of a large multi-protein complex. *In situ* hybridisation studies carried out in chick, mouse and human have indicated the highly conserved *MID1/Mid1* is expressed widely throughout embryogenesis although at varying levels depending on the tissue and cell type. However, the specific role of the MID1 protein in the development of these structures/tissues and how mutations of this gene gives rise to the various features seen among OS patients remains to be elucidated. As the various affected systems in OS patients appear to arise as a result of defective tissue fusion or remodelling during embryogenesis, elucidation of the molecular and cellular mechanisms by which the primordia of the face grow and then fuse to form the lip and primary palate will therefore shed light not only on our understanding of the developmental basis of CLP but also the processes leading to other common malformations (such as hypospadias and cardiac septal defects that also characterise OS patients).

A standard knockout of the murine *Mid1* gene was developed as part of a larger project to delineate the functional roles of *Mid1* in a mouse model. The generation involved replacement of the first coding exon of *Mid1* in ES cells with a *LacZ* reporter gene such that the reporter would be under the control of the endogenous *Mid1* cis-regulatory elements. Although the *Mid1* null mice do not display any gross external malformation in the current 129SvJ/MF1 genetic background, use of a *LacZ* reporter gene in the targeted DNA constructs enabled study of the expression pattern of *Mid1* by staining for β-galactosidase activity during early embryogenesis. Data presented in this thesis have revealed that *Mid1* is expressed in specific cell types within the craniofacial complex, the urogenital organ and surprisingly in the developing heart consistent with the defects seen in OS patients.

Detection of *Mid1* expression in the specific tissues during outgrowth and fusion of facial primordia suggests an important function of this gene in regulating these complex morphogenetic events. However, overlapping expression with the highly homologous *Mid2* gene suggests perhaps a level of functional redundancy between MID1 and its protein homologue, MID2. This would be consistent with: (1) the marked clinical variability in the presentation of OS, even among male patients from the same family and thus share identical *MID1* mutations, (2) the failure of the *Mid1* targeted knockout lines to display any gross facial malformation, at least in the current genetic background. To assist in addressing the functional redundancy between MID1 and MID2, specific antibodies recognised each protein were developed. Taken with recent evidence from early chick studies and the results presented in this thesis are consistent with this notion of redundancy also during later embryological stages.

In order to understand the cellular and developmental functions of MID1, inducible Madin-Darby canine kidney (MDCK) (epithelial) and Cos-1 (mesenchymal) cell lines that stably express either wild-type GFP-MID1 or one of a number of different mutant GFP-MID1 fusion proteins were then developed. These cells were used in preliminary investigations to address the role of MID1 in cellular processes such as cell migration, proliferation, cell death and the ability of cells to undergo epithelial-mesenchymal transitions (EMT), a key event in the fusion of epithelial-lined tissue such as in the facial prominences. These preliminary results showed that both epithelial and mesenchymal cell lines stably overexpressing wild-type or mutant MID1 did not effect either proliferation or apoptosis levels. However, in wound healing assays, MDCK cells stably overexpressing wild-type MID1 displayed delayed closure of the wounding area, in contrast to that seen with both MID1ΔCTD expressing cell lines where the rate of wound closure was notably more rapid than control cells. These early observations provide evidence that MID1 regulates the activation of epithelia, an early step in both EMT and cell migration.

This study has demonstrated that *Mid1* expression is expressed in all tissues normally affected in OS patients and, in particular, characterised in detail the expression of *Mid1* during the fusion of the facial prominences. This, together with an increasing knowledge about the cellular role of MID1, will greatly facilitate our understanding of the developmental processes controlled by the MID proteins and how their disruption

contributes to the clinical presentation of OS, and more specifically at least one of the pathways that lead to the susceptibility to CLP.

TABLE OF CONTENTS

Amendments

Tables 5.2 and 5.3: Data generated for cell proliferation (Table 5.2) and apoptosis (Table 5.3) analyses of stable, inducible cell lines expressing wild-type and mutant MID1 fusion protein were analysed statistically ($p < 0.05$, Student's *t* test). No significant differences were observed to support effects on cell proliferation or the amount of cell death presented in this thesis.

Figures 5.5 and 5.6: Assessment of monolayer epithelial (Figure 5.5) and mesenchymal (Figure 5.6) wound healing assays expressing wild-type and mutant MID1 proteins to indicate cell migration was based on the observation and comparison of the photomicrographs of the scratch wounds that were taken immediately after their formation (0 hour) and at a series of time points (12 hour intervals) until the healing process was completed. The rate of cell movement into the wounded area was compared to controls and used as a measure of the promotion or inhibition of cell migration.

Chapter One: General introduction

1.1 Craniofacial development: An introduction

The development of the craniofacial region is a complex step-by-step process following the establishment of the tubular body of the developing embryo. During this period of time, the developing embryo undergoes a series of critical morphogenetic events that involve the outgrowth of cell masses, the fusion of facial prominences and the differentiation of tissue, coordinated by a network of signalling molecules and transcription factors together with proteins conferring cell polarity and specificity of cell-cell interactions. The final stage in the development of this complex structure is the specification and differentiation of bones and muscles to give the head and face its final form. Notably, the main functions of the craniofacial structures are for digestion and respiration and to protect the brain and sensory organs.

The craniofacial structures are one part of the body highly sensitive to congenital abnormalities and these dysmorphologies occur primarily during the 5-12 weeks of development where growth, contact and fusion of facial prominences take place (Moore, 1988). It is believed that the complexity in their sequence of development makes the construction of the craniofacial complex particularly prone to even subtle genetic alterations and also to perturbations as a result of environmental teratogenic insults. This is reflected in the finding that one third of all major birth defects involve the head and face (Gorlin *et al.*, 2001b; Trainor, 2003). While there has been substantial progress in the studies of craniofacial development in the past decade, much of our knowledge is fragmentary and no unified developmental mechanism has emerged. In fact, little is known about the molecular and cellular regulation of craniofacial development. Therefore, elucidating the morphogenetic

pathways involved is very important in order to appreciate both normal and abnormal development of the craniofacial region and, of course, to understand the way it can be genetically or environmentally modified. There are a vast number of events underlying these complex morphogenetic processes, but this study will concentrate only on the outgrowth and fusion of the facial primordia involved in the formation of the lip and primary palate. Thus, processes involving the formation of bones, cartilages and muscles of the head and face will not be discussed in detail.

1.1.1 Early patterning of the head

The development of the vertebrate head is dependent on the establishment of a series of rhombomeres of the hindbrain and the branchial or pharyngeal arches. According to Hunt *et al.* (1998), the development of these two series of segmented structures is closely related where the neural crest cells, which are the principal source of the branchial arch mesenchyme, are derived from the lateral edge of the neural plate at the time of rhombomere formation. In their early development, the rhombomeres are organised into a series of seven segmental structures in the neural tube region that then becomes the hindbrain. Bilaterally, the lateral plate mesoderm of the ventral foregut region also becomes segmented to form a series of another five distinct bilateral swellings known as the branchial arches (Hunt *et al.*, 1998; Sperber, 2001).

The branchial arches form as a result of proliferating lateral plate mesoderm and subsequent reinforcement by the ventrally migrating cranial neural crest cells, also known as ectomesenchyme. Proliferation and differentiation of ectomesenchyme has been shown to dominate the formation of the craniofacial structures (reviewed by Santagati & Rijli, 2003). Structurally, branchial arches are separated externally by

small clefts called branchial grooves and corresponding small depressions called pharyngeal pouches separate each of the branchial arches internally (Nanci, 2003). There are six bilateral branchial arches that form in a cranial to caudal sequence with the fifth pair being only transitory structures in humans (Sperber, 2001). The first branchial arch is the precursor of both the maxillary and mandibular prominences, and is central to the development of the vertebrate face.

1.1.2 Development of the face

The face itself is derived from five prominences on the ventral surface of the developing embryo that surround the primitive oral cavity or stomatodeum. The prominences are the single frontonasal process and derivatives of the first branchial arch, the paired maxillary and mandibular processes. These prominences are undifferentiated buds of mesenchyme consisting of the neural crest-derived mesenchyme (ectomesenchyme) and mesoderm, covered by a layer of epithelial cells (Francis-West *et al.*, 2003; Nanci, 2003).

As development progresses, the facial prominences gradually become transformed. At about 28 days in human embryogenesis, a rapid proliferation of the underlying mesenchyme around the olfactory placodes at the frontal portion of the frontonasal prominence produce paired horseshoe-shaped ridges that subsequently invaginate. The lateral aspects of each horseshoe are referred to as the lateral nasal processes (LNP) and the medial aspects are called the medial nasal processes (MNP). The medial nasal processes together with the upper aspects of the frontonasal prominence (FNP), will give rise to the middle portion of the nose as well as the middle portion of the upper lip including the primary palate (Nanci, 2003; Sperber, 2001). Coordinated outgrowth and subsequent merging of these prominences are

essential for the face to begin to have a characteristic appearance and later become a complete and functional organ. Despite much information on the morphological events gathered so far, the molecular and cellular mechanisms by which the prominences of the face grow and then fuse, for example to form the lip and primary palate, remains unclear.

1.1.3 Formation of the lip and primary palate

The coordinated outgrowth of the facial prominences and their ultimate contact and fusion are crucial for normal formation of the face. Merging of two streams of ectomesenchyme of the paired mandibular processes form the lower lip. This is achieved by the elimination of a furrow or groove between these already attached primordia as a result of proliferation and migration of underlying mesenchyme. Unlike the formation of the lower jaw, the upper jaw is formed from the maxillary prominences of each side of the face and the ends of both lateral and medial nasal processes. Here, the ventral portion of the lateral nasal processes and the forward extent of the maxillary processes merge and then contact and fuse with the lateral tip of each freely projecting medial nasal process to form the nasal openings, upper lip and jaw as well as primary palate. In addition, partial fusion of the maxillary and mandibular prominences determines the actual size of the mouth (Cox, 2004; Francis-West *et al.*, 2003; Nanci, 2003; Sperber, 2001).

The mechanisms involved during growth and morphogenesis of the face described above are incredibly complex processes in embryogenesis. For this reason, the tissue interactions involved, particularly those controlling development of the lip and primary palate, are still not fully understood. Francis-West and her colleagues in their review stated that many previous studies have implicated epithelial cell death,

migration and an epithelial to mesenchymal transition (EMT) in lip and palate formation (Francis-West *et al.*, 2003). For instance, merging of the paired mandibular processes to form the lower lip predominantly involves epithelial migration whilst the fusion of the upper lip and primary palate involve all three mechanisms mentioned above (Cox, 2004; Francis-West *et al.*, 2003). Furthermore, observations of the surface of the maxillary and medial nasal processes have indicated that the pre-fusion epithelia involved undergo cytoskeletal reorganisation with the appearance of filopodia just prior to contact (Yee & Abbott, 1978). Taya and coworkers also observed filopodia on the surface of the medial edge epithelial (MEE) cells of wild-type mouse embryos just before fusion of the palatal shelf fusion whilst none were observed in TGF-ß3 null mice displaying cleft palate (Taya *et al.*, 1999). The importance of these filopodia in facilitating the fusion of the facial primordia will be interesting to investigate further. It appears that failure of any of the above mentioned processes involving the prominences during critical morphogenetic events could lead to a physical restriction of facial morphogenesis and a variety of different types of facial clefts (see Section 1.4.2).

1.2 Genetic basis of craniofacial development

1.2.1 Animal models for understanding craniofacial development and diseases

Numerous animal species have been manipulated for mutagenesis experiments to study developmental and molecular processes. However, mice, and to a lesser extent chicks, have proven to be better animal models for understanding craniofacial development and diseases, since they are likely to phenomimic human diseases and disorders. Although the mature chick's face develops into a beak structure, their similarities to mammals at early stages of growth and fusion of facial prominences

and also their accessibility to manipulation *in ovo*, have made them a choice as a model system to study the mechanisms controlling the outgrowth and patterning of the facial primordia. In support of this notion, Ashique *et al.* (2002) showed that the distinctive fusion of the lip and primary palate of the 'flat' chick face closely resembles human lip and primary palate formation. This study provided evidence that the pre-fusion epithelial cells of the maxillary, medial nasal and lateral nasal prominences are reprogrammed before fusion similar to the series of cellular changes that occur in the medial edge epithelium (MEE) before the fusion of the secondary palate.

Of the model organisms used to study craniofacial development, mice are the most widely used. According to Thyagarajan *et al.* (2003), other than their small size, short reproductive cycle and known genetic information, our ability to introduce precise genetic alterations into mouse embryonic stem cells and create from them a stable mouse line is the major factor for these choices. As a consequence, genetically manipulated mice are now widely used as animal models to assist us in understanding how human diseases develop. Recent advances in mouse knockout (KO) technology allow gene removal in both a temporal and spatial manner through the use of target sequence-specific exogenous recombinases to facilitate conditional silencing of target genes. This technique is advantageous compared to traditional gene silencing that required the removal of an entire gene or coding exon, resulting in a null allele. The traditional approach is also unable to be utilised for genes that are essential for cell viability as complete removal of these genes is usually severely detrimental to embryonic development and organism survival.

Over the past few years, a handful of knockout mouse models have been developed which display craniofacial phenotypes (see Section 1.2.2). Beside the

valuable information about *in vivo* gene function provided by these animal models, it is worth mentioning the variability shown among these different species compared to humans. Some of the gene knockout mouse models display unexpected phenotypes or no phenotypes, indicating the caution with which one must use such models when trying to accurately mimic and dissect human disease conditions. For example, our own attempts to produce a *Mid1* knockout mouse line to replicate the presentation of the X-linked Opitz GBBB syndrome (OS) have failed to produce, at least in the current genetic background, any of the obvious phenotypes seen in OS patients.

1.2.2 Genetic factors underlying craniofacial development

As mentioned earlier, craniofacial structures are derived from facial prominences consisting of mesenchymal cells that have originated from both neural crest and mesoderm, covered by an epithelial layer of ectoderm and endoderm. Specifically, the skeletal structures for each of the facial prominences are derived from the neural crest, whilst the mesoderm contributes to angioblasts[1] and myoblasts[2] (Francis-West *et al.*, 1998). For normal development of the craniofacial region, a multi-step process occurs starting with the formation and migration of neural crest, followed by correct outgrowth of the facial prominences and also the ultimate morphogenesis and differentiation of the skeletal elements. The development of each region of this complex is controlled by a unique set of genes and tissue interactions. Thus, this section will focus on the important genes that are expressed in the developing facial prominences and in tissue interactions that occur during facial development.

[1] Angioblasts are a collection of cells that develop into blood vessels and lymph vessels.
[2] Myoblasts are embryonic cells that develop into muscle fibres.

Many studies have been conducted to elucidate the tissue interactions that control patterning of the head (reviewed by Francis-West *et al.*, 2003). Recent studies by Couly and coworkers (Couly *et al.*, 2002) have revealed that endoderm has a major role in patterning the facial skeleton. Developing chick embryos have been shown to lose their skeletal structures when endoderm was removed but when endoderm was grafted in the developing face, it was able to induce the formation of ectopic skeletal structures (Couly *et al.*, 2002). This indicates that specific gene products produced by the pharyngeal endoderm are crucial for skeletal development.

Many different types of genes are involved in the regulation of developmental processes, some of which have been identified as controlling development of the face (reviewed by Francis-West *et al.*, 1998; Francis-West *et al.*, 2003; Richman & Lee, 2003; Wilkie & Morriss-Kay, 2001). The variety of mouse mutants that have demonstrated defects in craniofacial structures indicate the importance of numerous genes for the development of individual embryonic structures and organs. The key growth factors that control facial outgrowth include Sonic Hedgehog (Shh), Bone Morphogenetic Proteins (Bmps) and Fibroblast Growth Factors (Fgfs). Meanwhile, numerous transcription factors that are mediators of growth factor signals, including those of the homeobox-containing gene family such as Muscle-segment homeobox (*Msx*) and Distal-less related (*Dlx*) genes.

It has been shown that Shh is crucial for development and outgrowth of the frontonasal mass. According to Shimamura *et al.* (1995), mouse *Shh* is first expressed in the axial mesoderm but is then expressed abundantly in the facial primordium long after early patterning events. Consistently, generation of *Shh* knockout mice yielded a distinct phenotype in which the upper face was replaced by a proboscis-like extension lacking any skeletal structures (Chiang *et al.*, 1996). Recently, *Shh* expression has

also been shown to be highly restricted to the future sites of tooth development during the initiation of odontogenesis suggesting a role of Shh in stimulating epithelial proliferation (Cobourne *et al.*, 2001).

Another growth factor family, the Bmps, have been shown to control patterning, outgrowth and skeletal differentiation. The major players are Bmp4 and its closely related family member Bmp2, which are expressed in epithelium and in the underlying mesenchyme, respectively (reviewed by Francis-West *et al.*, 2003). Using a manipulation experiment in chicks, Barlow & Francis-West (1997) have shown that ectopic application of recombinant BMP2 or BMP4 to the chick mandibular or maxillary primordia induces the ectopic expression of *Msx1* and *Msx2* resulting in the bifurcation of Meckel's cartilage in the mandibular primordia and the palatine bone in the maxillary prominences, respectively. Interestingly, recent studies by Gong & Guo (2003) showed that *Bmp4* was expressed in a very distinctive pattern in the ectodermal layer at the putative site of fusion of facial prominences suggesting the importance of these factors in also facilitating these fusion events.

A number of members of the Fgf family are also expressed in the developing face. Both *Fgf2* and *Fgf8* are expressed in the epithelium, with *Fgf8* showing greater restriction in regional expression of the epithelium, whilst another Fgf member, *Fgf5* is localised to the mesenchyme (reviewed by Francis-West *et al.*, 2003). The role of these growth factors in outgrowth has been clearly demonstrated by conditional inactivation of *Fgf8* function and overexpression of the dominant-negative Fgfr2 receptor. Trumpp *et al.* (1999) showed that inactivation of *Fgf8* expression resulted in the loss of the mandibular and maxillary derivatives. Likewise, when dominant-negative Fgfr2 soluble receptor was transgenically expressed in mice, it was associated with cleft palate and a smaller face and skull (Celli *et al.*, 1998).

Of the transcription factors, members of the *Msx* gene family, *Msx1* and *Msx2*, are expressed in both migratory and post-migratory neural crest and also mediate epithelial-mesenchymal interactions (reviewed by Francis-West *et al.*, 1998). In support of this, a knock out of *Msx1* function in mice produces abnormalities of facial structures including cleft secondary palate, deficiency of alveolar bone in the mandible and maxilla as well as failure of tooth development (Mina, 2001). Conversely, transgenic mice overexpressing the *Msx2* gene display a similar phenotype to craniosynostosis i.e. premature fusion of the bones of the skull (Liu *et al.*, 1995). Interestingly, double knockouts of both *Msx1* and *Msx2* exhibit more severe facial phenotypes compared to individual knockouts, suggesting a level of functional redundancy between these two factors (Francis-West *et al.*, 1998). Other important transcription factors that are also expressed during craniofacial development are members of the Distal-less related (*Dlx*) family of genes. *Dlx1* and *Dlx2* are expressed in migratory neural crest as well as later in development, such as in the maxillary prominences (reviewed by Francis-West *et al.*, 1998). Other two members, *Dlx5* and *Dlx6* are expressed in the developing pharyngeal arches, brain and the limbs (reviewed by Panganiban & Rubenstein, 2002) where targeted inactivation of both *Dlx5* and *Dlx6* in the mouse resulted in severe facial and limb defects with *Dlx5/6*$^{-/-}$ embryos have an apparent homeotic transformation of the lower jaw into a maxilla-like structure (Beverdam *et al.*, 2002; Depew *et al.*, 2002; Robledo *et al.*, 2002).

As has been shown in palatogenesis, outgrowth and development of the lip and primary palate are also thought to be the result of an interaction between epithelium and mesenchyme. Identification of individual genes and their role in facilitating this morphogenetic event is therefore of considerable importance. Of

additional interest is the elucidation of the possible regulatory relationships with pathways known to be essential for palate development in mice, such as the recently identified Fgf10/Fgfr2/Shh signalling pathway (Rice *et al.*, 2004) or previously proposed Msx1 pathway by Zhang *et al.* (2002) involving Msx1, Bmp4, Shh and Bmp2.

1.3 Fundamental processes during craniofacial morphogenesis

This section describes briefly the involvement of epithelial-mesenchymal transition (EMT), epithelial cell death and epithelial cell migration in early embryogenesis. These cellular processes have been shown to play an important role during palatogenesis in many studies (Cuervo & Covarrubias, 2004; Shuler, 1995; Shuler *et al.*, 1991). There are also a few reports implicating them in regulating fusion process of the lip and primary palate in chick (McGonnell *et al.*, 1998; Sun *et al.*, 2000). However, whether the same basic mechanisms demonstrated in the secondary palatogenesis operate during the morphogenesis of the lip and palate remains to be elucidated.

1.3.1 Epithelial-mesenchymal transition (EMT)

Epithelia and mesenchyme are the two basic cell types that differ in their intracellular organisation and their relationships with the extracellular matrix as well as with adjacent cells. During the development of the vertebrate embryo, new mesenchymal tissue is locally generated from epithelial cells in a process known as epithelial to mesenchymal transition (EMT). Generally, EMT requires a phenotypic conversion of epithelia where transitioned epithelial cells lose their polarity, adherens junctions, tight junctions, desmosomes and also cytokeratin intermediate filaments in

order to rearrange their F-actin stress fibers and in some cases they express filopodia and lamellopodia (Kalluri & Neilson, 2003). This dynamic mechanism is very important in the formation of the body plan and is a source of mesenchyme in many places and at many stages during embryonic morphogenesis (Perez-Pomares & Munoz-Chapuli, 2002).

The importance of EMT in embryogenesis can be seen very early in embryonic development during the process known as gastrulation, where the epiblast actually undergoes EMT to form primary mesenchyme in the creation of triploblastic germ layers (Kalluri & Neilson, 2003). Furthermore, in vertebrate species, around the time of closure of the neural tube in chick and well before neural tube closure in mice, EMT is again initiated by a programme of gene expression at the most dorsal aspect of the forming neural tube. This process converts the epithelial neural crest into ectomesenchyme to enable their emigration from the neural epithelium to the ventral aspects of the developing embryo (Shook & Keller, 2003). Several lines of evidence also suggest that EMT is actually crucial for palatal shelf fusion by promoting the conversion of the medial edge epithelial (MEE) seam into a confluence of connective tissue across the palate (Martinez-Alvarez *et al.*, 2000; Nawshad *et al.*, 2004; Shuler *et al.*, 1991). In regard to the fusion process of the facial prominences, an investigation conducted in chicks by Sun *et al.* (2000) showed that EMT was the pivotal process for the 'removal' of seam epithelium to complete the fusion process of lip primordia. Any failure to replace this seam by a confluent and thickened mesenchymal bridge results in incomplete fusion producing a facial cleft.

1.3.2 Epithelial cell death and migration

As mentioned in Section 1.1.3, epithelial cell death and migration also play a very important role in craniofacial development. Both processes have been shown to be involved during the fusion of the palatal shelves to form the secondary palate (Cuervo & Covarrubias, 2004; Cuervo *et al.*, 2002; Martinez-Alvarez *et al.*, 2000; Takigawa & Shiota, 2004; Taya *et al.*, 1999), where the epithelial seam resulting from midline fusion of the medial edge epithelia (MEE) is rapidly removed through a combination of epithelial cell death and epithelial cell migration, as well as EMT. The elimination of this midline epithelial seam (MES) results in a complete shelf separating nasal and oral cavities. An early investigation of the role of these cellular processes during the fusion of facial primordia by McGonnell *et al.* (1998) clearly showed that epithelial cell death and epithelial cell migration are two of the major processes underlying shaping of the developing face.

Despite much success in revealing the developmental events of EMT, epithelial cell death and migration during craniofacial morphogenesis, very little is known about the molecular regulation of these important cellular processes. Members of transforming growth factor β (TGF-β) superfamily are regarded as main players in mediating these cellular processes during embryonic craniofacial morphogenesis, in particular during palatogenesis (Nawshad *et al.*, 2004). However, the role of other molecules in regulating cellular events during embryogenesis and possible interaction of these molecules in mediating normal and abnormal development of the craniofacial region not is fully understood. For this reason, identification of the other factors and their pathways that are likely participating in the above mentioned cellular processes is of importance.

1.4 Craniofacial malformation

1.4.1 Syndromes associated with craniofacial development

There are many syndromes in humans with phenotypes that involve abnormalities of the craniofacial structures. The defects may be restricted to specific regions of the face, such as facial prominences and their derivatives, as occurs in Treacher-Collins syndrome (Edwards *et al.*, 1997; reviewed by Francis-West *et al.*, 2003) or specific regions of the head may be affected, for instance the skull as occurs in craniosynostosis (Chun *et al.*, 2003). In addition, craniofacial defects may be found in association with cardiac and aortic arch anomalies as the heart and circulatory system also require a neural crest cell contribution from the hindbrain. Very interestingly, some syndromes can affect a particular developmental field, such as the ventral midline, as can be found in Opitz GBBB syndrome (Cox *et al.*, 2000; Robin *et al.*, 1996) and Holoprosencephaly[3] (Johnston & Bronsky, 1995; Nanni *et al.*, 2001).

Over recent years, rapid progress has been made in the identification of the gene mutations responsible for a number of human syndromes associated with craniofacial defects. This advanced understanding of the molecular pathology of craniofacial malformation syndromes has been achieved by family linkage studies, leading to candidate gene analysis and mutation identification (Francis-West *et al.*, 2003). The information is then used to produce mice with deficient gene function mimicking defects in the same genes involved in the human syndromes. A summary of the most prominent mouse mutants that have craniofacial defects generated so far by researchers worldwide has been compiled by Francis-West *et al.* (2003). In most instances, facial malformation and/or secondary palatal clefts are seen in these mouse

[3] Holoprosencephaly is a condition where the forebrain (prosencephalon) fails to divide into hemispheres or lobes, often accompanied by a deficit in midline facial development.

mutants, largely consistent with the defects displayed by the corresponding human syndromes.

1.4.2 Facial and palatal clefts

After post-migratory neural crest cells have populated the face, the mesenchyme proliferates and fills the facial prominences. As mentioned earlier, the correct growth and fusion of these prominences is required for normal face development, and any disruption of these processes can lead to facial and palatal clefts. It has been reported that clefts comprise approximately 15% of all reported abnormalities and represent the second most common malformation in the United States (Nanci, 2003). In some cases, these clefts are associated with other abnormalities, the combination of which helps define the various syndromes. These are normally referred to as syndromic clefts. Meanwhile, in most of the cases, these clefts occur in isolation and/or not associated with well-defined syndromes and they are referred to as non-syndromic clefts.

Failure of pairs of facial prominences to properly contact and/or fuse results in one of a variety of different facial clefts (Figure 1.1). Described as a relatively common congenital defect, unilateral cleft lip (which is more common on the left side) results from lack of fusion between the maxillary process and medial nasal process. If this failure of fusion occurs on both sides of the face, bilateral cleft lip results. Meanwhile, incomplete merging of the maxillary process and lateral nasal process causes an oblique facial cleft. Although considered very rare, incomplete merging of the two medial nasal prominences will transform the face with median cleft lip and in most cases various degrees of bifid nose are present. Incomplete merging of the maxillary and mandibular processes results in macrostomia, a situation

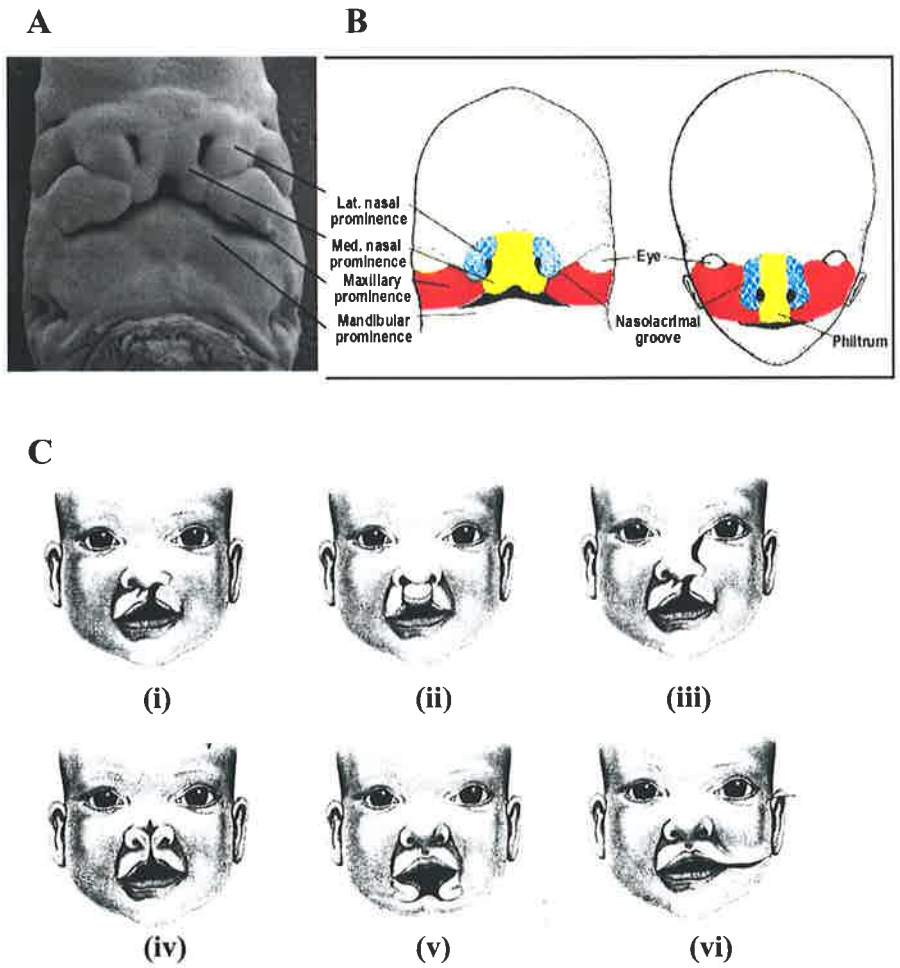

Figure 1.1 Craniofacial development and facial clefts

(A) Normal development of the midface depends on the proper fusion of facial primordia or prominences at about 5 weeks gestation in humans or 11.5 dpc in mice. (B) The contribution of each of these prominences to the final facial forms is depicted in colours. (C) Defects in this morphogenetic process result in different types of facial clefts i.e. (i) unilateral cleft lip, (ii) bilateral cleft lip, (iii) oblique facial cleft and cleft lip, (iv) median cleft lip and nasal defect, (v) median mandibular cleft, and (vi) unilateral macrostomia.

(A) and (B) were reproduced (with permission) from the website of the School of Medicine, University of North Carolina at http://www.med.unc.edu/embryo_images; and (C) was taken from Sperber (2001).

in which mouth size is larger than normal and this anomaly can often be unilateral. Lastly, the face also can suffer a rare midline mandibular cleft (Nanci, 2003; Sperber, 2001).

All facial clefts described above, primarily cleft of the upper lip as a result from defective development of the embryonic primary palate, often with secondary consequences for the palatine shelves (Nanci, 2003). Thus such clefts of the primary palate are often accompanied by clefts of the secondary palate (Figure 1.2). Although genetic and embryological studies indicate that both cleft palate (CP) and cleft lip with or without cleft palate (CLP) are etiologically distinct, its remains possible that they share some of the basic molecular and cellular mechanisms, particularly those involved in epithelial function during fusion. Collectively, the identification of the gene networks and also regulation of gene expression during lip and primary palate development should shed light on the precise molecular events that lead to human CLP.

1.4.3 Genetics of cleft lip and palate

The classification of cleft lip with or without cleft palate (CLP) comprises both isolated (non-syndromal) and syndromal forms and these are considered to be the most common features of all birth defects (Stanier & Moore, 2004). Patients with CLP frequently have complications affecting their feeding, speech, hearing, as well as psychological development and will need to undergo multiple rounds of surgical repair. CLP shows considerable geographical variation in live birth prevalence, ranging from 1 in 300 to 1 in 2500 births for cleft lip with or without cleft palate (CLP) to around 1 in 1500 births for cleft palate alone (CP). In humans, about 70-90% of all CLP cases are non-syndromic and show complex inheritance, with both genetic

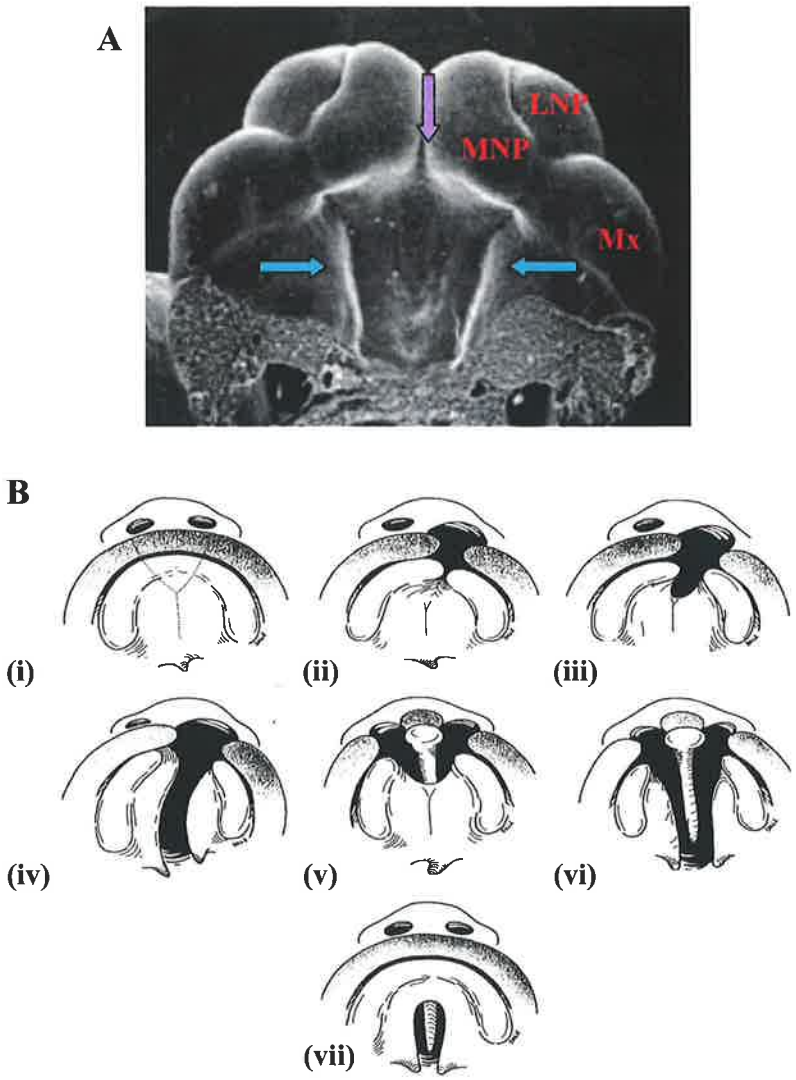

Figure 1.2 Palate development and palatal clefts

(A) Ventral view of the normally developing palatal shelves. The primary palate is completed as a result of merging of the medial nasal prominences (purple arrow) and the secondary palate forms by fusion of palatal shelves that originate from the maxillary prominences (blue arrow). (B) Defects in this morphogenetic process result in different types of palatal clefts i.e. (i) normal, (ii) cleft of lip and alveolus, (iii) cleft of lip and primary palate, (iv) unilateral cleft lip and palate, (v) bilateral cleft lip and primary palate, (vi) bilateral cleft lip and palate, and (vii) cleft palate only. [LNP: lateral nasal prominence; MNP: medial nasal prominence; Mx: maxillary prominence].

(A) was obtained from the website of the School of Medicine, University of North Carolina at http://www.med.unc.edu/embryo_images; and (B) was taken from Nanci (2003).

and environmental components (reviewed by Cox, 2004; Stanier & Moore, 2004; Wilkie & Morriss-Kay, 2001). The remaining syndromic cases have additional characteristic features including abnormalities of other parts of the body as seen in patients with Opitz GBBB syndrome (see Section 1.5.1). While studies on environmental factors have identified a contribution of numerous non-genetic risk factors such as anti-epileptic drugs, maternal alcohol and cigarette use, the contribution of genetic factors to CLP are the main focus of many current studies (Stanier & Moore, 2004). As discussed in Section 1.2.2, a variety of molecules have been implicated in facial development including growth factors such as Shh, Bmps and Fgfs and transcription factors such as those of the Msx and Dlx families. In fact, these transcription factors during maxillary and mandibular specification are regulated by Shh, Bmps and Fgfs signals (Richman & Lee, 2003). Supporting this, mutations in some of these molecules have been found to underlie human syndromes. For instance mutation in *Shh* is responsible for Holoprosencephaly, and most interestingly, gene-targeted mouse embryos of these molecules have facial clefts (for detail see Richman & Lee, 2003). There is no doubt that a similar approach will provide great opportunities to identify the different possible candidate genes for CLP in humans.

Recently, classic linkage analyses with families co-segregating for prominent CLP syndromes have been successfully used to identify human CLP genes (reviewed by Cox, 2004; Stanier & Moore, 2004). It is now becoming apparent that these so-called syndromic CLP genes may contribute to the population of isolated CLP. In this regard, at least six genes associated with syndromal forms of CLP have been identified, including *PTCH1*, *MID1*, *PVRL1*, *MSX1*, *p63* and *IRF6* (Cox, 2004). Although evidence of a significant association with the presentation and incidence of isolated CLP has so far only been shown for *MSX1*, *PVRL1* and *IRF6*, the

contribution of the other three genes remain to be determined. Of interest is *MID1*, a gene that has recently been shown to be responsible for X-linked Opitz GBBB syndrome (OS). In fact, CLP is one of the most common features in OS patients (So *et al.*, 2005). Furthermore, it is also interesting to speculate that *MID1* may not only contribute to the incidence of isolated clefts but also to the male bias in CLP given the gene is located on the X-chromosome.

1.5 Opitz GBBB syndrome

Opitz GBBB syndrome (OS; MIM 145410 and 300000) was first reported as two separate entities, BBB syndrome (Opitz *et al.*, 1969b) and G syndrome (Opitz *et al.*, 1969a), with the names being derived from the initials of the originally reported families. These two entities showed numerous midline defects and had significant phenotypic overlap, with the presence of laryngotracheo-esophageal (LTE) abnormalities considered to distinguish the G syndrome from the BBB syndrome (Allanson, 1988). However, Opitz (1987) re-examined the previously reported patients and found a boy in one of the original BBB families who had the G syndrome, providing strong evidence that the two syndromes actually represented the same condition. This finding was then supported by Verloes *et al.* (1989) who discovered a family where the propositus had G syndrome, including LTE cleft, whereas another relative had facial anomalies typical of the BBB syndrome. As a result, both syndromes were subsequently grouped and now referred to as Opitz GBBB syndrome (OS).

Initially, the mode of transmission of OS was not very clear. Males with OS are frequently more severely affected than females in the same family and this finding, as well as the pedigrees of the initially reported families, were consistent with

X-linked inheritance (Gaudenz *et al.*, 1998). However, evidence of male-to-male transmission in some families strongly suggested that OS could be inherited as an autosomal dominant trait (Opitz, 1987). Later, linkage data provided by Robin *et al.* (1995) indicated that OS was in fact a genetically heterogeneous disorder, with a locus on Xp22 and a second on 22q11.2. It was believed this was the first example of a classic multiple-congenital-anomalies syndrome shown to be genetically heterogeneous, with both X-linked and autosomal forms (Robin *et al.*, 1995). Clinical studies conducted later by Robin *et al.* (1996) showed that the two modes of inheritance have a virtually identical constellation of abnormalities and cannot be differentiated on the basis of the clinical phenotype.

1.5.1 The Opitz GBBB syndrome phenotype represents defects of the ventral midline

The pathology of OS can involve the entire ventral midline and present as a large spectrum of abnormalities involving major tissues and organs including the craniofacial complex, genitourinary system, cardiovascular and respiratory system (Figure 1.3) (Gorlin *et al.*, 2001a). As highlighted below, each of these malformations, specifically CLP, hypospadias and congenital heart defects (primarily defects in cardiac septation and vascular remodelling), occur with high incidence as isolated birth defects and therefore may reflect a common developmental mechanism. In considering the developmental processes that form these various affected structures, the most plausible explanation is a defect in tissue fusion and/or tissue remodelling (Cox, 2004; Schweiger & Schneider, 2003).

OS usually presents with characteristic facial anomalies including ocular hypertelorism (widely-spaced eyes) (98%), cleft lip with or without cleft palate (50%), low-set ears (45%) and broad nasal bridge (37%). Patients may also have

A

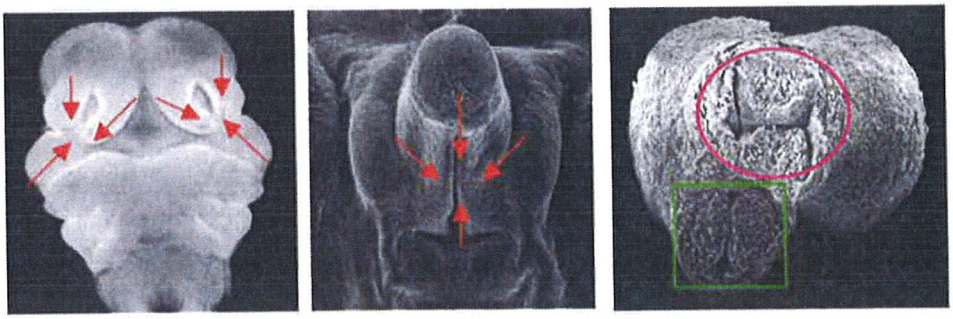

a b c

B

NOTE:

These images are included in the print copy of the thesis held in the University of Adelaide Library

a b c

Figure 1.3 Developmental defects in Opitz GBBB syndrome

(A) A defect in similar morphogenetic events may underlie formation of anomalies seen in OS patients; eg. during the formation of (a) the lip and primary palate, (b) male external genitalia, and (c) cardiac septa (endocardial and conotruncal cushions).

(B) The craniofacial abnormalities seen in OS patients include hypertelorism, a prominent nasal bridge or depressed nasal root, and posteriorly angulated ears (a and b). Cleft lip with or without cleft palate is common in more severe cases (c).
(A[a]) image of 10.5 dpc mouse embryo taken by Dr Alcasabas, Cox Laboratory; (A[b]) and (A[c]) were obtained from the website of the School of Medicine, University of North Carolina at http://www.med.unc.edu/embryo_images; and (B) from Dr Cox, University of Adelaide.

laryngotracheo-esophageal (LTE) defects including LTE clefting (50%) leading to swallowing difficulties, as well as a hoarse cry. These LTE anomalies are the most frequent cause of early infant death in OS patients if untreated (Cox *et al.*, 2000; Quaderi *et al.*, 1997; Schweiger *et al.*, 1999; So *et al.*, 2005). Commonly, the eyes display various degrees of upslanting or downslanting of the palpebral fissures (opening between the eyelids), epicanthus (congenital occurrence of a fold of skin obscuring the inner canthus of the eyes) as well as strabismus (Gorlin *et al.*, 2001a).

Besides ocular hypertelorism, the most prominent manifestation of OS is hypospadias (72%), which occurs in most affected males (So *et al.*, 2005). In fact, the co-presentation of ocular hypertelorism and hypospadias is considered as diagnostic of OS (Gorlin *et al.*, 2001a). The degree of hypospadias seen in OS varies from a mild coronal to a scrotal type with an associated ventral urethral groove (Gorlin *et al.*, 2001a). Males also often present with congenital anal anomalies such as imperforate or ectopic anus with rectourethral fistula, whilst affected females usually have normal genitalia with occasional splayed posterior labia majora and imperforate anus (Gorlin *et al.*, 2001a). Congenital heart defects in OS patients include atrial and ventricular septal defects, patent ductus arteriosus and also coarctation of the aorta. Minor respiratory system abnormalities might be present in some patients and may be associated with LTE defects causing respiratory complication which, as previously mentioned, is the major cause of significant morbidity and mortality. Developmental delay is also noted in two thirds of OS patients and at lesser frequency, anomalies of the central nervous system including agenesis of corpus callosum and cerebellar vermis hypoplasia (Gorlin *et al.*, 2001a; Graham *et al.*, 2003; So *et al.*, 2005).

As mentioned earlier, major malformations of patients with OS occur in both X-linked and autosomal dominant forms. Therefore, no clinical distinction can clearly

be assigned to one or other of the forms of OS although it has been noted that in both forms the phenotype is more complex and more severe in males than in females (Robin *et al.*, 1996). A study by Cox *et al.* (2000), who examined clinical features of OS patients with or without mutations in the X-linked *MID1* gene, revealed that all major characteristic features of OS can be seen in both groups except possibly anteverted nares. A more recent study by So *et al.* (2005) with a larger group of OS patients indicated that *MID1* mutation-positive cases show a significantly higher incidence of CLP, LTE anomalies and hypospadias compared to mutation-negative cases, who in contrast have a slightly higher incidence of cardiac structural defects. However, it should be noted that the overall incidence of cardiac defects in both forms of OS is likely to be underestimated, since dysphagia[4] is a common, and yet often poorly diagnosed feature. Nevertheless, the slightly higher incidence of congenital heart defects in mutation-negative cases may reflect the contribution of the principal autosomal OS locus, which is likely to be encompassed by the region commonly deleted in the "22q11 deletion syndrome" that accounts for approximately 5% of all congenital heart defects (McDonald-McGinn *et al.*, 2001). Intriguingly, all these abnormalities show remarkably variable inter-individual expressivity in patients, even within males in the same family who inherit an identical X-linked mutation (Cox *et al.*, 2000; So *et al.*, 2005). It is believed that this variability in presentation is influenced largely by other genetic and/or environmental factors but the molecular mechanisms underlying this variability are not well understood.

[4] Dysphagia is a difficulty in swallowing due to constriction of the oesophagus by aberrant remodelling of cardiac tissue during embryogenesis.

1.5.2 Molecular basis of X-linked Opitz GBBB syndrome

A linkage study performed on families segregating the OS phenotype revealed genetic heterogeneity of the disorder, with it being linked to DXS987 in Xp22 in three families and to D22S345 from chromosome 22q11.2 in another five families (Robin *et al.*, 1995). Another three additional studies conducted later by Fryburg *et al.* (1996), Lacassie & Arriaza (1996) and McDonald-McGinn *et al.* (1996) associated OS with a 22q11.2 microdeletion. Deletion of the overlapping region on 22q11.2 has also been found in other syndromes in which similar structures are affected, such as DiGeorge syndrome (DGS), velo-cardio-facial syndrome (VCFS) and conotruncal anomaly face syndrome (CAFS) (Scambler, 2000). In addition, other autosomal loci have also been implicated by cytogenetic anomalies in individual OS cases, including dup (5p12 – 13) (Leichtman *et al.*, 1991) and del (13q32.3 – 13qter) (Urioste *et al.*, 1995), although none have been confirmed by linkage studies.

Confirmation of the Xp22 localisation came from detailed studies conducted by May *et al.* (1997) linking OS to DXS7104 in Xp22 as well as molecular analysis of a pericentric inversion of the X chromosome, inv(X)(p22.3q36), segregating in a French OS family (Verloes *et al.*, 1995). These linkage and inversion breakpoint data clearly indicated Xp22.3 as the critical region for the OS gene. While the gene responsible for the autosomal form of OS has still not been identified, a positional cloning approach led to the identification of the Xp22.3 gene, *MID1* or *Midline 1* (Quaderi *et al.*, 1997). Initial mutational screening performed by this group in three X-linked OS families found nucleotide alterations in the region encoding the C-terminal portion of the MID1 protein confirming that *MID1* is indeed the gene for X-linked OS.

1.5.3 *MID1* gene and its protein organisation

The X-linked OS gene, *MID1*, covers a genomic region of about 300 kb and consists of nine coding exons and multiple non-coding exons (Cox *et al.*, 2000). The human *MID1* gene (also known as *TRIM18*) is located within Xp22.3, proximal to the human pseudoautosomal boundary (Perry *et al.*, 1998) whilst its murine homolog, *Mid1,* spans the pseudoautosomal boundary in *Mus musculus* (Dal Zotto *et al.*, 1998). Very interestingly, as noted by Dal Zotto *et al.* (1998), *MID1* is the first example of a gene subject to X inactivation in man while escaping it in mouse.

MID1 encodes a 667 amino acid microtubule-associated RBCC protein (or tripartite motif (TRIM) protein), a family of proteins so named because of a conserved N-terminal tripartite motif, consisting of a RING finger, two B-box zinc fingers and a leucine-rich α-helical Coiled-coil motif, with a C-terminal B30.2 domain and a fibronectin type III domain (FNIII) immediately N-terminal to the B30.2 domain (Figure 1.4) (Perry *et al.*, 1998; Schweiger & Schneider, 2003). The RBCC family has over 50 members (Reymond *et al.*, 2001). Some members of the RBCC protein family have been implicated in disease processes, including PML, RFP and TIF1 in tumourigenesis, especially when involved in specific chromosomal translocations resulting in fusion of the tripartite motif with other proteins (Dal Zotto *et al.*, 1998). However many of these RBCC proteins have not been characterised in any detail.

According to Reymond *et al.* (2001), despite some distinct roles and varied subcellular localisation, all RBCC proteins are thought to act as scaffolds for the assembly of larger multiprotein complexes. Each of their identified motifs or domains has been implicated either directly or indirectly in mediating protein-protein interaction. As for MID1, Short *et al.* (2002) showed that both the RING-finger and B-box motifs provided an interface for protein-protein interactions whereas the

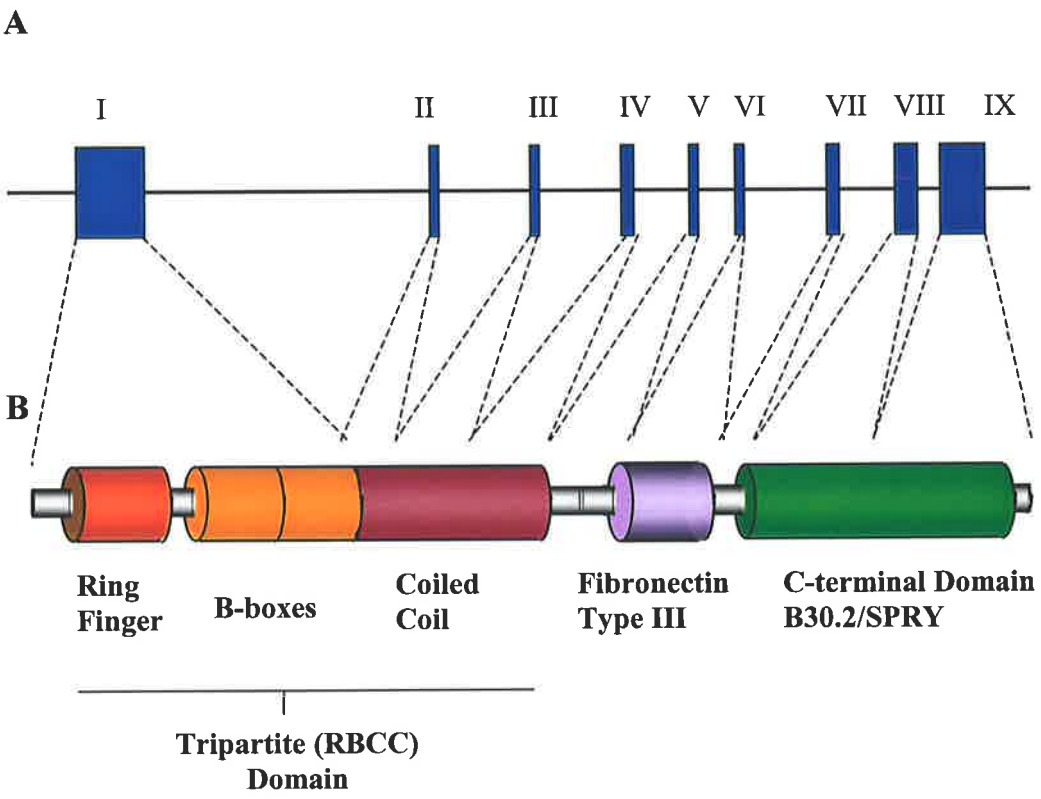

Figure 1.4 Schematic representation of the *MID1* gene and its protein product

(A) The *MID1* gene consists of nine coding exons (indicated by blue boxes and Roman numerals).

(B) The MID1 domains i.e. RING-Finger, B-Boxes, Coiled-Coil, FNIII and B30.2, are presented with the coloured cylinders from left to right. The regions encoded by each exon of the *MID1* gene are as indicated.

Coiled-coil motif provides the interface for oligomerisation, a property of almost all RBCC proteins (Reymond *et al.*, 2001). It has also been shown that MID1 forms homodimers with the Coiled-coil domain being both necessary and sufficient for this dimerisation (Short *et al.*, 2002). Notably, oligomerisation appears to be a prerequisite for the subsequent formation of high order protein complexes (Cox *et al.*, 2000; Short *et al.*, 2002). Another important region of the protein is the B30.2 domain that is also found at the C-terminus of over half of the RBCC proteins. Although the exact function of this B30.2 domain is still unclear, proteins possessing B30.2 domains have been reported to be involved in autoimmune diseases and developmental disorders, such as systemic lupus erythematosus (SLE) and OS, respectively.

1.5.4 Identification of *MID1* mutations as a causative gene in the X-linked OS

Identification of *MID1* mutations in unrelated OS affected individuals has confirmed that *MID1* is the gene responsible for the X-linked OS. To date, mutational analyses carried out by three groups (Cox *et al.*, 2000; De Falco *et al.*, 2003; So *et al.*, 2005) have shown mutations in the X-linked *MID1* gene in about 40% of patients with OS. All together, they reported 36 different mutations in sporadic and familial OS cases. Interestingly, in a case with no detectable open reading frame (ORF) mutation, haplotype data supported the notion that mutations in non-coding regions that affect the expression of *MID1* may also be present in some cases (Cox *et al.*, 2000). This hypothesis was further supported by Winter *et al.* (2003) who found a premature stop codon in one case that was due to a duplication of the first exon of the *MID1* gene, a mutation that was not detected by routine exon amplification during screening of mutations in the ORF.

To summarise, it is apparent that *MID1* mutations can be scattered throughout the gene, although more are represented in the 3' region. Missense and nonsense mutations, deletions, splice-acceptor and frame-shift mutations have all been found with most of them resulting in truncated protein products. This finding suggests that loss-of-function of MID1 is the mechanism underlying the pathogenesis of OS (Cox *et al.*, 2000).

1.6 Investigation of the *MID1* gene and its protein product

1.6.1 Expression pattern in the embryonic tissues supports *MID1* as a OS candidate gene

Following identification and isolation of the X-linked OS gene, *MID1*, in humans, its orthologues in other species such as in the mouse (*mMid1*) (Dal Zotto *et al.*, 1998) and chick (*cMID1*) (Richman *et al.*, 2002) were then successfully isolated. Comparison of their sequences with that of human have shown a strikingly high level of conservation. The murine *Mid1* gene shows 87% identity at the nucleotide level and 95% identity at the amino acid level, while the chick *Mid1* gene shows 84.4% identity at the nucleotide level and 95.4% identity at the amino acid level with human *MID1*.

Initial analysis of the expression of *MID1* using a multiple foetal and adult human tissue northern blot performed by Quaderi *et al.* (1997) revealed ubiquitous expression of two *MID1* transcripts (7.0 kb and 3.5 kb) with the most abundant expression detected in foetal kidney, as well as adult brain, heart and placenta. Meanwhile, *in situ* hybridisation studies performed in chick, mouse and subsequently human embryos have indicated a highly conserved pattern of expression throughout embryogenesis (Dal Zotto *et al.*, 1998; Pinson *et al.*, 2004; Richman *et al.*, 2002). These expression patterns were largely consistent with the tissues affected in patients

with OS. In the mouse, Dal Zotto *et al.* (1998) reported highest levels of expression in undifferentiated cells in the central nervous system (CNS), craniofacial complex and in the region of the developing external genitalia. While developing mouse embryos show generally more ubiquitous expression, interspecies differences are evident by the studies of Richman and colleagues, who reported slightly more localised *cMid1* expression patterns during chick embryogenesis (Richman *et al.*, 2002). Other than predominant expression reported in the myotome (condensing muscle block of the limb) and the midgut (at later stages of the chicken development), *cMid1* expression was also strongest in the facial ectoderm although detectable at lower levels in the proliferating mesenchyme that underlies epithelial tissues preparing for contact and fusion such as that in the facial prominences. Detailed characterisation of this *MID1* expression at different stages during fusion of the facial prominences is important in order to understand what role *MID1* is playing in regulating these crucial developmental processes. Of note, the developing heart was reported negative for *mMid1* expression in the original *in situ* hybridisation studies on mouse embryos (Dal Zotto *et al.*, 1998), but as discussed in the following chapter of this thesis does in fact express *Mid1* in a dynamic manner. Interestingly, this finding is more consistent with studies in both chick (Richman *et al.*, 2002) and human (Pinson *et al.*, 2004) and in line with the defects in the heart seen in affected OS patients.

1.6.2 The MID1 protein associates with the microtubule network

Investigation of the intracellular localisation of the MID1 protein has shown that both endogenous MID1 and overexpressed MID1 fusion proteins co-localise with the microtubule network throughout the cell cycle in all cell types tested (Figure 1.5) (Cox *et al.*, 2000) (Cainarca *et al.*, 1999; Schweiger *et al.*, 1999). In support of this

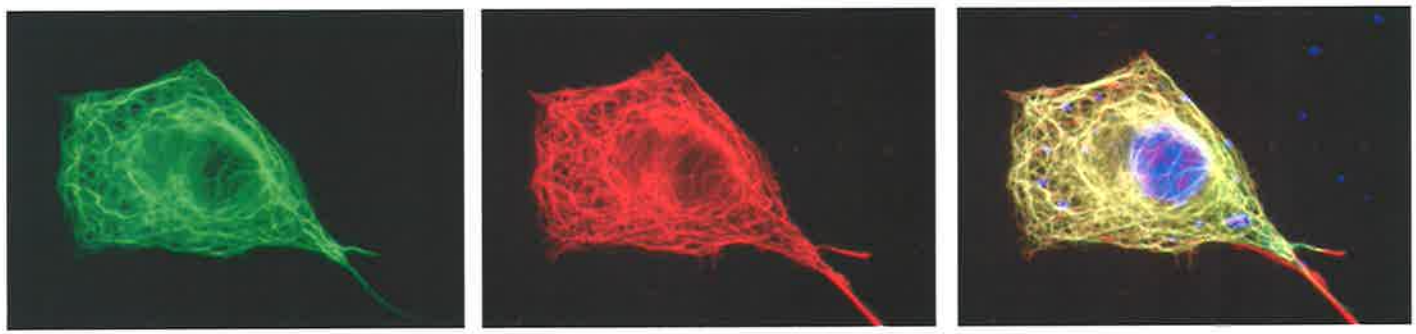

A B C

Figure 1.5 MID1 co-localisation on microtubules

Transient expression of wild-type GFP-MID1 fusion protein (A) in Cos1 cells. Microtubule network detected by staining with an anti-α-tubulin antibody (B). Merge of images (A) and (B) show co-localisation (C).
(Images courtesy of Kieran Short, Cox Laboratory).

observation, cell fractionation analysis performed by Schweiger *et al.* (1999) also confirmed this microtubule-association of MID1. Schweiger *et al.* (1999) also provided evidence that overexpression of MID1 protects microtubules from colcemid-induced depolymerisation similar to many other microtubule-associated proteins. However, similar protection from disassembly was not found by Cainarca *et al.* (1999) using vinblastine-induced depolymerisation. These seemingly contradictory findings might be due to the differences in the mechanisms of action of the distinct depolymerising drugs and thus the significance of these findings remain uncertain.

As mentioned in Section 1.5.3, MID1 likely functions in an oligomeric form, consistent with a number of other RBCC proteins. Short *et al.* (2002) demonstrated an altered cellular localisation upon overexpression of almost all domain-specific deletions of MID1 in Cos1 cells. The coiled-coil mutant, MID1ΔCC, was shown to result in a diffuse cytoplasmic distribution, suggesting loss of the ability to associate with microtubules and this was consistent with the observation that this same mutant had lost its ability to dimerise in a yeast two-hybrid assay. Short *et al.* (2002) also showed that unlike GFP-tagged MID1ΔRF, which only minimally affects microtubule localisation, MID1ΔBB, MID1ΔFNIII and MID1ΔCTD formed cytoplasmic clumps or speckles with variable cellular distributions. Interestingly, the aggregates of overexpressed GFP-MID1ΔBB and GFP-MID1ΔFNIII still appear to co-localise with microtubules, consistent with the altered microtubule-association of the overexpressed OS-associated mutation, MID1ΔM438 (deletion of a single Met codon in the FNIII domain) observed by Schweiger *et al.* (1999). Overexpression of the tested OS causative MID1 mutants in studies by two other groups ((Cainarca *et al.*, 1999) (MID1C266R) and (Cox *et al.*, 2000) (MID1E115X, MID1delExon2, MID1R368X and MID1L626P)) indicated that all affected cellular distribution, suggesting that

complete microtubule coverage by MID1 is important for its proper cellular function. Possible microtubule-associated cellular roles for MID1 include the regulation of cell proliferation, cell migration and/or the ability of cells to undergo epithelial-mesenchymal transition, a key event in the fusion of epithelial-lined tissue such as the facial processes.

1.6.3 Protein interactors of MID1 and its predicted functions

Early data presented by Schweiger *et al.* (1999) supported that MID1, like other RBCC proteins, might act as a scaffold to facilitate the formation of large protein complexes. Thus, identification of protein that interact with MID1 in these complexes is likely to give clues as to their cellular function. In this regard, three different groups (Liu *et al.*, 2001; Short *et al.*, 2002; Trockenbacher *et al.*, 2001) independently identified a mammalian homologue of TOR-associated protein in yeast (Tap42), called Alpha4 (α4), as a strong interactor of MID1. Alpha4 is recognised as a unique regulatory subunit of PP2-type phosphatases (such as PP2A) binding to the catalytical subunit (PP2Ac) independently of the common A- and B-type subunits, similar to the binding specificity of Tap42 (Murata *et al.*, 1997). In yeast, the association of Tap42 is a key component of the TOR (target of rapamycin) pathway. In both mammals and yeast, TOR is a protein kinase whose activity is increased in response to mitogenic and nutritional signals (Raught *et al.*, 2001). As has been shown in yeast, activation of TOR leads to enhanced phosphorylation of Tap42, which in turn increases its affinity for the catalytic subunit of PP2A (PP2Ac)/SIT4. The association of Tap42-PP2Ac/SIT4 lowers the catalytic activity of PP2Ac/SIT4 and in turn, affects many and diverse cellular functions, for example, gene transcription, cell cycle progression and cellular morphology (Harris *et al.*, 1999).

Both endogenous and overexpressed Alpha4, similar to PP2Ac, is found throughout the cytoplasm, although faint microtubule-association can be noticed in some cells overexpressing Alpha4 (Short and Cox, unpublished data). However, as it has been shown by Liu *et al.* (2001) and Short *et al.* (2002), when the levels of MID1 are not limiting (overexpressed MID1), Alpha4 is readily recruited onto microtubules. It is therefore likely that a phosphoprotein like MID1, at physiological levels, tethers at least a proportion of Alpha4 to the microtubules. The possible mechanisms for this interaction are: (1) MID1 could affect the local (microtubule-directed) activity of PP2-type phosphatases, or alternatively, (2) the Alpha4-MID1 interaction may direct PP2A phosphatase activity to specific targets on microtubule. However, evidence provided by Trockenbacher *et al.* (2001) supports the first hypothesis. An important *bona fide* role for the MID1-Alpha4 interaction is further supported by the finding of a putative mutation in the promoter region of *Alpha4* identified in a patient with a novel dysmorphism syndrome, with some similarity to OS (Graham *et al.*, 2003). Moreover, it was reported by Everett & Brautigan (2002) that the developmental expression of *Alpha4* overlaps with tissues affected in OS. Therefore, it will be interesting to further investigate how the disruption of MID1-α4-PP2A in the cells gives rise to the OS phenotypes and how it disrupts specific cellular events such as epithelial cell fusion.

Very recently, another independent research group (Berti *et al.*, 2004) reported the identification of a second MID1 interactor, MIG12, representing a novel protein with unknown function. Similar to Alpha4, MIG12 was found to be recruited onto microtubules by MID1, leading to increased resistance to the microtubule depolymerising drug, nocodazole. However, the functional significance of this interactor remains to be elucidated.

1.6.4 Functional correlations of MID1 and its homologue, MID2

Subsequent to the cloning of the *MID1* gene, sequence similarity searches performed by Buchner *et al.* (1999) and Perry *et al.* (1999) identified numerous highly related sequences represented in the EST databases. Retrieval and assembly of the full length cDNA revealed a highly homologous sequence, subsequently named *MID2*. This new gene shows 84% similarity with 70% identity at the nucleotide level and 77% identity at the protein level compared to *MID1*. Both genes display an identical structural organization comprising nine coding exons (note that *MID1* has an additional five non-coding exons at the 5' end of the first coding exon) with conserved exon sizes and splice junctions. As expected, MID2 is also an RBCC protein family with an essentially identical domain arrangement to that of MID1.

Consistent with the high level of primary sequence identity with MID1, MID2 has been shown to form both homo-dimers and hetero-dimers (with MID1) on microtubules and interact with Alpha4 at a comparable strength as judged by the reporter systems in the yeast two-hybrid assay (Short *et al.*, 2002). Intriguingly, recent studies in our laboratory (Zou and Cox, unpublished) have found a specific interactor of MID2, a PH domain-containing protein known as PEPP2. It has been shown that the interaction of MID2/PEPP2 is attenuated in the presence of excessive MID1 suggesting competitive binding between MID1 and PEPP2. Meanwhile, the expression pattern of the *Mid2* gene during early mouse embryogenesis showed that it was expressed at relatively low levels in most tissues as compared to *Mid1* but at noticeably higher levels in the developing heart (Buchner *et al.*, 1999; Perry *et al.*, 1999). The structural and functional similarity of both genes might suggest the possibility of a redundant or compensatory role of these genes in regulating certain

processes during early development. This redundancy issue is addressed in the following chapter of this thesis.

1.6.5 How disruption of MID1 function can lead to the development of the malformations seen in OS

As previously mentioned, the clinical presentation of OS represents defects in the ventral midline, reflecting disruption to tissue fusion and/or remodelling during early development of most organs. Moreover, the defects in all these tissues/organs, such as the craniofacial complex, heart and external genitalia, indicate that specific processes during their morphogenesis e.g. epithelial cell death, migration and/or EMT, might be compromised. Strikingly, all of these cellular events are known to be influenced by the activity of PP2A (Schweiger & Schneider, 2003). It is therefore of interest to understand how mutations in MID1 alter the levels of PP2Ac and thus perturb the regulation of one or more of these events. The first clues to answering this question have come from recent studies by this laboratory in collaboration with Professor Ray Runyan (Arizona, USA) that have shown an increase in endothelial cell activation and mesenchymal invasion of endocardial cushion explants, reflecting a promotion of EMT, following treatment with anti-sense oligonucleotides to either *cMID1* or *cMID2*. These endocardial cushions (both superior and inferior cushions) normally meet and fuse in the middle of the heart tube to separate the atria and ventricles of the heart. This fusion process is similar to that of facial prominences and the urethral folds that require the pre-fusion epithelial cells/sheets to make a contact and then ultimately conversion to mesenchyme to establish mesenchymal confluence (Cox, 2004). The early epithelial sheet breakage and mesenchyme conversion either following the application of anti-sense MID1 and MID2 oligonucleotides or

associated with the loss-of-function of MID1 seen in OS patients may disrupt proper fusion of endocardial cushions.

At the molecular level, the control of the EMT process during vertebrate development has been shown to be regulated by the Wnt signalling pathway through its two major components, E-cadherin and beta-catenin (Savagner, 2001). The effect of mutation in MID1 leads to the hypophosphorylation of microtubule-associated proteins (MAPs) as a result of the accumulation of PP2Ac. One consequence of hypophosphorylation of MAPs could be increased nuclear import of beta-catenin since this balance is regulated in part by PP2Ac (Schweiger & Schneider, 2003). Strikingly, the elevated levels of PP2Ac would therefore cause the destabilisation of cell adherens junctions initiating the transition of epithelium to mesenchyme, in line with the observation seen in the endothelial cushion of the heart discussed above. Similarly, the Wnt signalling pathway can be regulated also by the transforming growth factor β (TGF-β) signalling pathway through Smad molecules via serine-threonine phosphorylation. As a consequence of this latter hypothesis, further investigation of a functional interaction between MID1 and BMP4 signalling (a member of the TGF-β superfamily) is warranted given the recent reports that *Bmp4* is expressed in a very distinctive pattern in the pre-fusion facial epithelia in mice (Gong & Guo, 2003) and chicks (Ashique *et al.*, 2002). This functional interaction can also be extended to SHH, where both BMP4 and SHH have been shown to act antagonistically in many systems (Greene & Pisano, 2004). Intriguingly, a recent study by Granata & Quaderi (2003) showed that at least during establishment of the left/right body axis in chicks, *Mid1* acts upstream of *Bmp4* and plays an important role in mediating the mutually antagonistic interactions between *Shh* and *Bmp4*.

1.7 Aims of the thesis and approaches

The general aim of this thesis is to investigate the specific role of the *MID1* gene and its protein product in craniofacial morphogenesis, with emphasis in the development of the lip and primary palate and how disruptions of this gene can give rise to the various features seen among OS patients. As various affected systems in OS patients appear to arise as a result of defective tissue fusion or remodelling during embryogenesis, elucidation of the molecular and cellular mechanisms by which the primordia of the face grow and then fuse to form the lip and primary palate should shed light not only on our understanding of the developmental basis of CLP but also on the processes leading to other common malformations, such as cardiac septal defects and hypospadias. Therefore, to achieve the broad goals described above, the following specific aims were developed: (1) To characterise in detail the expression pattern of the *Mid1* gene in those tissues affected in OS patients, with respect to the cellular changes leading to fusion of the lip and primary palate, and (2) To investigate the specific role of the MID1 protein in key cellular events such as cell migration and proliferation, cell death and the ability of cells to undergo epithelial-mesenchymal transitions (EMT) that may operate during fusion of epithelial-lined tissues.

To provide support for the role of *MID1* during craniofacial development, the expression pattern of *Mid1* gene was analysed using *in situ* hybridisation on staged wild-type mouse embryos and X-gal staining of β-galactosidase activity in the *Mid1* knockout mouse embryos (Chapter Three). The same approaches were then extended to further characterise in detail the expression pattern of *Mid1* and other related genes, such as *Bmp4* and *Shh* that are also known to be expressed during fusion of facial prominences to form the lip and primary palate in mouse (Chapter Three). This chapter also provided further evidence of the possible functional redundancy between

MID1 and its protein homologue, MID2. As it has been suggested that MID1 and MID2 may have a partially redundant or co-ordinated function, mainly based on their high level of amino acid sequence similarity, specific antibodies recognising each protein were then generated (Chapter Four).

Lastly, to investigate further the specific role of MID1 protein in key cellular events during fusion of epithelial-lined tissues, stable and inducible epithelial (MDCK) and mesenchymal (Cos1) cell lines expressing either wild-type or one of a number of different mutant GFP-MID1 fusion proteins were developed. These cell lines were then used in preliminary investigations to study the role of MID1 in regulating cellular processes such as cell migration, proliferation, cell death and the ability of cells to undergo EMT, the key cellular processes regulating fusion of facial prominences (Chapter Five). Significantly, the information generated from these studies will greatly facilitate our understanding of the developmental processes controlled by the MID proteins and how their disruption contributes to the clinical presentation of OS, and more specifically at least one of the pathways that lead to the susceptibility to CLP.

Chapter Two: Materials and Methods

2.1 Abbreviations

Abbreviations listed below are primarily used in this chapter although some common abbreviations are also used occasionally in other chapters. In such cases, the abbreviations used are in accordance with those described here.

A_{600}: absorbance at 600nm

APS: ammonium persulfate

β-ME: 2-mercaptoethanol

BCIP: 5-bromo-4-chloro-3'-indolyphosphate p-toluidine salt

bp: base pairs

BSA: bovine serum albumin

CHAPS: 3-[(3-cholamidopropyl)-dimethylammonio]-1-propane sulfonate

DIG: digoxygenin

DMEM: Dulbecco's minimal essential medium

DNA: deoxyribonucleic acid

ssDNA: single-strandedDNA

dsDNA: double-strandedDNA

DNaseI: deoxyribonuclease I

dNTP: deoxyribonucleoside triphosphate

dH_2O: distilled water

dpc: days post-coitum

DTT: dithiothreitol

EDTA: ethylene-diamine-tetra-acetic acid

ELISA: enzyme-linked immunosorbent assay

EtOH: ethanol

FCS: foetal calf serum

GFP: green fluorescent protein

hrs: hours

HRP: Horseradish peroxidase

IPTG: isopropyl β-D-thiogalactopyranoside

kb: kilobase pairs

kDa: kilo Daltons

mins: minutes

NBT: nitro-blue tetrazolium chloride

OD: optical density

PBS: phosphate buffered saline

PBX: phosphate buffered saline with 0.1% Triton-X

PBST: phosphate buffered saline with 0.1% Tween-20

PCR: polymerase chain reaction

PEG: polyethyleneglycol

PFA: paraformaldehyde

PMSF: phenylmethanesulfonyl fluoride

RNA: ribonucleic acid

RNase: ribonuclease

RNase A: ribonuclease A

rpm: revolutions per minutes

SDS: sodium dodecyl sulphate

SSC: saline-sodium citrate buffer

SSPE: saline-sodium phosphate-EDTA buffer

STE: sodium tris-EDTA buffer

sec: seconds

TAE: tris-acetate-EDTA buffer

TBE: tris-borate-EDTA buffer

TE: tris-EDTA buffer

U: units

UV: ultraviolet light

V: volts

v/v: volume per volume

w/v: weight per volume

X-gal; BCIG: 5 Bromo-4-Chloro-3-indoyl β-D-galactopyranoside

2.2 Materials

2.2.1 Drugs, chemicals and reagents

All chemicals and reagents were of analytical grade or other highest grade obtainable. They were generally purchased from a range of manufacturers, with the major sources of the more important chemicals and reagents being obtained from Sigma, BDH Ltd, Bio-Rad, Boehringer Mannheim and Promega.

2.2.2 Enzymes

All restriction endonucleases and buffers were purchased from Pharmacia or New England Biolabs (NEB). Other modifying enzymes were obtained from the following sources:

RNase A and Lysozyme	Sigma
RNase Inhibitor	Promega
DNaseI (RNase-free)	Boehringer Mannheim

T7/T3 RNA polymerase	Boehringer Mannheim
SP6 RNA polymerase	Promega
Proteinase K	Boehringer Mannheim
T4 DNA ligase	Geneworks
T4 DNA polymerase	Geneworks
Klenow	Amersham
Taq DNA polymerase	Geneworks
Pfx polymerase	Invitrogen
SuperTaq polymerase	Ambion
PMSF	Sigma

Appropriate reaction buffers (either 5X or 10X) and additional supplements were supplied with all enzymes.

2.2.3 Stains and dyes

Bromophenol blue	Sigma
Ethidium bromide	Sigma

2.2.4 Antibiotics and indicators

Ampicillin	Sigma
Kanamycin	Sigma
Penicillin/Streptomycin	Invitrogen
Geneticin (G418)	Clontech
Doxycycline	Clontech
X-gal	Sigma
IPTG	Sigma

BCIP	Boehringer Mannheim
NBT	Boehringer Mannheim

2.2.5 Kits and assays

pGEM-T® Easy Vector System 1	Promega
QIAquick Gel Extraction kit	Qiagen
QIAprep Spin miniprep kit	Qiagen
QIAprep Spin midiprep kit	Qiagen
MAXIScript™ T7/T3 kit	Ambion
RETROscript® kit	Ambion
RNAqueous®-4PCR kit	Ambion
DIG RNA labelling kit	Boehringer Mannheim
Dual-Luciferase™ Reporter Assay	Promega
FuGENE™ 6 Transfection Reagent	Roche
Lipofectamine™ 2000	Invitrogen
CellTiter 96® Aqueous Assay	Promega
Caspase-Glo™ 3/7 Assay	Promega

2.2.6 Nucleic acid and protein molecular weight marker

1Kb PLUS DNA LADDER™, purchased from Invitrogen, consists of 12 fragments of the following sizes (in bp): 100, 200, 300, 400, 500, 650, 850, 1000, 1650, 2000, 5000 and 12000.

HyperLadder I, purchased from BIOLINE, consists of 14 regularly spaced bands of the following sizes (in bp): 200, 400, 600, 800, 1000, 1500, 2000, 2500, 3000, 4000, 5000, 6000, 8000 and 10000.

BENCHMARK™ Prestained Protein Ladder, purchased from GibcoBRL shows 10 major bands of the following sizes (in kDa): 8.4, 14.9, 19.6, 26.0, 37.4, 49.5, 63.8, 80.9, 113.7 and 176.5.

2.2.7 Solutions and buffers

All buffers were sterilised by autoclaving or filtration through a Sartorius[a] Minisart NML 0.2µm filter where necessary.

SSC (1X): 150mM NaCl
15mM sodium citrate

SSPE (1X): 150mM NaCl
10mM NaH_2PO_4
1mM EDTA pH 7.4

TAE (1X): 40mM Tris-acetate
20mM sodium acetate
1mM EDTA pH 8.2

TBE (1X): 90mM Tris-HCl
90mM boric acid
2.5mM EDTA pH 8.3.

TE (1X): 10mM Tris-HCl pH 7.5

0.1mM EDTA

PBS (1X): 7.5mM Na_2HPO_4

2.5mM NaH_2PO_4

145mM NaCl

Blotto solution: 5% (w/v) skim milk powder in 1 X PBS

Non-denaturing lysis buffer:

1% (v/v) Triton X-100

50mM Tris-HCl pH 7.4

300mM NaCl

5mM EDTA

0.12% (w/v) Sodium Azide

1mM PMSF (added prior to use)

Phenol/Chloroform: 50% (w/v) Phenol

48% (v/v) Chloroform

2% (v/v) Isoamyl alcohol (buffered with an equal volume of Tris-HCl, pH 8.0)

0.2% (v/v) ß-ME

Agarose gel loading buffer:

50% (w/v) glycerol

50mM EDTA

0.1% (w/v) bromophenol blue

2.2.8 Radionucleotides

[α-^{33}P] UTP (specific activity, 3000Ci/mmole) was purchased from Perkin Elmer.

2.2.9 Cloning and expression vectors

pBluescriptKS+ (pKS+)	Stratagene
pGEM®-T easy	Promega
pEGFP-C2	Clontech

2.2.10 Synthetic oligonucleotides

PRIMER	SEQUENCE (5' → 3') (restriction site linkers in bold)	ANNEAL TEMP. (°C)	SOURCE
T3	CGAATTAACCCTCACTAAAGGG	55	Geneworks
T7	GTAATACGACTCACTATAGGGC	55	Geneworks
EGFP-60r	GTTTACGTCGCCGTCCAGCTC	55	Sigma Genosys
EGFP-660	GATCACATGGTCCTGCTGGAG	55	Sigma Genosys
5' MID-fusion	GT**GAATTC**CTGAAGATGGAAACA CTGGAGTC	55	Bresatec
HM-MID2	CGATGGCCTGTAAAGGGCTTC	55	Biotech/Operon
mMID2P-F	GGAAACACTGGAGTCAGAATTGA CC	55	Sigma Genosys
mMID2P-R	CACCAGTTTGCATAAGGCACAGA TC	55	Sigma Genosys
mMID1-1Ec	GT**GAATTC**GAAACACGAGTGGAT CGGGAAG	56	Sigma Genosys
mMID1-2Ba	GT**GGATCC**CTCAAGGTCGCTGCT CCGTAC	56	Sigma Genosys
CMVTET-F	CAC**ATTAAT**TTTACCACTCCCTAT CAGTGATAGAG	55	Sigma Genosys
CMVTET-R	CAC**GCTAGC**GTTTAAACTTGGAC CTGGGAGTGGA	55	Sigma Genosys

2.2.11 MID1 domain deletions

	Region deleted	Amino acids deleted
MID1ΔBB	Two B-Boxes	Residue 72-211
MID1ΔCTD	B30.2 domain	Residue 490-667

2.2.12 Bacterial strains

The following *E. coli* K12 strain was used as host for recombinant plasmids in recombinant DNA procedures:

Strains	Genotype
E. coli DH5α	supE44 ΔlacU169 (p80 lacZΔM15) hsdR17 recA1 endA1 gyrA96 thi-1 relA1.

2.2.13 Bacterial growth media

All growth media were prepared in distilled and deionised water and sterilised by autoclaving, except for heat labile reagents, which were filter sterilised. Antibiotics and other labile chemicals were added after the solution had cooled to 50°C. Ampicillin (100μg/ml), kanamycin (70μg/ml) or chloramphenicol (33μg/ml) was added where appropriate to maintain selective pressure.

L-Broth: 1% (w/v) Bacto-tryptone (Difco)
0.5% (w/v) yeast extract (Difco)
1% (w/v) NaCl
Adjusted to pH 7.0 with NaOH

Plates: L-Broth with 1.5% (w/v) Bacto-agar (Difco)

SOC: 1% (w/v) Bacto-tryptone (Difco)

0.5% (w/v) yeast extract (Difco)

1% (w/v) NaCl, pH 7.0

10mM $MgCl_2$

10mM $MgSO_4$

20mM glucose

2.2.14 Tissue culture cell lines and media

2.2.14.1 Cell lines

Cos-1, Monkey Kidney cells

MDCK, Madin-Darby Canine Kidney

2.2.14.2 Media

All cells were grown in Dulbecco's modified Eagle medium (DMEM) (GibcoBRL) supplemented with 10% (v/v) FCS, 2mM L-glutamine, 100 units/ml penicillin and 100µg/ml streptomycin.

2.2.15 Antibodies

Anti-α-tubulin	Sigma
Anti-Vimentin	DHSB
Anti-β-Catenin	BD Biosciences
Anti-E-Cadherin	BD Biosciences
Anti-GFP	Rockland
Anti-DIG-alkaline phosphatase	Boehringer Mannheim

2.2.16 Miscellaneous materials

CHAPS	Sigma
D19 developer	Kodak
Hypam Hardener	ILFORD
L4 Emulsion	ILFORD
ProbeQuant™ G-50 Micro Columns	Amersham
Polymax T-Fixer	Kodak
Silica gels/desiccant packets	Sigma

2.3 Recombinant DNA methods

2.3.1 General molecular biology methods

The following methods were performed essentially as described in "*Molecular Cloning: A Laboratory Manual*" by Sambrock *et al.* (1989): Growth, maintenance and preservation of bacteria; quantitation of DNA and RNA; autoradiography; agarose and polyacrylamide gel electrophoresis; precipitation of DNA and RNA; phenol/chloroform extractions; end-filling or end-labelling of DNA fragments using the Klenow fragment of *E. coli* DNA polymerase I.

All manipulations involving viable organisms, which contained recombinant DNA were carried out in accordance with the regulations and approval of the Office of the Gene Technology Regulator (OGTR), Australian Government Department of Health and Ageing.

2.3.2 Restriction endonuclease digestions of DNA

All restriction endonuclease digestions of DNA dissolved in dH_2O (or 1 X TE) were carried out in the supplied 10X restriction buffer with addition of BSA where

appropriate. In analytical digests, 0.5-2µg of DNA were incubated with 2-3 units of the appropriate restriction enzyme in a reaction volume of 15µl for a minimum of 2 hrs at the temperature specified by the manufacturer. In preparative digests of DNA, more than 2µg of DNA were carried out using 2-3 units of restriction enzyme for each µg of DNA, in a reaction volume of 50µl, and allowed to proceed for up to 5 hrs at the appropriate temperature specified by the manufacturer.

2.3.3 Agarose gel electrophoresis of DNA

AMRESCO® biotechnology grade agarose (type 1) was used for the preparation of all horizontal agarose gels at appropriate percentage and size. Unless otherwise specified, the agarose was melted in 1X TAE to a final concentration of 1%. For small gels, molten agarose was poured onto a gel casting tray using a plastic comb to form the well slots. The gel was then placed in an electrophoresis tank and submerged in TAE. The DNA samples containing a suitable amount of loading buffer (at final concentration of 1X) were then loaded into the gel slots. 40-80V was applied to the tank until the bromophenol blue dye had migrated the required distance. The DNA was then stained with ethidium bromide (10mg/ml) in order to be visualised by illumination with long or medium wave UV light.

2.3.4 Phenol/chloroform extraction of DNA

The volume of DNA in solution was brought to a volume of 100µl or greater with sterile dH_2O. An equal volume of phenol/chloroform/isoamylalcohol was then added and the tube vortexed briefly and centrifuged for 5 mins at 14000rpm. The top layer was then removed to a clean tube and the sample was then EtOH precipitated as described below.

2.3.5 Ethanol precipitation of DNA

2µl of glycogen, 1/10th the volume of 3M NaAc (pH5.2) and 2.5 volumes of chilled absolute (100%) EtOH were added to the solution containing DNA, mixed thoroughly and the tube then placed at -20°C for at least 30 mins. The tube was centrifuged at 14000rpm for 20 mins and the resultant pellet washed in 70% (v/v) EtOH before being vacuum dried (SpeediVac) and resuspended in an appropriate volume of sterile dH_2O or 1 X TE.

2.3.6 Preparation of cloning vectors

Plasmids were linearised with appropriate restriction enzyme(s). The vector DNA was then electrophoresed on a 1% agarose gel and the gel stained with ethidium bromide. The linearised vector DNA was visualised under long wave UV light, excised and then extracted using the QIAquick Gel Extraction kit according to the manufacturer's instructions.

2.3.7 Preparation of DNA restriction fragments

DNA was incubated with the appropriate restriction enzyme(s) as described in Section 2.3.2. Restriction fragments were isolated from 1% agarose gel where bands representing restriction fragments were visualised under long wave UV light following staining with ethidium bromide, and then excised from the gel. DNA fragments were extracted using the QIAquick Gel Extraction kit following the supplier's protocols.

2.3.8 End-filling restriction endonuclease digested DNA

Both 5' and 3' overhangs were end-filled with T4 DNA polymerase. 1µg of restricted DNA was incubated with 0.2mM dNTP's, 1 X T4 DNA polymerase buffer and 2.5 units of the polymerase at 37°C for 1 hour. The enzyme was then heat inactivated at 68°C for 10 mins and the end product purified by phenol/chloroform extraction and then followed by EtOH precipitation.

2.3.9 Ligation of DNA

A 20µl reaction contained 20-50ng of vector DNA, a 3 molar excess of the insert DNA, 1X ligation buffer and 1 unit of T4 DNA ligase. The reactions were incubated for either 4 hrs at room temperature or overnight at 4°C. A control ligation with vector only was set up and included in the subsequent transformation to determine background levels of uncut or recircularised vector DNA.

2.3.10 Transformation of *E. coli* with recombinant plasmids

2.3.10.1 Preparation of competent *E. coli*

500ml of L-broth was inoculated with 5ml of an overnight culture of *E. coli* (*DH5α* strain) cells and grown to an OD_{A600} of 0.5-1.0. The culture was then chilled in an ice slurry for 15 to 30 mins and the cells then harvested by centrifugation at 4000g for 15 mins. The cells were then resuspended in 500ml of ice-cold MQ water, pelleted at 5000g, resuspended again in 250ml of ice-cold MQ water and pelleted again at 4000g. The pellet was then resuspended in 10ml of ice-cold 10% glycerol, repelleted at 3000g and finally resuspended in 1ml of ice-cold 10% glycerol. The competent cells were then dispensed into 45µl aliquots and then snap frozen in liquid nitrogen and stored at -80°C.

2.3.10.2 Transformation of competent bacteria

For transformation, cells were thawed at room temperature, added to ligation mixture and incubated on ice for at least 30 sec. Cells were then transferred to an ice-cold 2mm electroporation cuvette and electroporated in a Bio-Rad Gene Pulser set to 2500V, 25μFD capacitance and Capacitance Extender set to 500μFD. The cuvette was immediately washed out with 1ml of SOC and the suspension incubated at 37°C for 30 mins. Cells were then pelleted for 8 sec at 14000rpm, then about 800μl of the supernatant was removed and then the cells gently resuspended in the remaining SOC. The cell suspension was plated onto L-agar plates supplemented with either 100μg/ml ampicillin or 50μg/ml kanamycin and then incubated at 37°C overnight. If selection for β-galactosidase activity (blue/white colour selection) was required, 10μl of 10% IPTG and 10μl of 20% BCIG were added prior to plating.

2.3.11 Isolation of plasmid DNA

Small-scale and large-scale preparations of ultrapure DNA were prepared using the QIAprep Spin miniprep kit and the QIAprep Spin midiprep kit, respectively. In both instances preparations were performed according to the manufacturer's protocols.

2.3.12 Determination of DNA concentration

The concentrations of DNA samples were estimated by comparison to the bands of known concentration on an agarose gel, or by determining UV absorbance of the DNA solution at 260nm and estimating the DNA concentration (50μg of dsDNA and 30μg of ssDNA per absorbance unit).

2.3.13 Automated sequencing of PCR products

All automated sequencing runs were performed at the IMVS Molecular Pathology Sequencing Unit, Adelaide, South Australia. Automated sequencing reactions were carried out using 4-6µl of terminator ready mix (version 2 or version 3), 2µl of template DNA (500µg), 1µl of primer (100µg) and approximately 11-13µl of dH_2O. The cycles completed on a Peltier Thermal Cycler (MJ Research) were: 96°C for 30 secs, 50°C for 20 secs, 60°C for 4 mins with 25 completed cycles.

2.3.14 Polymerase chain reaction (PCR) amplification of DNA

PCR's were performed in 50µl volumes containing 0.2mM dNTP's, 1 X PCR reaction buffer, 2mM $MgCl_2$, 1.0µM each primer, 2U of *Taq* DNA polymerase and 1.0µM template DNA. Amplifications was performed in a Peltier Thermal Cycler (MJ Research) programmed with an initial template denaturation at 94°C for 3 mins followed by 35-45 cycles of denaturation at 94°C for 1 minute, a primer annealing step and extension at 72°C. Annealing temperature and extension time varied depending on the primer pairs.

2.3.15 Preparation of PCR products for cloning

PCR products were EtOH precipitated as detailed in Section 2.3.5, resuspended in dH_2O and then digested with the appropriate restriction enzyme. The digest was gel purified as detailed in Section 2.3.7 and then an appropriate amount of the purified fragments used in ligation reaction as detailed in Section 2.3.9.

2.4 Methods for RNA analysis and β-galactosidase activity

Sterile equipment was used in all procedures that involved the analysis of RNA. Gloves were worn at all times. Solutions and plasticware were autoclaved (120°C for 15 minutes) and glassware was baked (200°C for 5 hours).

2.4.1 Embryos collection and fixation

Prior to the commencement of the studies described in this thesis, an approval was obtained from the Animal Ethics Committee, the University of Adelaide for the use of animals in this research project (# S/22/99 and # S/37/01). For the collection of mouse embryos, timed matings for both wild-type and *Mid1* knockout mice were established and the morning on which the vaginal plug was found designated as day 0.5 dpc. After female mice were sacrificed, the uteri were dissected and immediately transferred to sterile ice-cold PBS. Individual conception sites were then dissected in PBS under a Zeiss SVII stereoscope. Precise staging of dissected embryos was performed using Kaufman's Atlas of Mouse Development (Kaufman, 1998). Embryos were fixed using freshly prepared 4% PFA dissolved in PBS. Following fixation, embryos for whole-mount *in situ* hybridisation were dehydrated in a graded methanol series diluted in PBX (25%, 50%, 75% and 100% methanol) and stored at -20°C, while embryos for sectioning were dehydrated in a graded ethanol series diluted in PBS (25%, 50%, 75% and 100% ethanol). All histology work involving embedding in paraffin and sectioning of the embryos (standard histological techniques) were performed in the Department of Pathology, the University of Adelaide. Embryos were embedded in paraffin wax, sectioned at 5-7μm and mounted on SuperFrost® Plus slides.

2.4.2 Preparation of hybridisation probes

Hybridisation reactions were performed using DIG-labelled RNA probes for whole-mount *in situ* hybridisation to mouse embryos and ^{33}P-labelled RNA probes for the *in situ* hybridisation to tissue sections. Prior to the synthesis of RNA transcripts, cDNA templates were first linearised using appropriate restriction enzymes, purified by phenol/chloroform extraction (Section 2.3.4) and then ethanol precipitated (Section 2.3.5), with the DNA pellet being resuspended in dH_2O or 1 X TE.

2.4.2.1 Synthesis of DIG-labelled RNA probes

DIG-labelled RNA probes were synthesised using a range of reagents bought from Boehringer Mannheim. The incubation reaction comprised: 1µg linearised DNA template, 2µl 10X reaction buffer, 2µl 10X nucleotide cocktail (10mM GTP, 10mM ATP, 10mM CTP, 6.5mM UTP, 3.5mM DIG-UTP), 2µl DTT, 25U RNase Inhibitor (RNasin), RNase-free dH_2O to 20µl and 30U RNA polymerase. After gentle mixing, the reaction was incubated at 37°C for 2 hrs. The DNA templates were then removed by the addition of 2µl of RNase-free DNase 1 (10U/µl) to the reaction and incubated at 37°C for a further 10 mins. The reaction mixture was then diluted with sterile 1 X TE buffer to a volume of 50µl and loaded onto a ProbeQuant™ G-50 micro column and centrifuged into a sterile eppendorf tube. The probe was stored in an equal volume of hybridisation solution (recipe in Section 2.5.3) at -20°C. The probe concentration was estimated after separation on an agarose gel containing 0.5µg/ml ethidium bromide.

2.4.2.2 Synthesis of ^{33}P-labelled RNA probes

The ^{33}P-labelled RNA probes were synthesised using a MAXIScript™ T7/T3 *in vitro* transcription kit (Ambion). The incubation reaction comprised: 2µg linearised DNA template, 1µl 10X reaction buffer, 2µl 5X nucleotides cocktail (10mM GTP, 10mM ATP, 10mM CTP), 0.6µl cold UTP, 0.5µl RNase Inhibitor (RNasin; 20U/µl), 5-10µl ^{33}P-rUTP (3000 Ci/mmol) (radioactive label was first dried in a speedy-vac apparatus), RNase-free dH_2O to 10µl and 30U RNA polymerase. After gentle mixing, the reaction was allowed to proceed at 37°C for 2 hrs. The DNA templates were then removed by the addition of 1µl of RNase-free DNase 1 (10U/µl) to the reaction and incubated at 37°C for a further 10 mins. The reaction mixture was then diluted with sterile STE (150mM NaCl, 10mM Tris-HCl, pH 8.0, 1mM EDTA) buffer to a volume of 50µl and loaded onto a ProbeQuant™ G-50 micro column and centrifuged into a sterile eppendorf tube. The probe was then stored at 4°C after the addition of 2.5µl Vanadyl, 0.5µl β-ME and 20U RNasin. The probe concentration was determined using a Scintillation counter (in cpm/µl). The size and integrity of the probe was also determined by electrophoresis of the probe onto a 10 cm X 15 cm X 5 mm pre-prepared 6% polyacrylamide gel (SequaGel®; National Diagnostics) followed by exposure on X-ray film without intensifier screens overnight.

2.4.3 Whole-mount *in situ* hybridisation to mouse embryos

Embryos were first rehydrated by washing for 10 mins at each step on a rocking platform in a graded methanol series in PBX (75%, 50% and 25% methanol) and then twice in PBX alone. The embryos were transferred into 2 ml tubes using a cut pipette tip and treated with 10µg/ml proteinase K diluted in PBX for 5-25 mins at

room temperature (the length of treatment determined by the size of the embryos). The proteinase K solution was then removed and the embryos rinsed briefly with PBX before being refixed for 20 mins with fresh 0.2% glutaraldehyde, 4% PFA in PBX. Following this refixation step, the embryos were washed 3 times for 5 mins each with PBX on a rocking platform. The embryos were then rinsed with 2 ml of hybridisation solution (50% formamide, 5X SSC, 2% blocking powder (Boehringer Mannheim; dissolved directly in this mixture), 0.1% Triton X-100, 0.1% CHAPS, 1mg/ml tRNA (or yeast RNA), 5mM EDTA, 50µg/ml heparin) and the embryos were allowed to settle in the tube before replacement of fresh hybridisation solution and approximately 1µg/ml of DIG-labelled RNA probe. The hybridisation involved incubation overnight at 65°C.

Following hybridisation, the embryos were subjected to a number of post-hybridisation washes (at 65°C unless otherwise stated): 2X SSC, 0.1% CHAPS containing 25% formamide, three times for 10 mins; 2X SSC, 0.1% CHAPS for 20 mins; 0.2X SSC, 0.1% CHAPS, three times for 20 mins; KTBT (50mM Tris-HCl pH 7.5, 150mM NaCl, 10mM KCl, 0.1% Triton X-100) twice for 10 mins each at room temperature. The embryos were then pre-blocked with 10% sheep serum in KTBT for 1-3 hrs at room temperature on a shaking platform, followed by incubation with 1:2000 dilution of anti-DIG-alkaline phosphatase antibody in 10% sheep serum in KTBT, and rocked overnight at 4°C.

For post-antibody washes and histochemistry, the embryos were washed with KTBT at least 5 times for 1 hour each at room temperature, then overnight at 4°C on a shaking platform. Finally, the embryos were incubated in the dark with NTMT containing 4.5µl/ml NBT stock solution and 3.5µl/ml BCIP stock solution. The reaction was periodically monitored and when an appropriate strength signal was

observed, the colour reaction was stopped by washing several times with PBX. The embryos were then fixed in 4% PFA for 1-2 hrs at room temperature, and stored in PBS at 4°C.

2.4.4 *In situ* hybridisation to tissue sections

Slides containing paraffin embedded tissue sections were melted at 55°C for 5 mins, then deparaffinised (twice for 5 mins each in Safsolvent), hydrated (2 mins each in 100%, 80% and 50% ethanol) and subjected to a number of pre-hybridisation washes (at room temperature unless otherwise stated): 2X SSPE for 2 mins; 0.25% acetic anhydride in 0.1M triethanolamine-HCl (pH 8.0) for 10 mins; 2X SSPE for 2 mins followed with fresh 2X SSPE for another 10 mins. The sections were then air dried and warmed on a slide warmer block at 52°C. Hybridisation solution was applied to the warmed sections, which were then overlaid with siliconised coverslips. The hybridisation solution was 50% formamide, 2X SSPE, 10% polyethleneglycol (molecular weight: 6000), 1mg/ml yeast RNA, 0.5mg/ml salmon sperm DNA, 500mM βME and 0.5% Blotto. ^{33}P-labelled RNA probes were used at a final concentration of 20,000cpm/µl. Hybridisation was performed at 52°C for 20hrs in a humidified chamber.

Following hybridisation, the sections were subjected to a number of washes to remove non-specifically bound probe: 2X SSPE at 52° for 1 hour; 0.1X SSPE at 65°C 1 hour; 2X SSPE containing RNase A (20µg/ml) at 37°C for 30 mins; 0.1X SSPE at 65°C for 30 mins as a final stringency wash. The sections were dehydrated (2 mins each in 50%, 80% and 100% ethanol) and air-dried. The sections were then coated with Ilford L4 nuclear track emulsion, dried and exposed at 4°C in light-proof boxes.

The time of exposure varied from 5-14 days, depending on the probe and the tissue under investigation.

The emulsion was developed with Kodak D19 developer (diluted 1:1 with water) for 2.5 mins, rinsed briefly in water for 10-15 secs, followed by fixation with Ilford Hypam Rapid Fixer for 5 mins. After washing the slides in running tap water for a few minutes, the slides were counterstained with Haematoxylin and Eosin and coverslips were affixed with Dako® fluorescent mounting medium. The slides were then analysed under dark and bright field illumination.

2.4.5 Reverse transcription-PCR (RT-PCR)

Total RNA from both wild-type and *Mid1* knockout mice tissues was prepared using RNAqueous®-4PCR kit (Ambion) following the manufacturer's instruction. The concentration and purity of RNA were determined by reading the absorbance in a spectrophotometer at 260 nm and 280 nm. Two-step RT-PCR was then performed using a RETROscript® kit (Ambion) following the manufacturer's protocols. Approximately 1µg of total RNA was used to generate cDNA with oligo(dT) as a primer and MMLV reverse transcriptase (100U). 5 µl of the cDNA product was used for PCR amplification using the following primers: mMID2P-F – GGAAACAC-TGGAGTCAGAATTGACC and mMID2P-R – CACCAGTTTGCATAAGGCACA-GATC. Cycle conditions were denaturation, 95°C for 30 seconds; annealing, 59°C for 30 seconds; and extension, 72°C for 30 seconds. 15µl of amplified product were resolved by electrophoresis through 1% (w/v) agarose gels in 1 X TAE.

2.4.6 *LacZ* staining

Whole-mount staining for detection of β-galactosidase activity in *Mid1* knockout embryos was performed on embryos of various ages (9.5 dpc to 15.5 dpc). Dissected embryos were first rinsed in PBS then fixed in 4% PFA prepared in PBS for about 8 mins at room temperature. Following fixation, samples were washed three times for 15 mins each time in *LacZ* wash buffer (2mM $MgCl_2$, 0.01% sodium deoxycholate, 0.02% Nonidet-P40 (NP-40) in PBS). Staining was carried out in 0.5mg/ml X-gal, 5mM potassium ferrocyanide and 5mM potassium ferricyanide dissolved in *LacZ* wash buffer at 37°C for 6 hrs to overnight, with gentle shaking and protected from light. After completion of staining, embryos were washed three times for 10 mins in PBS and stored in 70% EtOH at 4°C.

2.5 Methods for generation of polyclonal and monoclonal antibodies

Synthetic peptides used in this study were synthesised by Auspep Pty. Ltd., Victoria, Australia. The purity of the peptides were >90% as determined by mass spectra and high performance liquid chromatography (HPLC). All steps involving animal handling, including standard immunisation and bleed protocols were provided by the School of Molecular & Biomedical Science's Research Support, University of Adelaide. All other steps involved in the generation of these polyclonal and monoclonal antibodies were performed by the author unless otherwise stated.

2.5.1 Generation of polyclonal antibodies

Pre-bled New Zealand White rabbits were initially immunised with 0.5mg of Diphtheria Toxoid (DT)-conjugated synthetic peptide in Freund's complete adjuvant. After 3 weeks, the rabbits were given booster injections every other week with 0.5mg

of conjugate in incomplete adjuvant until maximum titers were reached, about 7-13 weeks after the primary immunisation. The animals were bled after each boost and ELISA was used to titrate the antibodies of each bleeding. When a high antigen-specific titre was achieved, serum was then prepared from collected blood by centrifugation at 4,000rpm, 4°C for 10 mins. Serum was stored in aliquots in screw-top tubes at -20°C.

2.5.2 Generation of monoclonal antibodies

A BALB/c mouse was immunised by one intraperitoneal injection of 60µg of the respective DT-conjugated synthetic peptides in 50% Freund's complete adjuvant followed by at least two injections in 50% Freund's incomplete adjuvant at 3 week intervals. When high titers of antibodies were detected in the mouse blood by ELISA, the mouse was sacrificed and the spleen removed. Splenocytes were obtained by crushing the spleen with a Dounce homogeniser and then fused with murine myeloma SP2/O cells for hybridoma production. 100 X 10^6 splenocytes were incubated with 20 X 10^6 SP2/O cells in 50% PEG (molecular weight 1500) for 90 sec at 37°C. Cells were then distributed in 96-well plates and hybridomas selected by incubation in the presence of HAT (Hypoxanthine-Aminopterin-Thymidine). Primary hybridoma supernatants were then screened using ELISA. Identified candidate hybridomas were then expanded. The limiting dilution procedure was performed using a FACScan (Becton Dickinson) to identify the positive hybridoma clones. Supernatants were harvested and filter- sterilised through 0.45 µm filters. All supernatants were stored at -20°C in 10ml aliquots.

2.5.3 ELISA procedures

Costar 96-well vinyl assay trays (ELISA plates) were coated with 50µl of PBS containing 10µg/ml of synthetic peptides as an antigen at room temperature for 60 mins. The wells were each washed once with 150µl of PBST and then blocked with 200µl of PBS containing fat-free milk ('Diploma' skim milk; 3% w/v) at room temperature for 60 mins, followed by another wash with PBST. Primary antibodies (immune sera or hybridoma supernatants) diluted in PBS supplemented with 3% fat-free milk were then added to each well, and incubation continued for 60 mins at room temperature, before extensive washing with PBST. HRP-conjugated secondary anti-species IgG diluted at 1:500 in PBS supplemented with 3% fat-free milk was added to each well and incubated at room temperature for another 60 mins. The plates were finally washed three times with 150µl of PBST. The bound antibodies were detected by colour development following the addition to each well of O-phenylenediamine dihydrochloride in 0.1M sodium citrate supplemented with 0.03% H_2O_2, pH 5.5. The reaction was stopped 10 mins later by 2.5M sulphuric acid, and the absorbance was measured at 492nm using a microtiter plate spectrophotometer.

2.6 Methods for mammalian cell culture

2.6.1 Maintaining cultured cell lines

All cultured cell lines were routinely grown in 75-150 cm^3 flasks (Falcon) at 37°C in an atmosphere of 5% CO_2. Cell lines were maintained by subculturing approximately 1:10 to 1:20 dilutions every 3-4 days. Harvesting and subculturing adherent cells was completed by first removing the culture media, washing twice with PBS before the addition of 1-2ml of trypsin/EDTA solution. The cells were left at 37°C until they began to detach from the surface of the flask, after which 8ml of

culture media was added and the flask washed to remove any remaining cells. Harvested cells were washed twice in PBS and pelleted by centrifugation at 1,200g for 2 mins before being resuspended in the appropriate buffer.

2.6.2 Transfection of cultured cells

Cells were seeded into appropriately sized dishes to approximately 60-80% confluency in growth media. The cells were allowed to attach to the surface of the flask or inserted coverslip for at least 4 hrs and transfected with a mixture of either FuGENE™ 6 (Roche) or Lipofectamine™ 2000 (Invitrogen) diluted with DMEM and the appropriate DNA construct (as per manufacturers recommendations). Following at least 24 hrs of expression, cells were utilised for either protein extraction or immunofluorescence.

2.6.3 Generation of stable cell lines

For the generation of stable cell lines, semi-confluent cells grown in DMEM with 10% FCS were first stably transfected with 1µg of DNA constructs expressing a tetracycline-controlled transactivator using Lipofectamine™ 2000 (Life Technologies), according to the manufacturer's instructions. Cultures were placed under selection by the addition of 300µg/ml Geneticin (G418) 48 hrs after transfection and maintained under these conditions until colonies formed. After 2-3 weeks, colonies were isolated and expanded. These single stable Tet-On cell lines were then cotransfected with the inducible GFP reporter plasmids expressing full-length or one of a number of deletion forms of MID1 using Lipofectamine™ 2000 as described above. Following a series of expansions, expression of the exogenous GFP-fusion protein was induced by the addition of doxycycline (1-2µg/ml) for about 12-16

hrs. The fluorescence positive cells were then subjected to fluorescent-activated cell sorting (FACS) with a FACScan (Becton Dickinson). Clonal cell lines obtained were frozen at –80°C and in liquid nitrogen for longer term.

2.6.4 Assay for Luciferase activity

Luciferase activity was measured using a Dual-Luciferase™ Reporter Assay System (Promega) and measurements determined in a Berthold model LB9502 luminometer. The assays for firefly luciferase activity and *Renilla* luciferase activity were performed according to the manufacturer's protocols.

2.6.5 Immunofluorescent analysis of cultured cells

Twenty-four hours post-transfection, cells plated on coverslips were rinsed twice in PBS and fixed with 3.5% PFA in PBS. Following permeabilisation with 0.2% Nonidet-P40 in PBS, microtubule or cell cytoskeleton were stained with the appropriate dilution of primary antibody for 1 hour. Excess primary antibodies were washed off with PBS and attached antibodies were then detected with appropriate dilutions of conjugated secondary antibodies. The coverslips were inverted and mounted onto glass slides for visualisation under appropriate wavelength light on an Olympus AX70 microscope and images captured using a Photometrics CE200A cooled CCD camera.

2.6.6 Non-denaturing protein extraction from cultured cells

10cm plates containing either transfected or untransfected cells that were 80-90% confluent were rinsed twice with ice-cold PBS. Cells were collected by physical removal with a cell scraper or cell lifter in 1ml of ice-cold non-denaturing lysis buffer

and then transferred to a microcentrifuge tube. Following a brief vortex for 10 sec, the cells were incubated on ice for 30 mins and centrifuged at 13,000rpm for 20 mins. Clear supernatant was collected and stored at -20°C.

2.6.7 Protein concentration determination (Bradford assay)

Bradford reagent (Biorad) was diluted 1:5 with MQ water. Between 1-5µl of total protein was made up to 200µl with dilute Bradford reagent and mixed by pipetting. The assay solution was placed into a 96 well plate and the absorbance at 590nm was measured on a UV spectrophotometer. BSA protein standard assays were obtained between the ranges of 0-40mg/ml. Approximate concentration of the test sample was determined against a linear plot produced by the BSA standard. All assays were completed in duplicate and the mean result determined.

2.6.8 Protein gel electrophoresis and Western blotting

All SDS-PAGE of protein samples and subsequent western transfer to nitrocellulose or nylon membranes and Coomassie blue staining of gels was performed exactly as described by Harlow & Lane (1988). Nitrocellulose and nylon blots were washed thoroughly with PBST and then blocked for 1 hour in 5% blotto. Primary and secondary antibody incubations were carried out overnight at 4°C or for 45 mins at room temperature with the appropriate dilution of antibody in the aforementioned blocking solution. All secondary antibodies were conjugated to HRP (Amersham) and then detected by Enhanced Chemuluminescence (Amersham).

2.6.9 Isolation of genomic DNA from tissue culture cells

Confluent cells grown in 10cm culture plate (~3 X 10^7 cells) were harvested, washed once in ice-cold PBS and resuspended in 700µl of digestion buffer (10mM Tris-HCl, pH 8.0, 100mM NaCl, 25mM EDTA, pH 8.0 and 0.5% SDS) with 0.1mg/ml proteinase K added before use. Samples were then incubated with shaking at 50°C for 12-18 hours in tightly capped tubes. The digestion was then extracted with an equal volume of phenol/chloroform/isoamyl alcohol by centrifugation at 1700g for 10 mins in a swinging bucket rotor. The aqueous (top) layer was then transferred to a new tube and genomic DNA was precipitated with 0.5 volume of 7.5M ammonium acetate and 2 volumes (of original amount of top layer) of 100% EtOH, followed by washing with 70% EtOH and resuspension in 500µl of 1 X TE at 4°C overnight.

2.6.10 Proliferation and apoptosis assays

For proliferation and apoptosis assays on permanent cell lines, 5 X 10^3 cells were seeded into 96-wells plate and incubated for 24 – 48 hours with or without doxycycline induction (2µg/ml). Proliferation was measured using CellTiter 96® Aqueous One Solution Cell Proliferation Assay (Promega). Briefly, 20 µl of the CellTiter solution were added for the last 4 hours of the incubation period and absorbance measured at 490 nm using a spectrophotometer. Apoptosis was detected in the same setting using Caspase-Glo™ 3/7 Assay (Promega). For this assay, 100 µl of the reagent were then added and incubated at room temperature for up to 3 hours. Luminescence of each sample was measured in a plate-reading luminometer. Both proliferation and apoptosis assays were performed in triplicate.

2.6.11 Wound healing assays

Cells for *in vitro* wound healing assays were grown to confluency in 15 cm tissue culture dish with 20 mm grids. The monolayer cells were then wounded with a sterile yellow pipette tip being scraped along the surface, generating a wound spanning about 15-20 cell diameters. The cells were then grown with or without induction with doxycycline. The healing process of these cells was judged by monitoring the closure of the wound over a period of up to 60 hours in complete tissue culture media. Wound closure was observed at a series of time points using a Nikon TE200 microscope and photographed with a Photometrics Coolsnap™ fx camera. All images were then processed using Photoshop software.

Chapter Three: Characterisation of *Mid1* expression during early mouse embryogenesis

3.1 Introduction

Mutations in the *MID1* gene have previously been identified as a cause of X-linked Opitz GBBB syndrome (OS) (Cox *et al.*, 2000; Quaderi *et al.*, 1997; So *et al.*, 2005), a congenital defect affecting the development of midline structures. Craniofacial and external urogenital abnormalities are the two principal features of OS, but cardiac abnormalities, developmental delay (found in two-thirds of patients) and central nervous system (CNS) defects resulting in mental retardation are also common. To date, *MID1* orthologues have been successfully isolated from the mouse (Dal Zotto *et al.*, 1998) and chick (Richman *et al.*, 2002), providing an excellent opportunity to investigate the developmental function of this gene during early embryogenesis. Quaderi *et al.* (1997) performed an initial northern blot analysis of the tissue expression of the *MID1* gene using a cDNA as a probe. This analysis of multiple foetal and adult human tissues revealed ubiquitous expression of this gene, with abundant expression found in foetal kidney, adult brain, heart and placenta. Later expression studies conducted during early mouse (Dal Zotto *et al.*, 1998) and chick (Richman *et al.*, 2002) embryogenesis showed that expression patterns were largely consistent with the tissues affected in OS patients. However, detailed characterisation of *Mid1* expression in craniofacial tissues, particularly during key morphogenetic time points, has not been carried out but is relevant in terms of understanding the possible cellular role(s) of MID1 in lip and palate formation.

As discussed in Chapter One, the development of the vertebrate face is a complex process that begins with the formation of five prominences on the ventral surface of the developing embryo. The prominences are the single frontonasal process

and the paired maxillary and mandibular processes. Following the formation of the nasal pits on the ventral side of the forebrain, subsequent growth of two prominences on the medial and lateral sides of these pits form the medial and lateral nasal prominences. As the medial, lateral and maxillary prominences reach the appropriate size, fusion of these facial primordia is initiated resulting in the formation of the upper lip and primary palate (Nanci, 2003; Sperber, 2001). In order for the fusion to occur, the epithelial layers of these facial primordia need to be in contact with each other and then these epithelial cells subsequently removed to establish the mesenchymal confluence of the upper lip and primary palate. Failure of either the growth and/or fusion of these primordia results in the presentation of cleft lip with or without cleft palate (CLP), one of the prominent features of OS.

It has been shown that signalling from key growth factors such as FGFs, BMPs and SHH is critical for early development of the craniofacial complex, particularly outgrowth and morphogenesis of the facial primordia (reviewed by Cox, 2004). Recent studies by Gong & Guo (2003) revealed that *Bmp4* was expressed in a distinct spatial and temporal manner near and at the site of fusion of the midface. Meanwhile, early evidence of the interaction between *Shh, Mid1* and *Bmp4* has come from an investigation by Granata and Quaderi (2003) who showed that *Mid1* acts upstream of *Bmp4* and plays an important role in mediating the mutual antagonistic interaction between *Shh* and *Bmp4* in patterning of the left/right axis in developing chicken embryos. Such regulatory interactions might not only play a part during the establishment of Henson's node but also be important in regulating the formation of other tissues/structures such as the lip and primary palate. This hypothesis has been investigated further in this study and results presented in this chapter provide some evidence of possible regulatory relationships involving the *MID1* gene.

Further study of *MID1* mutations in X-linked OS patients performed by our laboratory (Cox *et al.*, 2000) have revealed that most mutations produce a truncated protein product, suggesting that loss-of-function of MID1 protein is the mechanism underlying the pathogenesis of OS. Based on these findings, a standard knockout of the murine *Mid1* gene was developed in collaboration with Professor Alan Ashworth, Institute of Cancer Research (ICR), London. The development of this knockout mouse line has provided an excellent stepping-stone to complement the gene expression studies initiated in this research project. Therefore, the results presented and discussed in this chapter were carried out using both wild-type and *Mid1* knockout embryos and provide some important information about the developmental role of *MID1* in affected tissues in OS patients, especially craniofacial primordia.

3.2 Results

3.2.1 *Mid1* developmental expression analysis by *in situ* hybridisation studies

Initially, mRNA *in situ* hybridisation studies using serial sections of wild-type mouse embryos were carried out to characterise in detail the expression pattern of *Mid1* during craniofacial morphogenesis. Two different clones of the *Mid1* coding sequence were used to generate ^{33}P-labelled riboprobes. The 485 bp PCR fragment from the 5'-end encompassing the first coding exon of the gene (corresponding to nucleotides 303-788) was synthesised using the following primers: 5' MID-fusion: GT**GAATTC**CTGAAGATGGAAACACTGGAGTC and HM-MID2: CGATGGCC-TGTAAAGGGCTTC. The other cDNA fragment, the 316 bp PCR fragment corresponding to nucleotides 1812-2128 (covering the region used by Dal Zotto *et al.* (1998)), was synthesised using the following primers: mMIDI-1Ec: GT**GAATTC**GAAACACGAGTGGATCGGGAAG and mMID1-2Ba: GT**GGATC-**

CCTCAAGGTCGCTGCTCCGTAC. Standard PCR amplification was performed using mouse genomic DNA as a template. The resultant cDNA fragments were isolated and cloned into pBluescript KS+ and then linearised with appropriate restriction enzymes to transcribe either sense or antisense ^{33}P-labelled riboprobes. Wild-type mouse embryo tissue sections were prepared and RNA *in situ* hybridisation experiments were performed as described in Chapter Two. The 485 bp riboprobe did not produce any signal whilst the 316 bp riboprobes produced an expression signal as viewed under dark field illumination after 10 days exposure (see below).

These *in situ* hybridisation studies showed that during the development of the craniofacial complex, murine *Mid1* is widely expressed albeit at generally low levels (Figure 3.1). However, at 10.5 dpc, *Mid1* expression is higher in the proliferating neuroepithelial tissues of the telencephalic vesicles and ventricle, in the branchial arches and in the epithelium of the larynx and oropharynx. Other than these tissues, *Mid1* transcripts were also detected strongly in the dorsal root ganglion, as well as in the neural tube.

3.2.2 Generation and characterisation of *Mid1* knockout mice

As previously mentioned, a standard knockout of the murine *Mid1* gene was developed in collaboration with Professor Alan Ashworth, ICR (London). In brief, the generation of these knockout animals involved replacement of the first coding exon of *Mid1* in embryonic stem (ES) cells with a *LacZ* reporter gene such that the reporter would be under the control of the endogenous *Mid1* cis-regulatory elements. These targeted ES cells were then injected into blastocysts and allowed to integrate with other cells of the inner cell mass. The blastocysts were then introduced into pseudopregnant dams. Resultant chimeric animals were bred and offspring harbouring

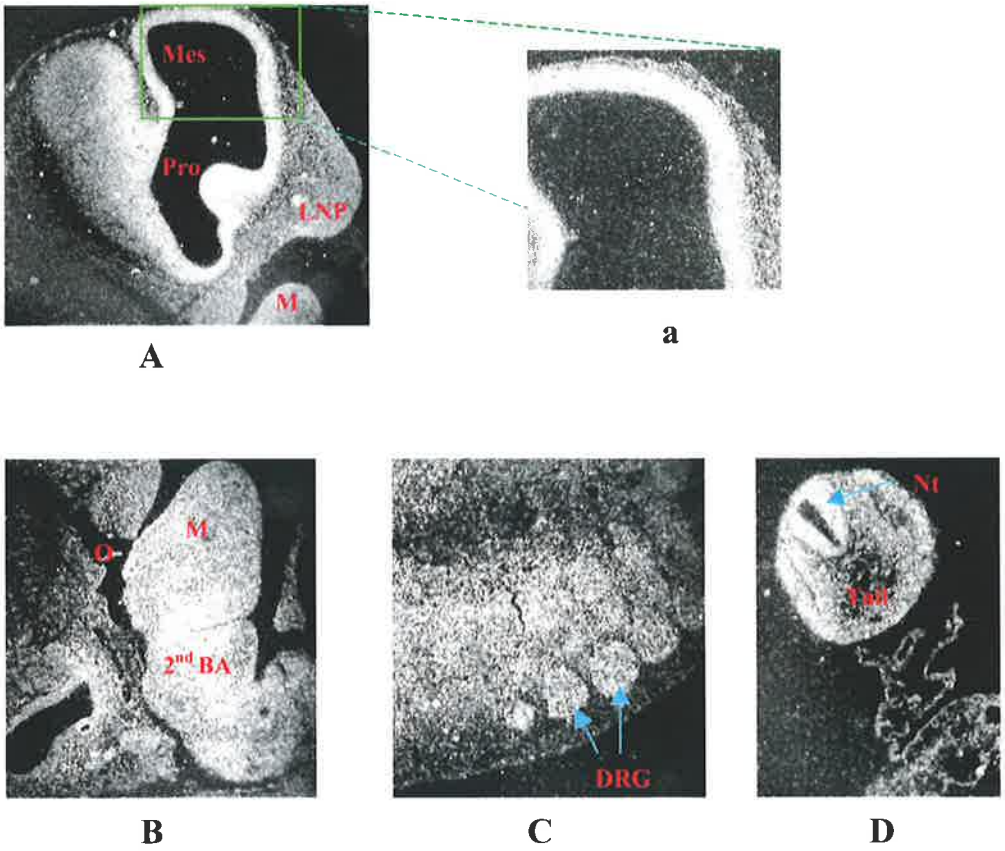

Figure 3.1 *Mid1* expression by *in situ* hybridisation on mouse embryos

Expression pattern detected by *in situ* hybridisation on sagittal sections of 10.5 dpc mouse embryos showing strong *Mid1* expression in the prosencephalon and mesencephalon, and moderate expression in the lateral nasal prominence (A) as well as in the mandibular prominence (A and B). Picture (a) is an enlargement of indicated area in (A) showing localised *Mid1* transcript in the neuroepithelium. *Mid1* expression was also detected in the 2nd branchial arch and in the epithelium of oropharynx (B). Other than in the craniofacial complex, *Mid1* mRNA also showed prominent expression in dorsal root ganglia (C) and neuroepithelium of neural tube (of the tail region) (D). [Pro, Prosencephalon; Mes, mesencephalon; LNP, lateral nasal prominence; M, mandibular process; BA, branchial arch; O, oropharynx; DRG, dorsal root ganglia; Nt, neural tube].

the deleted *Mid1* alleles used as founders in subsequent breeding regimes. Mice heterozygous for the *Mid1* mutant alleles were bred to produce hemizygous and homozygous null-mutant mice. Surprisingly, in the current 129SvJ/MF1 genetic background, these *Mid1* knockout mice do not appear to have any gross external malformations (data not shown), although alterations in facial morphology and other subtle changes are being investigated further by our laboratory. However, modifications made in the construction of the targeted DNA constructs with the replacement of a *LacZ* reporter gene used to generate these knockout mice have enabled the further investigation of the expression pattern of *Mid1* gene during early embryogenesis by staining embryos for β-galactosidase activity (see next section).

3.2.3 *Mid1* developmental expression analysis by *LacZ* staining

3.2.3.1 Mid1 expression during early mouse embryogenesis

By staining for β-galactosidase activity (*LacZ* staining), identification of the embryonic sites of *Mid1* expression could be achieved with greater sensitivity than by *in situ* hybridisation. This was deemed to be important, and a more robust method of analysis given the low expression of the *Mid1* gene. In addition to whole-mount *LacZ* staining, some of these *LacZ* stained embryos were embedded in paraffin wax and sectioned at 8-10 μm. These sections were then counterstained with eosin.

Whole-mount *LacZ* staining of these *Mid1* knockout mouse embryos from day 9.5 post-coitum (dpc) to 11.5 dpc revealed a localised expression pattern of *Mid1* in various tissues with a very distinct profile of expression pattern detected in the craniofacial region (Figure 3.2). *Mid1* expression was noted throughout the epithelia (ectoderm) of the mandibular and maxillary processes, medial and lateral nasal prominences, as well as the frontonasal prominences (Figures 3.2 and 3.3). A closer

Figure 3.2 *Mid1* expression by *LacZ* staining on mouse embryos

Whole-mount *LacZ* staining of β-galactosidase activity of *Mid1* knockout mouse embryos. (A) Expression pattern detected in 9.5 dpc mouse embryo showing prominent *Mid1* expression in the developing neural tube with localised expression in the otic pit and olfactory placode. Lower levels of *Mid1* expression were also present in the mandibular component of first branchial arch at this stage of development. At (B) 10.0 dpc and (D) 10.5 dpc, localised expression can be detected in the craniofacial region (mandibular and maxillary processes, as well as medial and lateral nasal prominences), developing heart and urogenital tissues. The facial expression appears to be predominantly in the ectoderm although mesodermal expression in the mandibular processes is also evident. (C) Sagittal section through a 10.0 dpc embryo showing localised expression in specific tissues including neuroepithelial tissues (arrowhead). (E) Expression in the craniofacial region remains strong at 11.5 dpc. No expression is evident in either forelimb or hindlimb (D and E). [Ot, otic pit; Op, olfactory placode; Tv, telencephalic vesicle; LNP, lateral nasal prominence; Mx, maxillary process; M, mandibular process; BA, branchial arch; Nt, neural tube; H, heart; U, urogenital; FL, forelimb; HL, hindlimb].

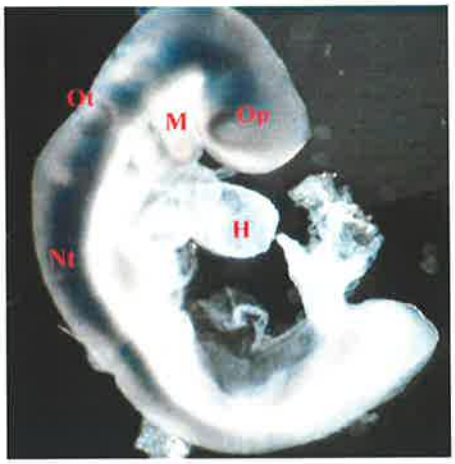

A

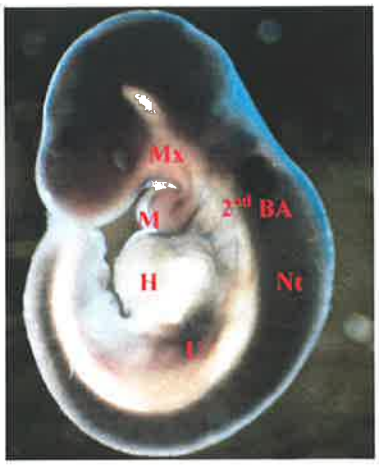

B

C

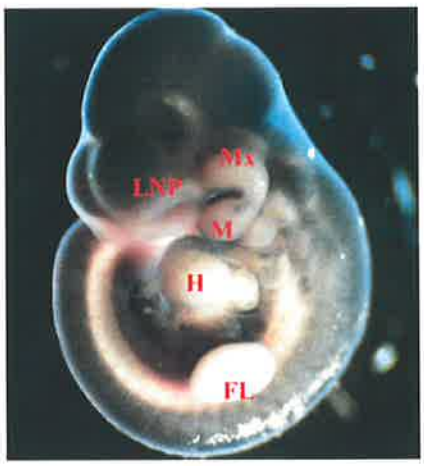

D

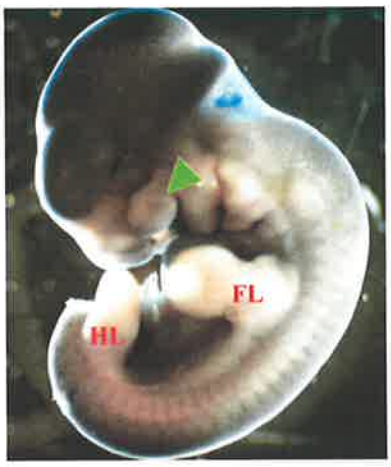

E

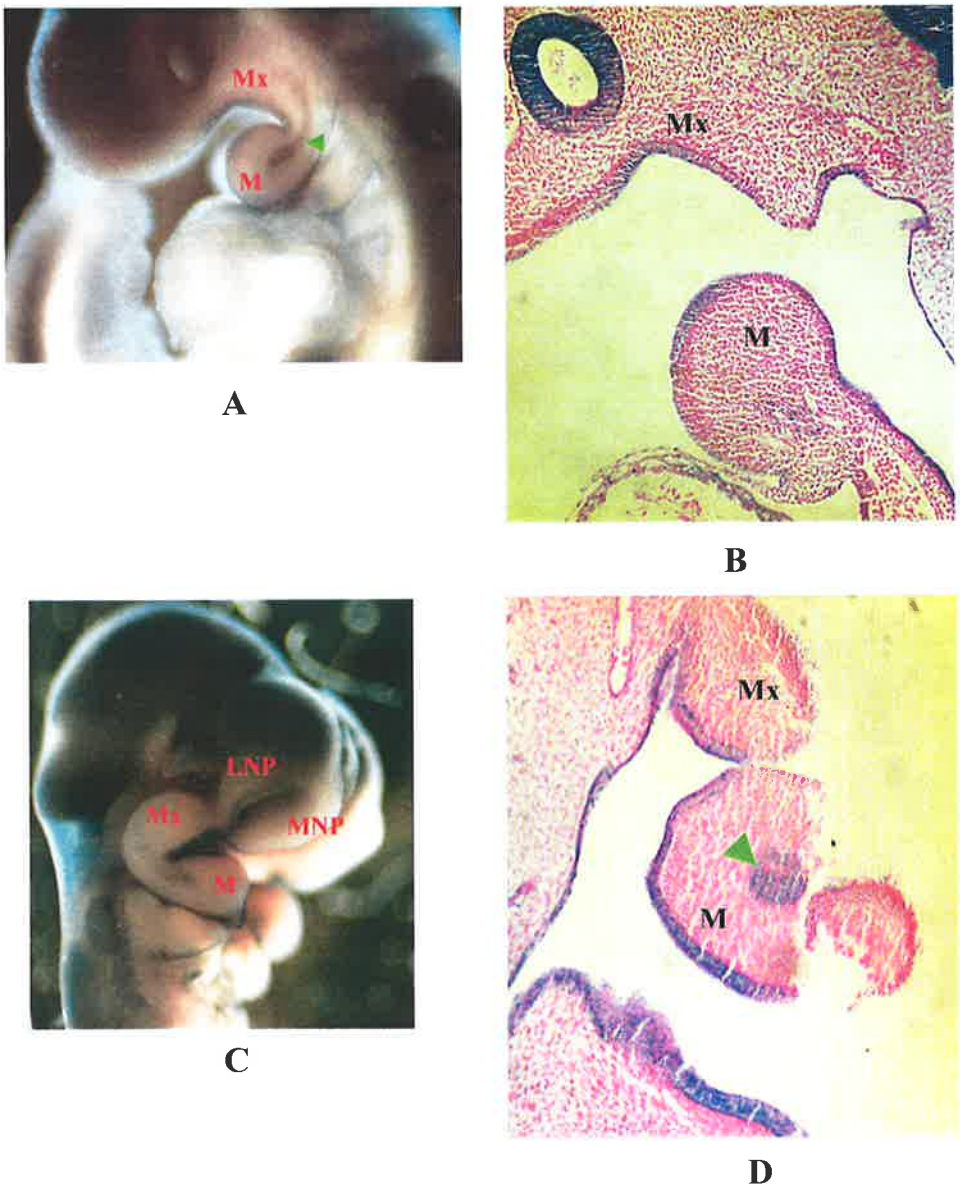

Figure 3.3 *Mid1* expression in the craniofacial complex

Closer views of the developing face of *Mid1* knockout embryos at (A) 10.0 dpc and (C) 10.5 dpc clearly show *Mid1* expression in the epithelial cells lining the facial prominences and mesodermal core (arrowheads in A and D). (B) and (D) are sagittal sections through 10.0 dpc and 10.5 dpc embryos, showing the precise site of *Mid1* expression during outgrowth of the facial prominences. [MNP, medial nasal prominence; LNP, lateral nasal prominence; M, mandibular process; Mx, maxillary process].

view of the developing face at 10.5 dpc, prior to fusion of midfacial prominences, clearly showed localised expression of *Mid1*, near and at the site where the fusion of facial prominences takes place (Figure 3.3) (further details in the next section).

Apart from the craniofacial region, *Mid1* was also dynamically expressed in cardiac tissue throughout morphogenesis of the heart (Figure 3.4). Initially, expression was detected in dorsal aspects of the early heart at 10.5 dpc, with expression at 11.5 dpc in the outflow tract of the heart. Changes in expression were noted by 12.5 dpc, with more prominent expression in the ventricles of the heart. *Mid1* expression was also detected in the urogenital region, with very high levels of expression found in the developing neural tube (Figure 3.2).

3.2.3.2 *Expression of Mid1 during fusion of facial primordia to form lip and primary palate*

As highlighted above, a very distinct pattern of *Mid1* expression has been detected in the craniofacial tissues using whole-mount *LacZ* staining of *Mid1* knockout mouse embryos. These localised expression patterns during the outgrowth of facial primordia, prior to fusion, was maintained to later stages at 11.0 dpc, where the three facial primordia (maxillary, lateral and medial nasal prominences) approach to one another (Figure 3.5A). This expression remained strong at 11.5 dpc, right at the time that these midfacial prominences eventually make contact and undergo fusion to form the upper lip and primary palate (Figure 3.5B-D). At this stage, fusion of the lateral and medial nasal prominences can be observed at the anterior aspect of the nasal pit (Figure 3.5D, hatch). *Mid1* expression was apparent in the epithelial layers of the lateral nasal process and medial nasal process flanking the nasal pit (Figure 3.6A and 3.6B). In the most posterior region of nasal pit, where a confluent mesenchymal bridge has been achieved, the expression of *Mid1* remains strong in the ectodermal

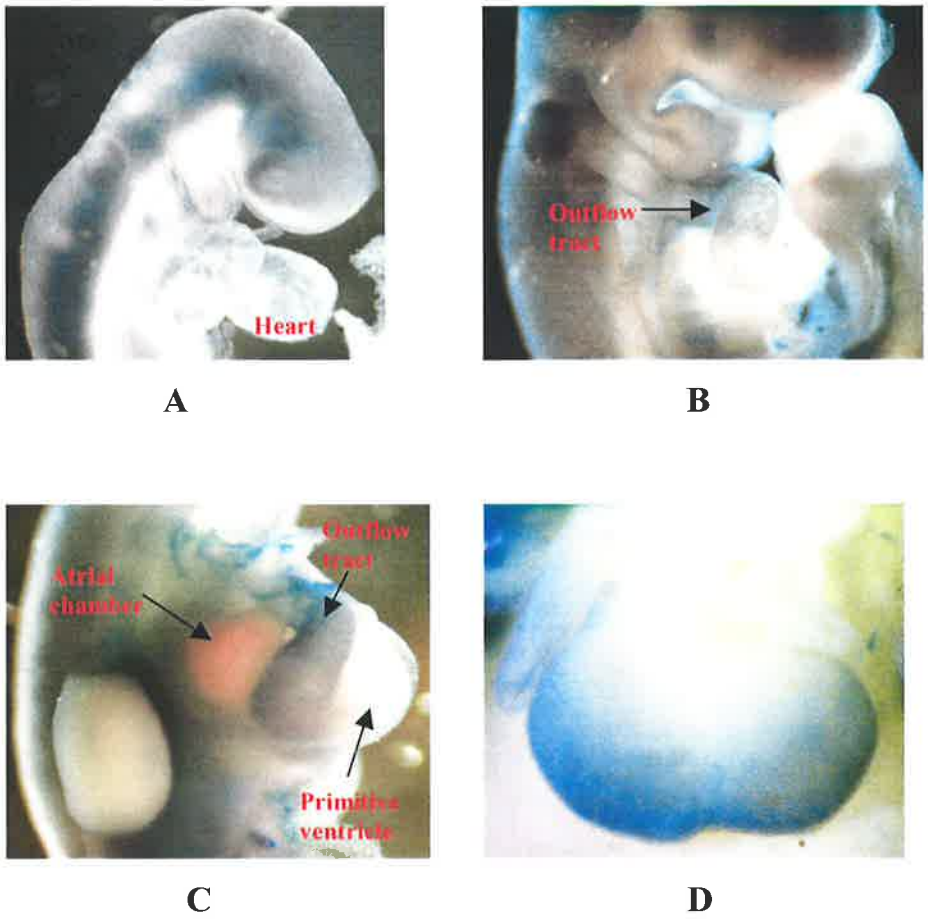

Figure 3.4 *Mid1* expression in the developing heart

Expression of *Mid1* in the developing heart as shown by *LacZ* staining. (A) Although expression could not be detected at 9.5 dpc in any part of the heart, at (B) 10.0 dpc and (C) 10.5 dpc, expression was evident in the dorsal aspect of the developing heart. (D) By 12.5 dpc there was more prominent expression in the ventricles.

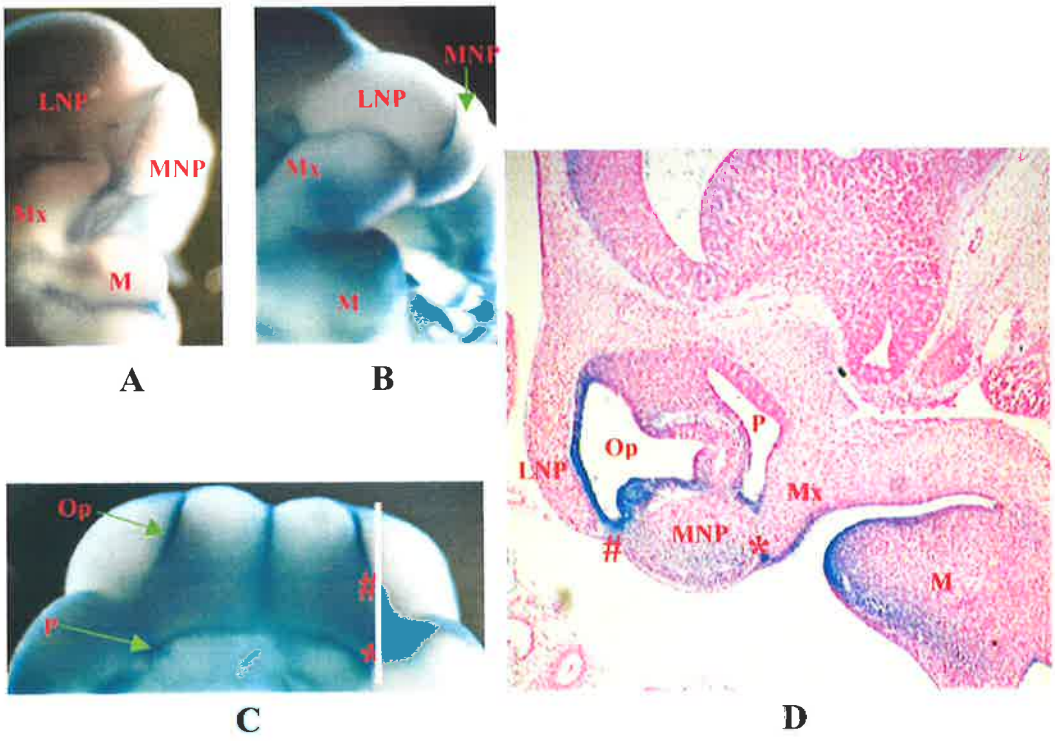

Figure 3.5 Expression of *Mid1* at the putative site of fusion of facial primordia

Lateral view of developing face of (A) 11.0 dpc and (B) 11.5 dpc mouse embryos where fusion of facial primordia occurs to form the lip and primary palate. *Mid1* is expressed at the putative site of fusion of three facial processes, Mx, MNP and LNP. (C) Ventral view of 11.5 dpc face (as viewed from underneath) showing the site of fusion, which is more clearly shown in sagittal section in (D). The site of the section is depicted by a vertical white line in (C). Fusion between the LNP and MNP (denoted by #) occurs around the olfactory pit (Op). Meanwhile, fusion between MNP and Mx (denoted by *) occurs underneath the enclosing pit (primitive posterior naris) that will then become the definitive choana after the formation of the palate. [LNP, lateral nasal prominence; MNP, medial nasal prominence; Mx, maxillary process; M, mandibular process; P, pit; Op, olfactory pit].

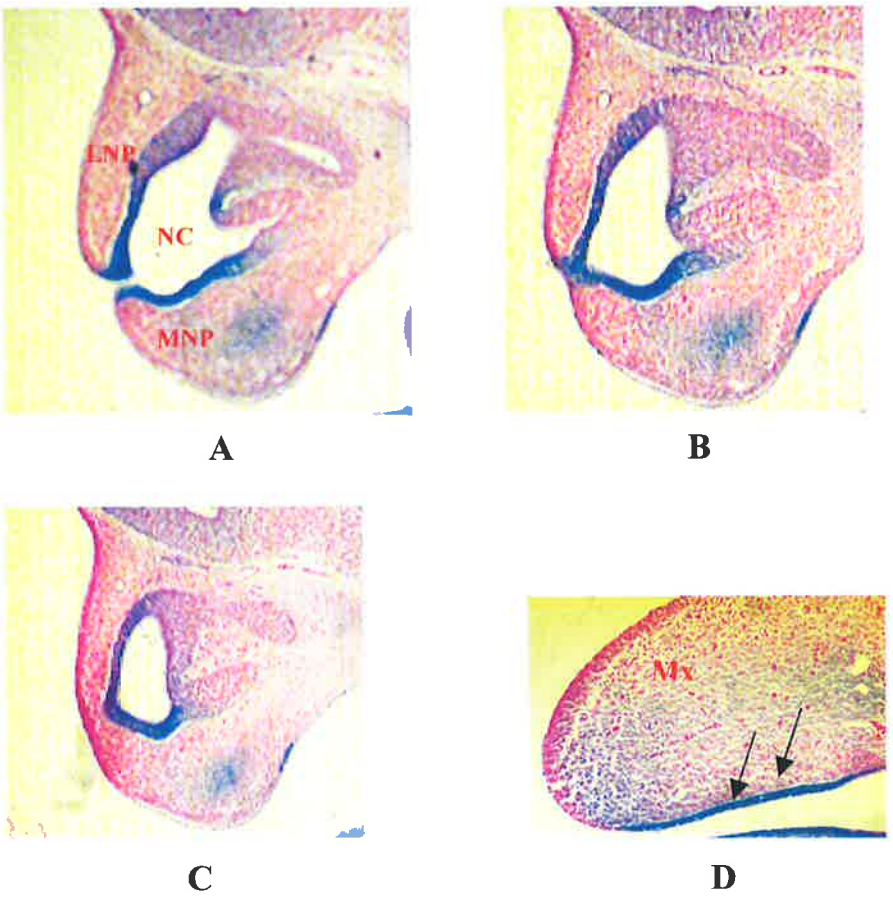

Figure 3.6 Expression of *Mid1* during fusion of medial and lateral nasal prominences

(A-C) Sagittal sections through the nasal pit region of 11.5 dpc *Mid1* knockout embryos showing localised staining of β-galactosidase in the ectodermal layer of nasal cavity. (D) Distribution of *Mid1* in the maxillary process is apparent in mesenchyme although ectodermal expression remained strong at the area of the maxillary contribution to the primary palate (arrows). [LNP, lateral nasal prominence; MNP, medial nasal prominence; Mx, maxillary process].

layer lining the nasal cavity (Figure 3.6C). *Mid1* was also noted to be expressed at the site of fusion between maxillary and medial nasal process that form the primary palate (Figure 3.5D, asterisk).

In the older embryos i.e. at 12.0 dpc, after fusion was completed and the midface had developed, some *Mid1* expression was detected in the mesenchyme of the upper lip although the expression in the ectodermal layer of the nasal cavity and nasal septum could still be seen (Figure 3.7). After the formation of the lip and primary palate was completed, outgrowth and fusion of the palatal shelves occurred to form the secondary palate. *Mid1* was also noted to be expressed in the medial edge epithelia of the palatal shelves (Figure 3.8, arrowheads).

3.2.4 Regulatory relationships between *Mid1* and other molecules involved in craniofacial morphogenesis

To investigate further the existence of a regulatory relationship between *Mid1, Shh* and *Bmp4* as suggested earlier (Granata & Quaderi, 2003), *Mid1* knockout embryos were used to assess the expression of these genes in tissues lacking Mid1 compared with wild-type embryos. Digoxigenin riboprobes were prepared by linearising *Shh* (gift of Rathjen Group, University of Adelaide) and *Bmp4* (obtained from Ms S. Donati, Cox Laboratory) cDNA plasmid clones followed by *in vitro* transcription. Whole-mount *in situ* hybridisation and immunostaining were performed using standard techniques as described in Chapter Two.

Whole-mount *in situ* hybridisation of *Bmp4* showed a similar pattern of expression for both *Mid1* knockout and wild-type mouse embryos (Figure 3.9). Similarly, no obvious differences were observed for the expression pattern of *Shh* transcripts in both types of embryos tested (Figure 3.10).

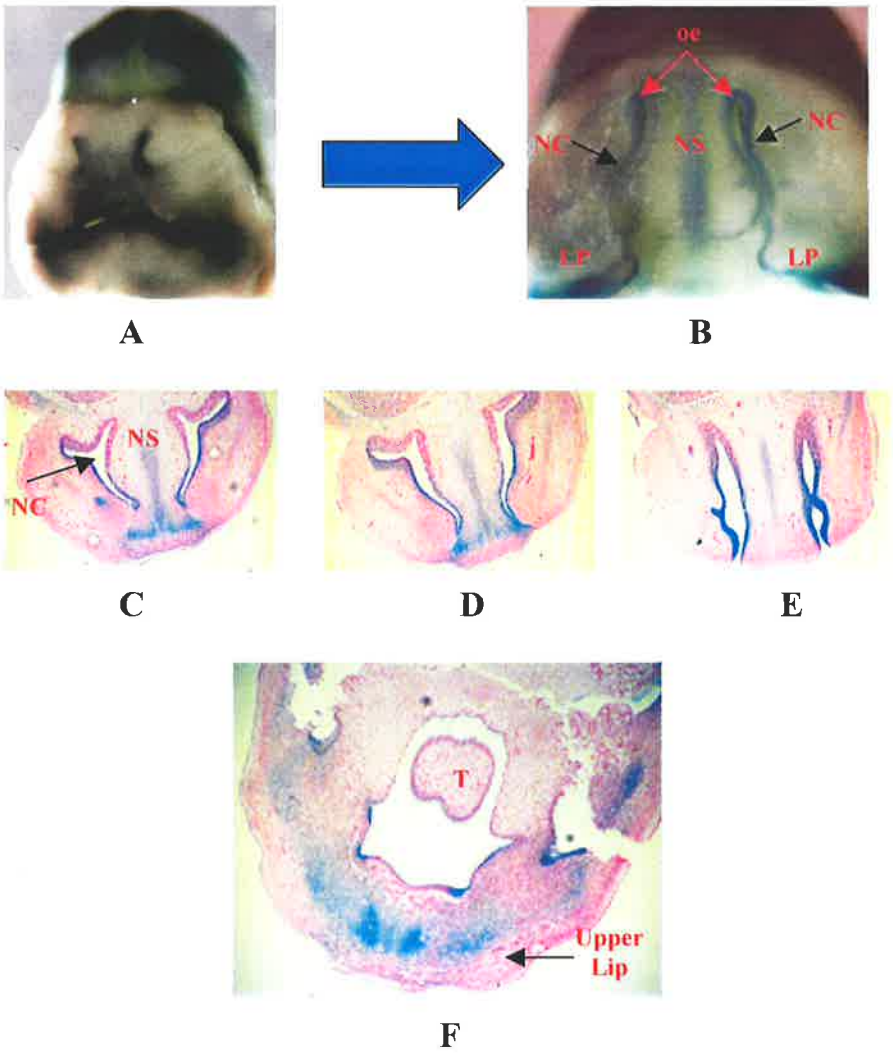

Figure 3.7 Expression of *Mid1* in facial tissues after fusion of facial primordia

(A) Frontal view of 12.0 dpc *Mid1* knockout mouse post-fusion face. Cross-section through the face revealing β-galactosidase staining in the olfactory epithelium (B). (C-E) Frontal sections showing *Mid1* expression around the nasal cavity including the nasal septum. At this stage, some β-galactosidase staining can be detected in the mesenchyme of the upper lip (F). [NC, nasal cavity; NS, nasal septum; LP, lateral palatine process; T, tongue; oe, olfactory epithelium].

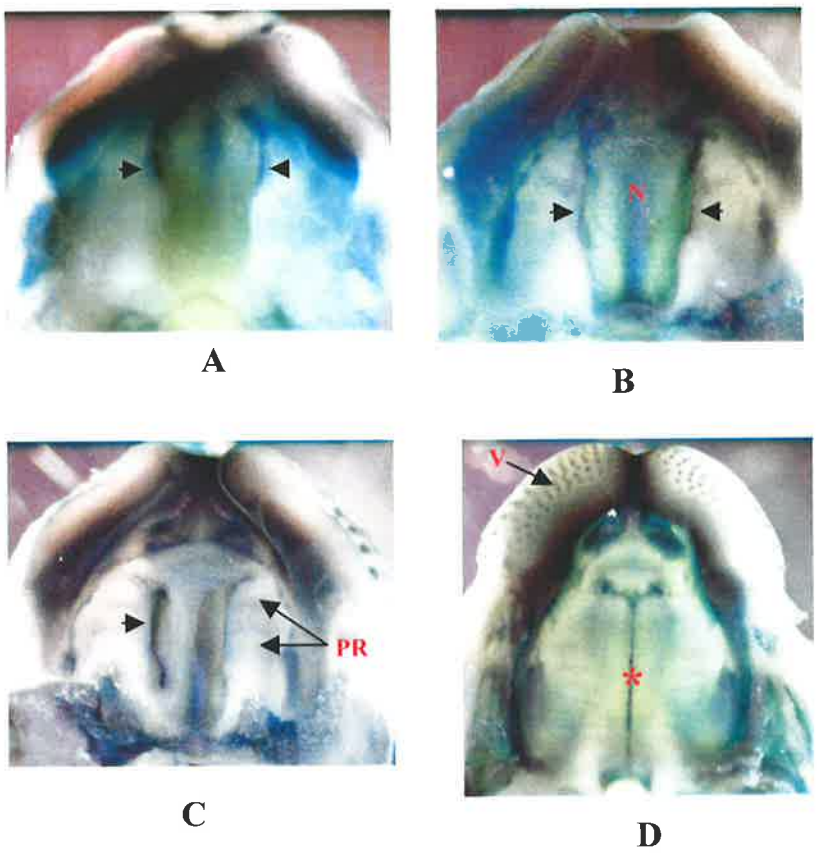

Figure 3.8 Expression of *Mid1* in the developing secondary palate

Mid1 is expressed in the palatal shelves (small arrows) throughout outgrowth and fusion of the secondary palate at (A) 12.5 dpc, (B) 13.5 dpc, (C) 14.5 dpc and (D) 15.5 dpc. Asterisk in (D) shows an initial site of apposition and subsequent fusion of the palatal shelves. [PR, prominent rugae; V, vibrissae; N, roof of the primitive nasopharynx].

Figure 3.9 Expression of *Bmp4* on *Mid1* knockout and wild-type mouse embryos

Whole-mount *in situ* hybridisation of 11.5 dpc (A-C) and 10.5 dpc (D and E) of *Mid1* knockout (A-E) and wild-type (A'-E') mouse embryos. The expression pattern of *Bmp4* transcripts in both *Mid1* knockout and wild-type embryos in all tissues was similar. [LNP, lateral nasal prominence; Mx, maxillary process; M, mandibular process; FL, forelimb; HL, hindlimb].

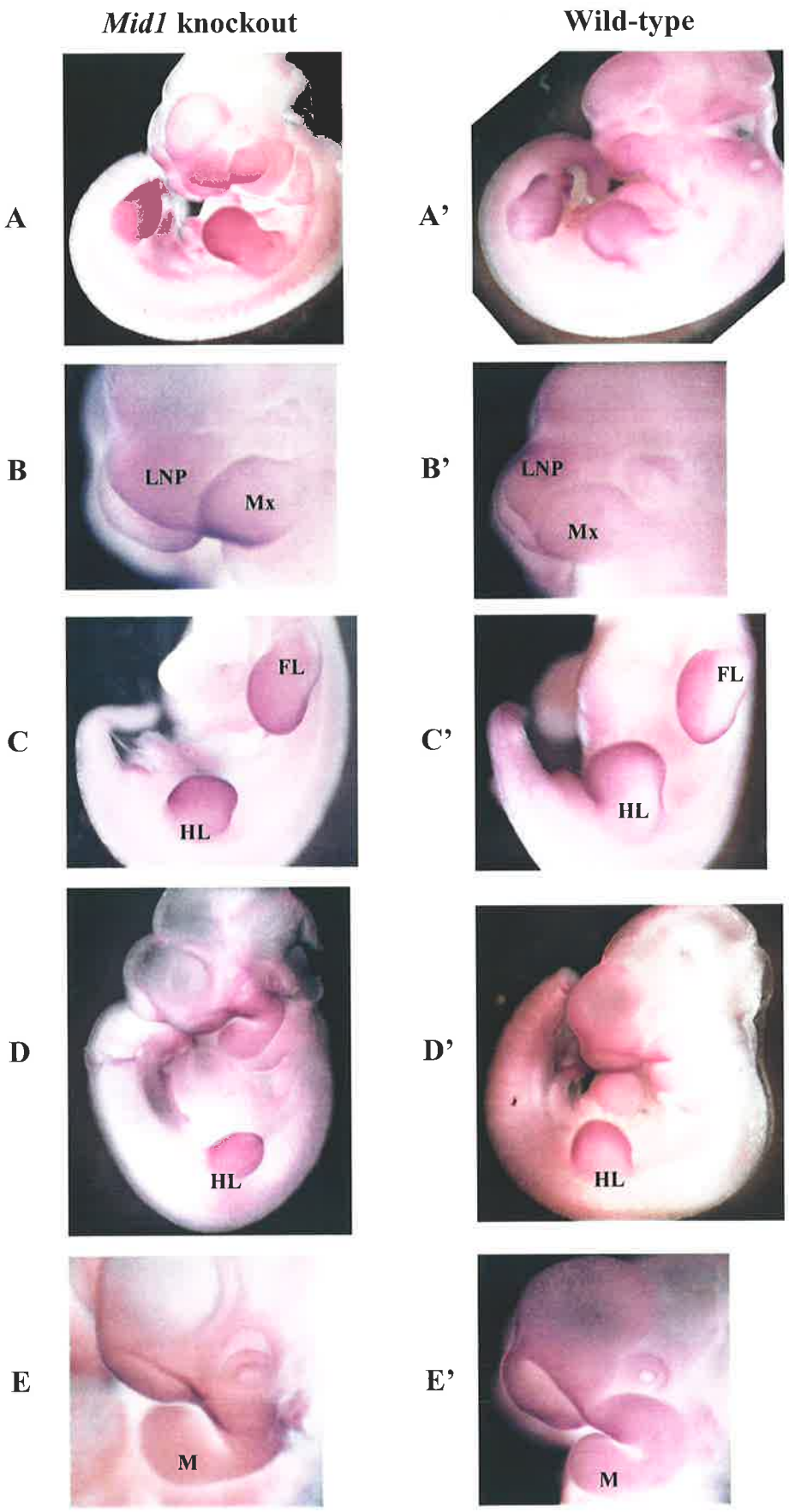
Mid1 knockout
Wild-type
A
A'
B
B'
LNP
Mx
LNP
Mx
C
C'
FL
HL
FL
HL
D
D'
HL
HL
E
E'
M
M

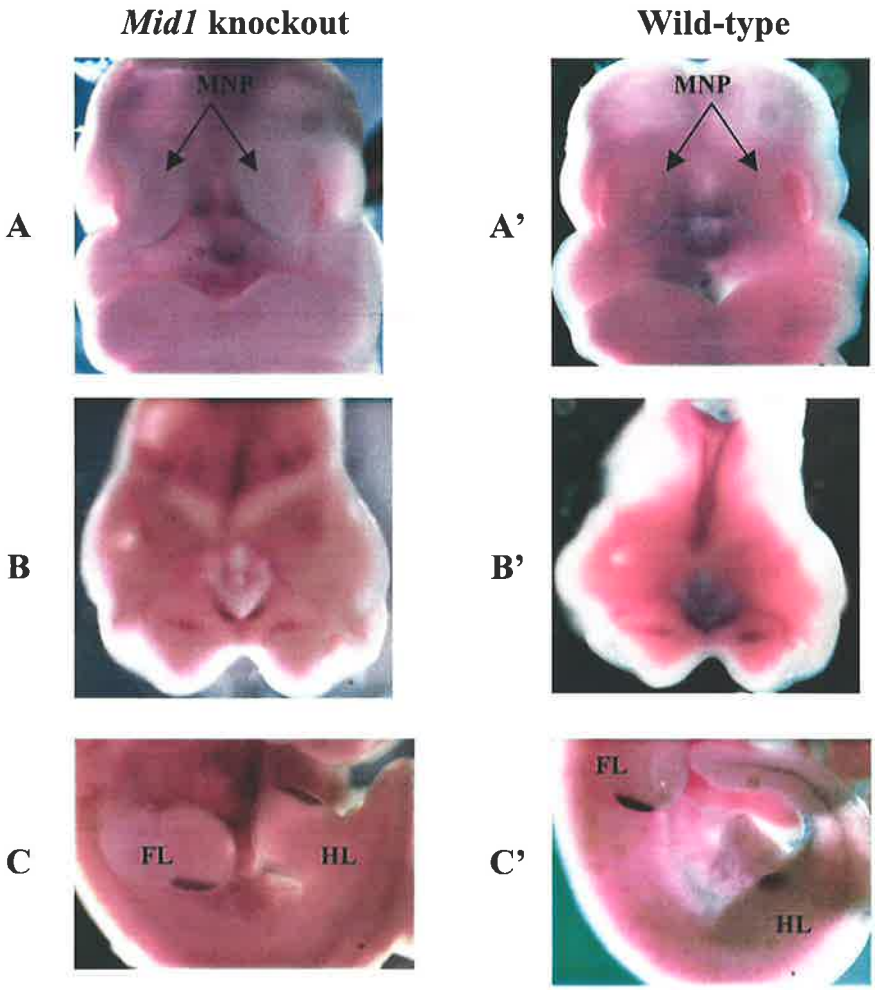

Figure 3.10 Expression of *Shh* on *Mid1* knockout and wild-type mouse embryos

Whole-mount *in situ* hybridisation on 10.5 dpc of *Mid1* knockout (A-C) and wild-type (A'-C') mouse embryos. The expression patterns of *Shh* transcripts for both *Mid1* knockout and wild-type embryos showed no obvious differences. [MNP, medial nasal prominence; FL, forelimb; HL, hindlimb].

To further investigate this putative regulatory relationship, homozygous *Mid1* knockout females were crossed with heterozygous *extra-toes* $Gli3^{XtJ}$ mouse mutant males to produce double $Mid1^{-}/Gli3^{XtJ}$ heterozygotes and $Mid1^{-}/Gli3^{wt}$ mice. The zinc finger transcription factor, Gli3, is recognised as a major downstream regulator of Shh signalling. Due to the time constrains, only a handful of embryos from these crosses were obtained and independent of information regarding genotype, all embryos were stained for β-galactosidase activity as previously described. With the exception of the limbs, no obvious differences were observed in the pattern of β-galactosidase for both *Mid1* knockout and embryos from the above crosses. In the limb, roughly half of the embryos displayed β-galactosidase activity in the apical ectodermal ridge (AER) (Figure 3.11), a site not normally expressing *Mid1*. This proportion of embryos showing altered expression is consistent with the expected Mendelian ratio of $Gli3^{XtJ}$ heterozygote embryos.

3.3 Discussion

In order to understand the role of *MID1* during embryonic development, expression studies of this gene have been carried out in many different species. Initial whole-mount expression studies performed by Quaderi *et al.* (1997) reported that, although ubiquitously expressed during early mouse embryogenesis (9.0 dpc – 10.5 dpc), *Mid1* transcription was higher within the frontonasal processes, the branchial arches and the central nervous system (CNS). Following these whole-mount expression studies, Dal Zotto *et al.* (1998) conducted *in situ* hybridisation studies on tissue sections at later stages of development (12.5 dpc – 16.5 dpc) and reported that *Mid1* expression was high, particularly in undifferentiated cells in the central nervous, gastrointestinal and urogenital systems during mouse development although

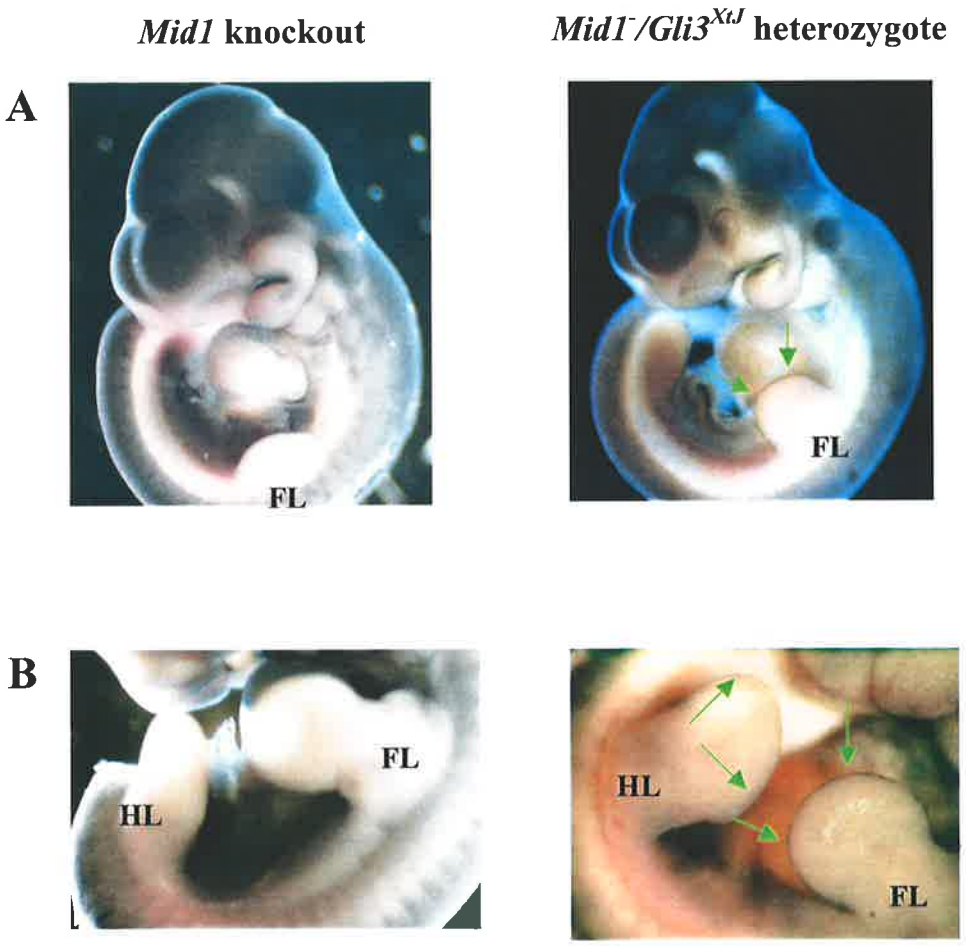

Figure 3.11 *Mid1* expression in *Mid1* knockout and presumed *Mid1*⁻ /*Gli3*$^{Xt J}$ heterozygous embryos

Staining of β-galactosidase in (A) 10.5 and (B) 11.5 dpc of the *Mid1* knockout and presumed *Mid1*⁻/*Gli3*$^{Xt J}$ heterozygote embryos clearly show *Mid1* expression in the apical ectodermal ridge (AER) of the limbs (arrows). [FL: forelimb; HL: hindlimb].

expression was reportedly not detected in the heart. Apart from these studies, detailed characterisation of *Mid1* during craniofacial morphogenesis has received little attention. The *Mid1* expression data presented in this chapter emphasise the importance of *Mid1* during craniofacial morphogenesis, as it was widely transcribed during outgrowth of facial prominences. During the course of this project, other investigators have reported *Mid1* expression studies in the chick (Richman *et al.*, 2002) and also in humans (Pinson *et al.*, 2004). Interestingly, *MID1/Mid1* expression reported in these two species was more localised compared to the expression pattern detected in the mouse, suggesting perhaps different regulation and levels of expression of this gene in these species. In summary, *in situ* hybridisation studies carried out in this investigation and by others have shown that the highly conserved *MID1/Mid1* is expressed widely throughout embryogenesis, although at varying levels depending on the tissue and cell type. In part, this variability could be attributed to the presence of an endogenous retrovirus in the human *MID1* promoter (Landry *et al.*, 2002) and the fact that the mouse *Mid1* gene (compared with human) spans the pseudoautosomal boundary, escaping X-inactivation and possessing duplications (i.e. repetitive sequences) of its 3' end (Dal Zotto *et al.*, 1998).

As previously mentioned, a standard knockout of the murine *Mid1* gene was developed mainly to delineate the functional roles of Mid1 in a mouse model. The approach adopted was based on genotype-phenotype assessments of OS patients that indicated that the OS phenotype results from a loss-of-function of MID1 (Cox *et al.*, 2000). However, these mice do not show any highly penetrant external malformations, as seen in OS patients. The most plausible explanation for this is the possibility of a level of functional redundancy between Mid1 and its homologue, Mid2, in this species where the two genes share high sequence identity and are

expressed in most of the same tissues (Buchner *et al.*, 1999) (see below). The 129SvJ/MF1 genetic background may also be a contributing factor. Furthermore, the absence of obvious craniofacial malformation, particularly facial clefting, was not entirely unexpected considering that development of uni-/bi-lateral clefts of the primary palate is rare in mice, in part due to the extended period of growth of the embryonic facial tissues associated with the formation of the elongated snout and the inbred nature of the strains used (Cox, 2004). With respect to possible non-facial OS-related anomalies, defects of the external genitalia in mice, such as hypospadias, need to be assessed by scanning electron microscopy (SEM) (Yamada *et al.*, 2003). The external genitalia and the heart of these knockout animals are being investigated further by our laboratory as part of ongoing research undertaken to delineate the developmental role of *MID1* in these organs.

The use of a *LacZ* reporter gene in the gene targeting construct for the development of the *Mid1* knockout mice, as mentioned earlier in this chapter, provided an opportunity to further investigate the profile of expression of *Mid1* by staining for β-galactosidase activity in knockout embryos. The results presented in this chapter clearly show localised expression of *Mid1* by *LacZ* staining, that differs in some aspects to the expression profile provided by *in situ* hybridisation studies. Possibility of a longer half-life and stability of β-galactosidase as to *Mid1* mRNA were taken into consideration in their correlation of the spatial and temporal expression pattern. Nevertheless, the data presented here demonstrate that murine *Mid1,* like in chick and humans, is expressed in specific tissues during craniofacial morphogenesis. Most notably, highest levels of *Mid1* expression were found in the epithelia of the facial prominences prior to and around the time of fusion of the

primary palate, suggesting a likely important function of this gene in regulating this complex morphogenetic event.

Apart from the craniofacial region, *Mid1* mRNA expression studies showed expression of this gene in the developing heart in both human and chick (Pinson *et al.*, 2004; Richman *et al.*, 2002), but supposedly not in the mouse (Dal Zotto *et al.*, 1998). The use of whole embryo staining for β-galactosidase activity in *Mid1* knockout mouse embryos, however, has indicated that murine *Mid1* is expressed during heart development and in a dynamic fashion albeit at low levels relative to other tissues. Interestingly, at 10.5 dpc, *Mid1* is expressed in the dorsal aspects of the heart tube, consistent with the timing of cushion and outflow tract development. The cardiac defects seen in OS patients arise as a result of perturbation in the morphogenesis or remodelling of these early structures suggesting the expression data are *bona fide*. Also consistent with the chick and human studies is the prominent levels of *Mid1* expression in the developing neural tube. This is interesting given that only a low incidence of neurological problems have been reported in OS patients (So *et al.*, 2005).

The profile of gene expression of *MID1/Mid1* during early embryogenesis has raised the question of how MID1 contributes to the development of organs lying in the ventral midline of the body and how loss-of-function of this protein leads to the highly characteristic OS phenotype. Identification of the genetic pathways in which MID1 is involved and the cellular mechanisms governed by them is a crucial step in answering this question. As the findings of Granata and Quaderi (2003) suggested a regulatory relationship between MID1, SHH and BMP4 in the early events determining left/right asymmetry, expression patterns of both *Shh* and *Bmp4* were investigated in the tissues deficient in Mid1. The results presented here however

showed no clear differences in the expression patterns of both *Shh* and *Bmp4* mRNAs in *Mid1* knockout and wild-type embryos. These results can be interpreted and supported by arguments of redundant mechanisms substituting MID1 function in the majority of tissues by its protein homologue, MID2. Interestingly, very recent data (Granata *et al.*, 2005) revealed that the alterations of *Shh* and *Bmp4* ectopic expression in the previous report were a result of 'accidently' knocking down both *Mid1* and *Mid2* using an antisense Mid1 morpholino that bound to both MID sequences. These researchers showed that MID2 is able to compensate for an absence in MID1 during chick left/right determination and this capability may explain the observation of normal *Shh* and *Bmp4* expression in the *Mid1*-deficent tissues reported in this thesis. In addition, it might also explain of why our *Mid1* targeted knockout lines did not display any gross facial malformations. Our laboratory is now in the process of addressing this issue by breeding the *Mid1* knockout mice into different genetic background as well as initiating the production of a *Mid1/Mid2* double knockout mouse strain (this will be discussed in the last chapter of this thesis).

Further investigation of a regulatory relationship involving *Mid1* was pursued in this study by crossing homozygous *Mid1* knockout mice with mice heterozygous for the transcription factor Gli3 (known as *extra-toes* or $Gli3^{Xt\!J}$). X-gal staining of the embryos from this cross showed ectopic *Mid1* expression in the apical ectodermal ridge (AER) of limbs in around half the embryos, the presumed $Mid1^{-}/Gli3^{Xt\!J}$ heterozygotes. Although these embryos were not genotyped, endogenous *Mid1* expression has never been reported in the AER and so this suggests that *Mid1* is derepressed by the *extra-toes* mutation. This derepression must however be indirect as *Gli3* is only expressed in limb mesoderm (Schweitzer *et al.*, 2000) while the ectopic expression of *Mid1* is restricted to the ectoderm (AER). Notably, *Bmp4* is also

strongly expressed in the AER, although also in mesoderm subjacent to the ectoderm. This result is interesting considering only a handful of other genes, e.g. *Shh* itself, have been noted to be changed in *Gli3* heterozygotes; the expression of most genes e.g. *Bmp4* and *Fgf8,* being altered only in homozygous *Gli3* embryos. These data support the notion of the regulatory relationship between Shh, Mid1 and Bmp4 in tissues outside the early gastrulating chick embryo although confirmation of this in developing facial tissue will await assessment of *Mid1* (β-galactosidase) expression in homozygous $Gli3^{XtJ}$ embryos.

Chapter Four: Investigation into the functional relationship between MID1 and MID2

4.1 Introduction

One of the intriguing observations among patients with X-linked Opitz GBBB syndrome (OS) is the clinical variability in presentation even among male patients from the same family, i.e. those sharing identical hemizygous *MID1* mutations (Cox *et al.*, 2000). This marked phenotypic variability of the OS phenotype could be due to a number of factors including epigenetic phenomena, the influence of the *in utero* environment, or a level of functional redundancy with the homologous MID2 protein.

Support for the notion of some degree of functional redundancy between MID1 and MID2 in tissues where their expression domains overlap is provided by numerous data from different groups. Studies into MID function show that both MID1 and MID2 are microtubule-associated proteins (Buchner *et al.*, 1999; Perry *et al.*, 1999) and able to bind Alpha 4 (α4), a regulatory subunit of PP2-type phosphatases (Short *et al.*, 2002; Trockenbacher *et al.*, 2001). This similarity in expression and function suggests that natural variation in *MID2* expression or activity may account for some of the intrafamilial variability in clinical presentation of OS. In addition, Granata and colleagues (2005) have recently provided the first evidence from studies of MID function during early gastrulation in the chick, that the two proteins do have at least partially redundant roles *in vivo*.

Investigation of the tissue-specific expression of both MID1 and MID2 is somewhat hampered by their high level of identity both at the nucleotide and protein levels. Remaining somewhat unresolved is the difficulty in reliably distinguishing between *MID1* and *MID2* based on their expression profile during early embryogenesis. As achieving reproducible RNA *in situ* hybridisation data using

probes outside the homology regions of these two genes has proven difficult, the possibility of using MID1- and MID2-specific antibodies in immunocytochemistry was considered a feasible approach and one that would provide valuable tools for ongoing studies. Therefore, this chapter reports attempts to produce MID1- and MID2-specific antibodies, their characterisation and subsequent investigations with the aim of ultimately addressing the role of functional redundancy between these two proteins homologues in different tissues with the developing embryo.

4.2 Results

4.2.1 Preparation and production of MID1- and MID2-specific antibodies

4.2.1.1 Selection of peptides for raising anti-peptide sera

The *MID1* homologue, *MID2,* was initially identified after sequence similarity searches of the EST databases using the *hMID1* cDNA sequence (Perry *et al.*, 1999). Similar to *MID1*, *MID2* also maps to the X-chromosome but to the long arm at band Xq22 (compared to *MID1* at Xp22). MID1 and MID2 protein sequences show very high similarity overall (77% identity and 92% similarity) and display an identical structural organisation (Figure 4.1).

For the selection of MID1 and MID2 peptides for use in raising anti-peptide sera, both protein sequences were analysed by two independent custom anti-peptide antibody suppliers: Auspep Pty. Ltd. (Victoria, Australia) and Alpha Diagnostic International (San Antonio, USA) in order to provide the best advice as to the choice of antigenic peptides. Peptides from the N-terminus of MID1 corresponding to residues 96-109, SPSETRRERAFDAN, and the N-terminus of MID2 corresponding to residues 96-108, SPSESRRERTYRP, were selected based on guided assessments (Figure 4.2). Each peptide was synthesised with an extra cysteine residue added to the

(A)

```
hMID1     (1) METLESELTCPICLELFEDPLLLPCAHSLCFNCAHRILVSHCATNESVESITAFQCPTCR
mMid1     (1) METLESELTCPICLELFEDPLLLPCAHSLCFNCAHRILVSHCATNEPVESINAFQCPTCR
hMID2     (1) METLESELTCPICLELFEDPLLLPCAHSLCFSCAHRILVSSCSSGESIEPITAFQCPTCR
mMid2     (1) METLESELTCPICLELFEDPLLLPCAHSLCFSCAHRILVSSCSSGESIEPITAFQCPTCR

hMID1    (61) HVITLSQRGLDGLKRNVTLQNIIDRFQKASVSGPNSPSETRRERAFDANTMTSAEKVLCQ
mMid1    (61) HVITLSQRGLDGLKRNVTLQNIIDRFQKASVSGPNSPSETRRERAFDANTMSSAEKVLCQ
hMID2    (61) YVISLNHRGLDGLKRNVTLQNIIDRFQKASVSGPNSPSESRRERTYRPTTAMSSERIACQ
mMid2    (61) YVISLNHRGLDGLKRNVTLQNIIDRFQKASVSGPNSPSESRRERTYRPSSAMSSERIACQ

hMID1   (121) FCDQDPAQDAVKTCVTCEVSYCDECLKATHPNKKPFTGHRLIEPIPDSHIRGLMCLEHED
mMid1   (121) FCDQDPAQDAVKTCVTCEVSYCDECLKATHPNKKPFTGHRLIEPIPDSHIRGLMCLEHED
hMID2   (121) FCEQDPPRDAVKTCITCEVSYCDRCLRATHPNKKPFTSHRLVEPVPDTHLRGITCLDHEN
mMid2   (121) FCEQDPPRDAVKTCITCEVSYCDRCLRATHPNKKPFTSHRLVEPVSDTHLRGITCLDHEN

hMID1   (181) EKVNMYCVTDDQLICALCKLVGRHRDHQVAALSERYDKLKQNLESNLTNLIKRNTELETL
mMid1   (181) EKVNMYCVTDDQLICALCKLVGRHRDHQVAALSERYDKLKQNLESNLTNLIKRNTELETL
hMID2   (181) EKVNMYCVSDDQLICALCKLVGRHRDHQVASLNDRFEKLKQTLEMNLTNLVKRNSELENQ
mMid2   (181) EKVNMYCVSDDQLICALCKLVGRHRDHQVASLNDRFEKLKQTLEMNLTNLVKRNSELENQ

hMID1   (241) LAKLIQTCQHVEVNASRQEAKLTEECDLLIEIIQQRRQIIGTKIKEGKVMRLRKLAQQIA
mMid1   (241) LAKLIQTCQHVEVNASRQEAKLTEECDLLIEIIQQRRQIIGTKIKEGKVIRLRKLAQQIA
hMID2   (241) MAKLIQICQQVEVNTAMHEAKLMEECDELVEIIQQRKQMIAVKIKETKVMKLRKLAQQVA
mMid2   (241) MAKLIQICQQVEVNTAMHEAKLMEECDELVEIIQQRKQMIAVKIKETKVMKLRKLAQQVA

hMID1   (301) NCKQCIERSASLISQAEHSLKENDHARFLQTAKNITERVSMATASSQVLIPEINLNDTFD
mMid1   (301) NCKQCLERSASLISQAEHSLKENDHARFLQTAKNITERVSMATASSQVLIPEINLNDTFD
hMID2   (301) NCRQCLERSTVLINQAEHILKENDQARFLQSAKNIAERVAMATASSQVLIPDINFNDAFE
mMid2   (301) NCRQCLERSTVLINQAEHILKENDQARFLQSAKNIAERVAMATASSQVLIPDINFNDAFE

hMID1   (361) TFALDFSREKKLLECLDYLTAPNPPTIREELCTASYDTITVHWTSDDEFSVVSYELQYTI
mMid1   (361) TFALDFSREKKLLECLDYLTAPNPPAIREELCTASYDTITVHWTSEDEFSVVSYELQYTI
hMID2   (361) NFALDFSREKKLLEGLDYLTAPNPPSIREELCTASHDTITVHWISDDEFSISSYELQYTI
mMid2   (361) NFALDFSREKKLLEGLDYLTAPNPPSIREELCTASHDTITVHWISDDEFSISSYELQYTI

hMID1   (421) FTGQANVVSLCNSADSWMIVPNIKQNHYTVHGLQSGTKYIFMVKAINQAGSRSSEPGKLK
mMid1   (421) FTGQANVVSLCNSADSWMIVPNIKQNHYTVHGLQSGTKYIFTVKAINQAGSRSSEPGKLK
hMID2   (421) FTGQANFISLYNSVDSWMIVPNIKQNHYTVHGLQSGTRYIFIVKAINQAGSRNSEPTRLK
mMid2   (421) FTGQANFISLYNSVDSWMIVPNIKQNHYTVHGLQSGTRYIFIVKAINQAGSRNSEPTRLK

hMID1   (481) TNSQPFKLDPKSAHRKLKVSHDNLTVERDESSSKKSHTPERFTSQGSYGVAGNVFIDSGR
mMid1   (481) TNSQPFRLDPKSAHRKLKVSHDNLTVERDDSSSKKSHAPERFAGQGSYGVAGNVFIDSGR
hMID2   (481) TNSQPFKLDPKMTHKKLKISNDGLQMEKDESSLKKSHTPERFSGTGCYGAAGNIFIDSGC
mMid2   (481) TNSQPFKLDPKMTHKKLKISNDGLQMEKDESSLKKSHTPERFSGTGCYGAAGNIFIDSGC

hMID1   (540) HYWEVVISGSTWYAIGLAYKSAPKHEWIGKNSASWALCRCNNNWVVRHNSKEIPIEPAPH
mMid1   (540) HYWEVVTSGSTWYAIGLAYRSAPKHEWIGKNAASWALCRCHNHWAVRHDGKETPIAPAPH
hMID2   (540) HYWEVVMGSSTWYAIGIAYKSAPKNEWIGKNASSWVFSRCNSNFVVRHNNKEMLVDVPPH
mMid2   (540) HYWEVVMGSSTWYAIGIAYKSAPKNEWIGKNASSWVFSRCNSNFVVRHNNKEMLVDVPPQ

hMID1   (600) LRRVGILLDYDNGSIAFYDALNSIHLYTFDVAFAQPVCPTFTVWNKCLTIITGLPIPDHL
mMid1   (600) LRRVGVLLDYDNGSIAFYDALSSVHLHTFHAALAQPVCPTFTVWNKCLTIVTGLPIPDHL
hMID2   (600) LKRLGVLLDYDNNMLSFYDPANSLHLHTFDVTFILPVCPTFTIWNKSLMILSGLPAPDFI
mMid2   (600) LKRLGVLLDYDNNMLSFYDPANSLHLHTFDVTFILPVCPTFTIWNKSLMILSGLPAPDFI

hMID1   (660) DCTEQLP------------------
mMid1   (660) DCTEQRP------------------
hMID2   (660) DYPERQECNCRPQESPYVSGMKTCH
mMid2   (660) DYPERQECNCRPQESPYVSGMKACH
```

(B)

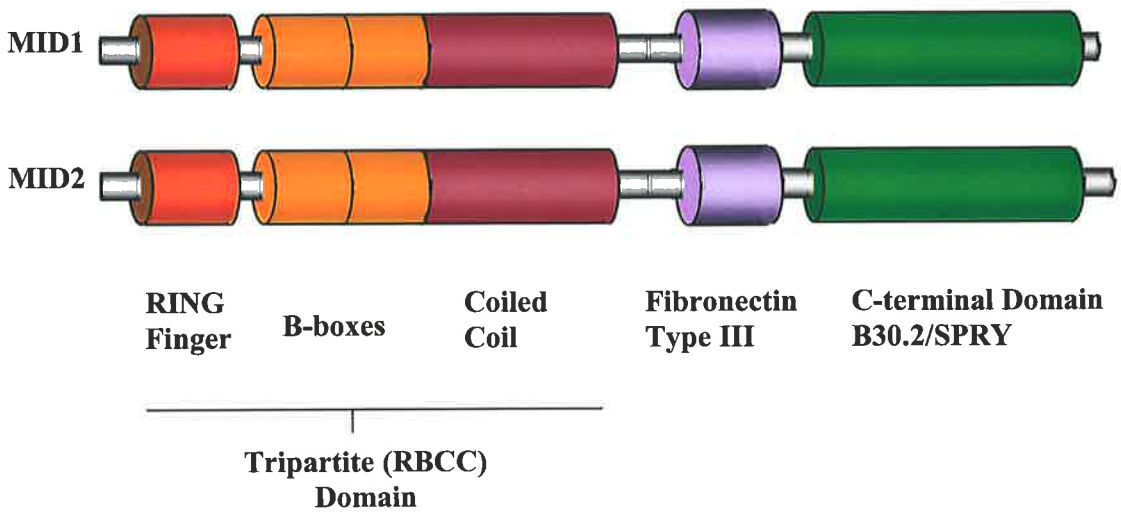

Figure 4.1 (A) Sequence alignment of human/mouse MID1 and MID2 proteins

MID1 and MID2 protein sequences were obtained from Genbank and aligned using the Vector NTI® Suite (v.6) programme. Block in grey and yellow indicate identical (identity) and similar (similarity) amino acid residues, respectively. Red font indicates identity which not conserved across all four protein sequences.

(B) Domain organisation of the MID1 and MID2 proteins

Schematic representation of highly conserved MID1 and MID2 domain organisation with N-terminal RBCC tripartite motif (RING-finger: residue 10-60; B-box1: residue 114-164; B-box2: residue 170-212; and Coiled-Coil domain: residue 219-345) followed by a Fibronectin type III domain (residue 382-475) and a C-terminal B30.2 domain (residue 538-658). The difference is largely restricted to a 19-amino acids extension at the C-terminal of MID2.

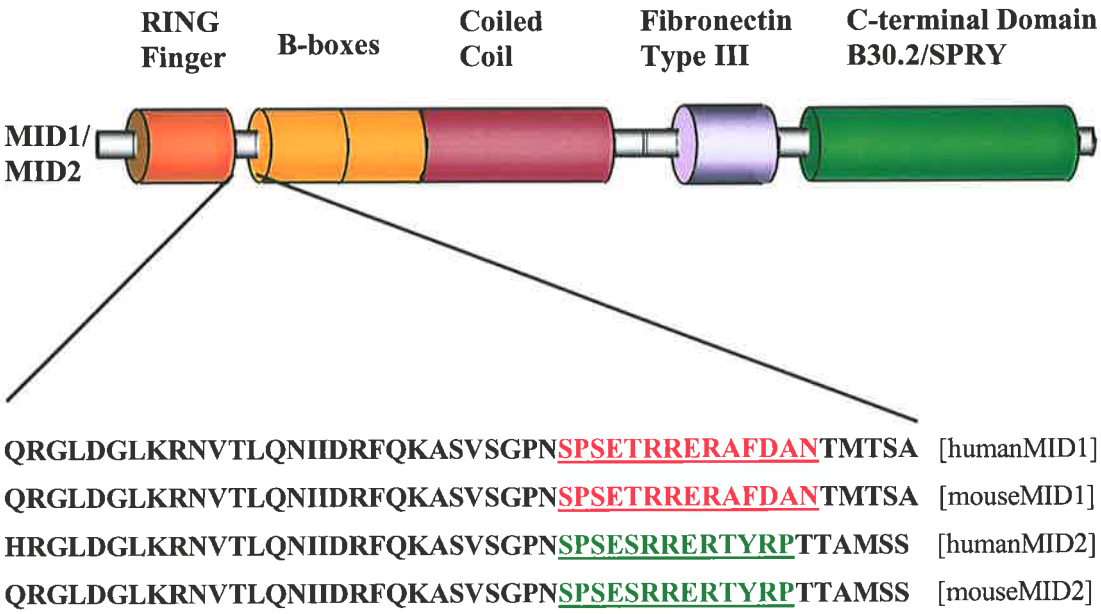

Figure 4.2 Amino acid sequences for designing the MID1 and MID2 synthetic peptides

Amino acids from the conserved N-terminal sequence of MID1 and MID2 selected (underlined and coloured) for the synthetic peptide preparation and predicted to be immunogenic.

C-terminus for coupling to the immunogenic carrier protein, Diphtheria Toxoid (DT) to ensure the immunogenicity of the peptides. The rationale for the choice of these peptides was based on the relative hydrophilicity and flexibility as recommended by the suppliers as well as showing the greatest difference in primary sequence between the homologues. In addition, the peptides chosen reside between motifs in a region predicted to be unstructured (see Figure 4.2). High purity peptides (>90%) certified by high performance liquid chromatography (HPLC) were then obtained from Auspep Pty. Ltd (Figure 4.3).

4.2.1.2 Production of anti-MID1 and anti-MID2 antibodies

For production of MID1 and MID2 antibodies, standard immunisation procedures were performed in three BABL/c mice for each peptide (Chapter Two). The mice were bled prior to immunisation to collect pre-immune serum. Animals were bled again a week after the second and fourth booster injections to determine titers of the antibodies produced. The immunoreactivity of pre- and post-immune sera against MID1 and MID2 synthetic peptides showed reactivity when analysed by ELISA assay (Figure 4.4). However the antisera against the two MID proteins varied considerably in titer, with the anti-MID1 antisera being relatively weak compared to that of anti-MID2 antisera. Pre-immune sera did not react with any of the peptide antigens. Based on these immunoreactivity titers, another two booster injections of MID1 peptide were administered to increase immunoreactivity against MID1. Unfortunately, this effort did not give a significant increase in the antibody titer (data not shown).

Hybridomas for the production of monoclonal antibodies against MID1 and MID2 were generated by fusion of the splenocytes obtained from the mice described

Figure 4.3 High Performance Liquid Chromatography (HPLC) analysis of the synthetic peptide

Graphs show the HPLC chromatogram of synthesised (A) MID1 and (B) MID2 synthetic peptides for use in the production of anti-peptide antibodies.

(A)

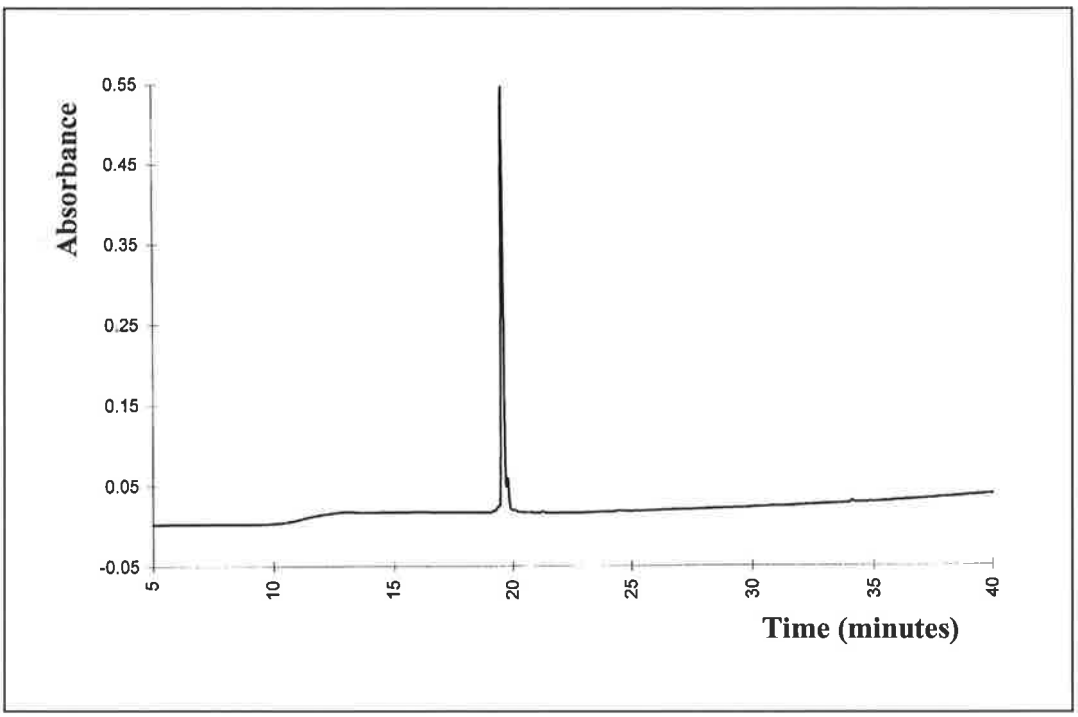
Absorbance
0.55
0.45
0.35
0.25
0.15
0.05
-0.05
5
10
15
20
25
30
35
40
Time (minutes)

(B)

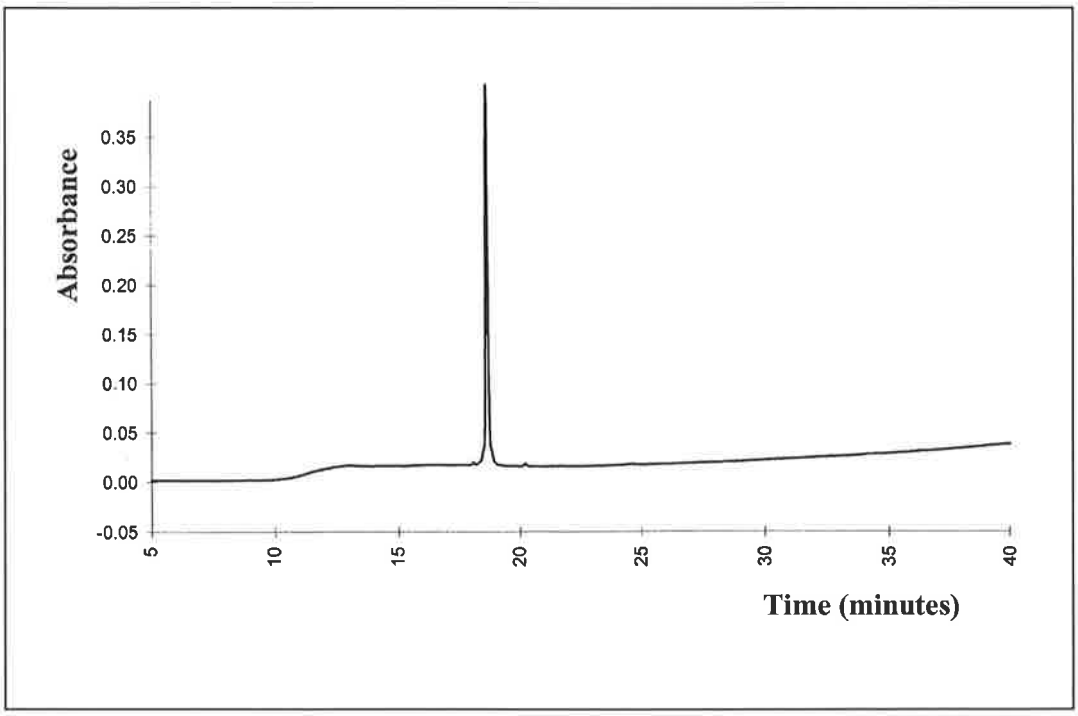
Absorbance
0.35
0.30
0.25
0.20
0.15
0.10
0.05
0.00
-0.05
5
10
15
20
25
30
35
40
Time (minutes)

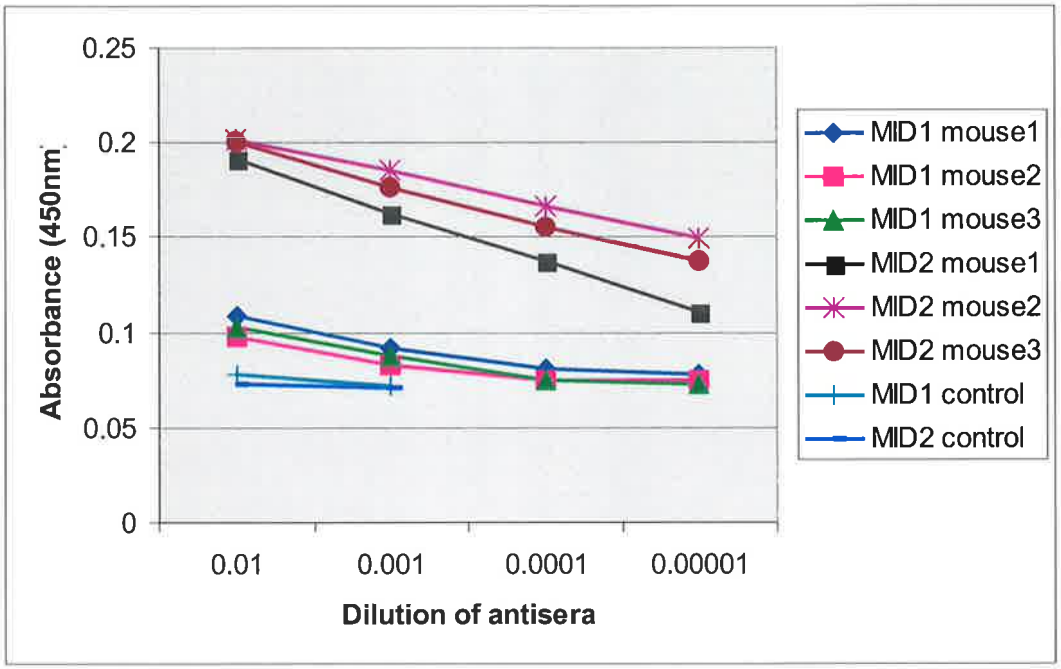

Figure 4.4 ELISA characterisation of the anti-peptide antisera

Immunoreactivity of mouse antisera against MID1 and MID2 synthetic peptides in ELISA. MID1 control and MID2 control are pre-immune sera obtained from the mice before immunisation.

above with murine SP2/O myeloma cells (Chapter Two). The culture supernatants in each well of the 96-well plates were tested using ELISA against the synthetic peptides used for immunisation to detect any hybridoma clones that secreted either anti-MID1 or anti-MID2 monoclonal antibodies. The first attempt failed to produce any positive clones. However, in the second attempt, 18 wells of "anti-MID2" supernatants were positive whilst none of "anti-MID1" supernatants tested positive. The screen stringency was then increased to select hybridomas that stably produced antibodies and free from false-positive wells. At this stage, only one well gave a strong positive response indicating that this well contained a hybridoma secreting an anti-MID2 monoclonal antibody. However, repeated attempts to clone the antibody-producing cell using the limiting dilution technique were not successful. As an alternative approach to isolate a stable clone of hybridoma cells, a fluorescent-activated cell sorting (FACS) approach was adopted which successfully generated 4 positive single-cell hybridomas. These hybridoma cells were grown and expanded to produce tissue culture supernatants with high concentrations of monoclonal antibody against MID2.

Following the failure to identify and isolate MID1 monoclonal antibody producing hybridomas, the same MID1 synthetic peptide was re-employed in an attempt to generate anti-MID1 antisera from rabbits. The process involved standard immunisation of the pre-bled New Zealand White rabbits, with booster injections administered as described in Chapter Two. Surprisingly, the immunoreactivity of the polyclonal antiserum against the immunised antigen, as assessed by ELISA, showed greater reactivity compared to the antiserum obtained from the mice (Figure 4.5).

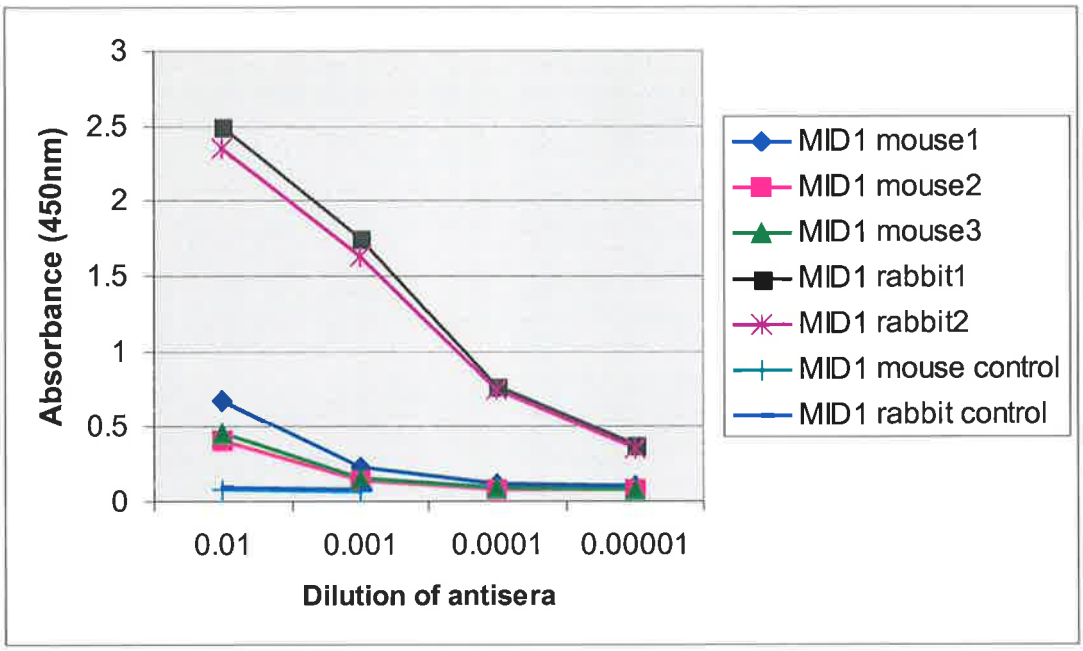

Figure 4.5 Comparison of rabbit and mouse anti-MID1 peptide immunoreactivity

Immunoreactivity of mouse and rabbit antisera against MID1 synthetic peptide in ELISA. MID1 mouse control and MID1 rabbit control are pre-immune sera obtained from the mice and rabbits before immunisation, respectively.

4.2.2 Characterisation of MID1- and MID2-specific antibodies

In order to characterise the MID1- and MID2-specific antibodies produced in this study, ELISA using the immunisation peptides as antigen was performed. These studies showed little cross-reactivity of the antibodies with the non-immunising synthetic peptides indicating the specificity of the monoclonal antibody against the MID2 synthetic peptide and polyclonal antibody against MID1 peptide (Figure 4.6). These antibodies were then used in immunocytochemical studies of Cos-1 cells transiently expressing either MID1- or MID2-GFP fusion protein to check the ability to recognise their native proteins. Cultured Cos-1 cells fixed 24 hours post-transfection were incubated with neat MID1 polyclonal or MID2 monoclonal antibodies and at antibody dilutions of 1/10, 1/100, 1/1000 and 1/10,000. Appropriate secondary antibody that is specific for the source of the primary antibody i.e. goat anti-rabbit and goat anti-mouse for MID1 polyclonal and MID2 monoclonal, respectively (both obtained from Sigma) was used at dilutions suggested by the supplier. Surprisingly, both MID1 and MID2 antibodies were repeatedly unable to detect the expression of the GFP-fusion proteins in these cells where observation by fluorescence microscopy confirmed of their GFP fluorescence on microtubules. As an alternative, Western blot analysis using protein extracted from the above transiently transfected Cos-1 cells were then performed. The antibodies also did not readily recognise the MID native proteins in this assay system.

In an attempt to improve recognition by the antibodies, an enrichment of each was performed using affinity purification. For the purification process (provided by the Institute of Medical and Veterinary Sciences (IMVS), Adelaide, Australia), MID1 polyclonal and MID2 monoclonal antibodies were subjected to affinity chromatography using immobilised Protein A and Protein G, respectively. Repeat

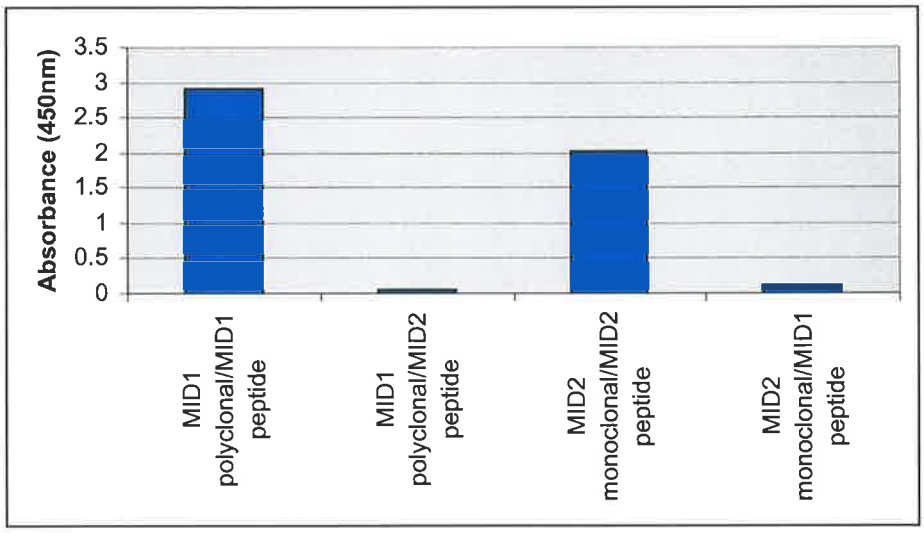

Figure 4.6 Specificity of MID1 polyclonal and MID2 monoclonal antibodies

ELISA assay showing specificity of MID1 polyclonal antibody against MID1 peptide and MID2 monoclonal antibody against MID2 peptide. No cross-reactivity was detected when these antibodies assayed against other synthetic peptides.

immunocytochemical and Western blot analyses using these purified and concentrated MID1 and MID2 antibodies also did not effectively improve the recognition of native protein by these antibodies.

4.2.3 Investigating the functional relationship between MID1 and MID2

To gain insight into the functional relationship between MID1 and MID2, the levels of *Mid2* mRNA in wild-type and *Mid1* knockout mouse embryos were investigated using reverse transcription-PCR (RT-PCR) analysis. Total RNA from 11.5 dpc and 12.0 dpc wild-type and *Mid1* knockout embryos were extracted using RNAqueous®-4PCR Kit (Ambion) and the concentration of the purified RNA determined by spectrophotometric analysis. A set of primers designed to amplify exon 1-derived coding sequence of *Mid2* was used for PCR amplification to ascertain whether the expression of *Mid2* mRNA may be upregulated in *Mid1* knockout mice as part of a compensatory mechanism. Different amplification cycles i.e. 20, 24, 28 and 32 cycles were tested (cycle conditions were denaturation, 95°C for 30 seconds; annealing, 59°C for 30 seconds; and extension, 72°C for 30 seconds) for verification of linear amplification. This RT-PCR analysis of the *Mid2* mRNA extracted from wild-type and *Mid1* knockout mouse embryos revealed similar apparent levels of amplified product in both tissues (Figure 4.7). Attempts to further investigate the level of Mid2 protein in the same tissues using Western blot analysis were not successful due to the inability of the anti-MID2 monoclonal antibody produced in this study to detect native protein.

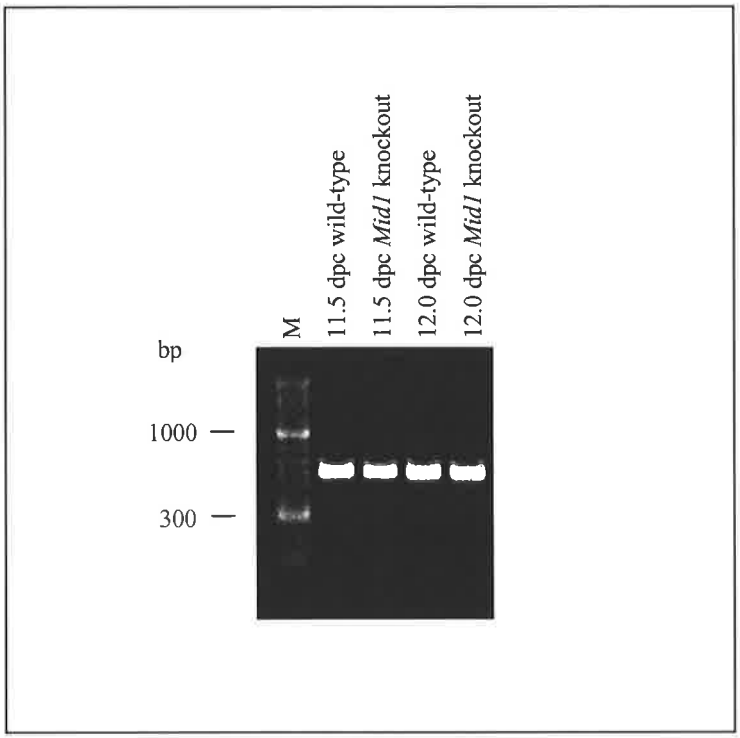

Figure 4.7 RT-PCR of wild-type and *Mid1* knockout mouse embryos

RT-PCR analysis of both wild-type and *Mid1* knockout mouse embryonic tissues. No upregulation of *Mid2* mRNA level in both 11.5 and 12.0 dpc mouse tissues tested. PCR analysis was performed at 32 cycles and M refers to the molecular weight marker lane. The same result was obtained using a smaller cycles.

4.3 Discussion

Variability in the clinical phenotype of the X-linked Opitz syndrome (OS) may be caused by a number of factors. One possibility is mutations with less severe consequences on protein levels or function i.e. mutations in non-coding regions of the *MID1* gene, such as the promoter elements, although this has not received any support from family data (Cox *et al.*, 2000; So *et al.*, 2005). Nevertheless, recent evidence presented in this thesis (Chapter Three) and by other studies (Granata & Quaderi, 2003; Granata *et al.*, 2005; Short *et al.*, 2002) is consistent with the notion that some level of functional redundancy between MID1 and its protein homologue, MID2 may exist. In this regard MID2 may be playing a compensatory role in the absence or loss-of-function of MID1, with variation in MID2 expression contributing to the phenotypic variability seen in OS patients. This redundant and compensatory mechanism may also explain the grossly normal appearance of our *Mid1* knockout mouse.

In order to investigate further the possibility of functional redundancy between the highly homologous MID1 and MID2 proteins, this study reported the production of MID1- and MID2-specific antibodies using synthetic peptides as antigens. Besides addressing compensatory mechanisms of the MID proteins, these antibodies were also anticipated to be useful in detecting dynamic changes in MID1 and MID2 protein localisation during fusion of facial primordia, the developmental mechanism of particular interest for this study.

One of the real challenges in producing useful anti-peptide antibodies is to choose peptides that are not only antigenic but also have a native protein-reactive antigenicity value. Well-designed anti-peptide antibodies can become a powerful tool for the identification and quantification of proteins containing the peptide sequence

chosen (Walter, 1986). Therefore, assistance in choosing the specific peptides against which MID1 and MID2 antibodies were to be raised was obtained from two independent custom-made anti-peptide antibody suppliers: Auspep Pty. Ltd. (Victoria, Australia) and Alpha Diagnostic International (San Antonio, USA). MID1 and MID2 protein sequences were analysed for hydrophilicity and flexibility by a number of predictive algorithms to determine the peptide antigenicity. Once identified, these short peptide sequences were compared against total protein in GenBank to ensure that the selected peptides were unique and did not share a region of homology by chance with any unrelated protein. The MID1 peptide selected in this study coincidently overlapped the peptide previously utilised by another research group (Schweiger *et al.*, 1999) in their attempt to produce a polyclonal antibody against MID1. Importantly, the amino acid sequences selected in this study are highly conserved across all MID1 and MID2 species, respectively, and therefore we anticipated that the generated antibodies would be specific for the MID protein against which they were raised, yet useful for detecting these proteins in different vertebrate model systems.

In this chapter, the development and purification of MID1 polyclonal and MID2 monoclonal antibodies is described. An attempt to produce a MID1 monoclonal antibody failed due to low immunoreactivity of the MID1 peptides in the mouse although it could not be ruled out that this could be caused by poor solubility of the MID1 peptide. Conversely, when injected in the rabbit, the same antigen produced higher-titer antisera, suggesting that the rabbit and mouse differ in their ability to respond to the peptide sequence. The immunoreactivity of the antibodies produced against synthetic peptides was verified by ELISA. Antibodies elicited by each peptide reacted strongly with the peptide used to raise them, and as predicted, showed no

cross-reactivity to one another. This result thus directly indicates that the amino acid sequences selected were able to produce unique and specific antibodies to recognise either MID1 or MID2 proteins. Unfortunately, both of these specific antibodies failed to directly detect their native protein obtained from various sources using different assay systems tested. Their native protein epitope recognition capability also showed no significant improvement after affinity purification. The failure of MID1 polyclonal antibody produced in this study to recognise MID1 protein in Western blots and immunocytochemical analyses was surprising considering its sequence overlapped significantly with a peptide previously used to raise anti-MID1 antisera that successfully recognised native proteins, albeit weakly. However, it is noteworthy to mention that the amino acids selected by Schweiger and her colleagues have higher similarity to the MID2 protein and therefore, it might be expected that their antibody would cross react with MID2. Furthermore, technical differences in experimentation e.g. type of cells used for immunocytochemical analysis may be a contributing factor in the successful detection of native protein. An additional possibility is that the failure to recognise the epitopes in their native states may be due to differences in conformation (i.e. functional state) of the protein itself. In this regard, there is growing evidence suggesting that, like some other characterised RBCC proteins, both MID1 and MID2 proteins exist in higher order protein complexes (Zou and Cox, unpublished; Cainarca *et al.*, 1999) and even complexed with Hsp90, a chaperone (Matts and Cox, unpublished). In such complexes, the target peptide sequence may not readily accessible to the antibodies or be altered in conformation. We therefore anticipate that better understanding of the MID1 and MID2 three-dimensional protein structures will greatly assist the production of specific antibodies in the future to delineate the role of MID protein in the development of craniofacial tissues/structures.

A level of a functional redundancy between two highly homologous proteins involved during early embryonic development has been shown to exist in a number of animal models. Phenotypic comparison between double-null mice with the relevant single-null mouse model provides definitive evidence that the compensatory mechanisms act as a powerful modulator of the expressivity of mutant alleles. One of the examples is in members of the homeobox transcription factors, Msx1 and Msx2 where double knockouts of both *Msx1* and *Msx2* mice exhibit a more severe facial phenotype, e.g. the presence of bilateral clefts of the primary palate, that is not seen in either individual knockout mouse (reviewed by Francis-West *et al.*, 2003). Some level of functional redundancy has also been found for two members of the *Distalless* gene family, *Dlx5* and *Dlx6*. Targeted inactivation of both *Dlx5* and *Dlx6* in mice resulted in severe developmental defects of craniofacial and limb structures (Beverdam *et al.*, 2002; Depew *et al.*, 2002; Robledo *et al.*, 2002) where defects in the facial skeletal and middle ear ossicles have been reported for $Dlx5^{-/-}$ mice (Acampora *et al.*, 1999). It was therefore of interest that recent findings (Granata & Quaderi, 2003; Granata *et al.*, 2005; Short *et al.*, 2002) including data presented in this thesis have implicated MID2 in the pathogenesis of OS through functional redundancy, although the precise role of the proteins is still not fully understood. Therefore, we hypothesised that in the absence or loss-of-function of MID1, MID2 may be upregulated as part of a compensatory mechanism. Although the antibodies generated in this study were unable to be used to specifically address this issue at the protein level, the opportunity to further investigate the involvement of MID2 in the presentation of OS came by way of availability of *Mid1* knockout mouse tissues. Data obtained from RT-PCR of *Mid2* mRNA in wild-type and *Mid1* knockout tissues however showed no upregulation of *Mid2* was evident in the tissues lacking Mid1. Although this finding does not refute

the hypothesis that MID1 and MID2 have redundant functions, it suggests that if MID2 can compensate for loss of MID1, it does so at its normal endogenous levels. Resolution of this issue is likely to only be achieved with the development of a *Mid1/Mid2* double knockout mouse strain. This is currently a focus of research in our laboratory.

Chapter Five: Investigation into the cellular and developmental functions of MID1 protein

5.1 Introduction

The X-linked Opitz GBBB syndrome (OS) gene, *MID1*, encodes for a 72 kDa RING finger (RBCC) protein that harbours conserved functional domains (Chapter One, Figure 1.4). In trying to delineate the function of MID1, previous work by our laboratory and that of others, showed that each of its identified motifs or domains could be implicated either directly or indirectly in mediating protein-protein interactions (Cainarca *et al.*, 1999; Reymond *et al.*, 2001; Short *et al.*, 2002). As in other members of the RBCC protein family, MID1 is thought to function as part of a multiprotein complex of between 250 kDa and 1 MDa (Zou and Cox, unpublished data; Cainarca *et al.*, 1999). Although little is known about the identity or function of other components in these complexes, MID1 at least has been shown to associate with cytoplasmic microtubules along their length and throughout the cell cycle. This has been demonstrated by immunofluorescence detection of endogenous MID1, transient expression of GFP-MID1 fusion proteins, and in the cellular fractionation experiments (Cox *et al.*, 2000; Schweiger *et al.*, 1999).

Most *MID1* mutations found in patients with X-linked OS are truncating mutations although missense changes and in-frame deletions and insertions have also been found. Interestingly, without exception the resultant mutant protein has been shown to have lost its ability to distribute along the microtubule network. For the truncated proteins, most form cytoplasmic clumps. Together these observations led to the assumption that OS is caused by loss of function of MID1 (Cox *et al.*, 2000). Undoubtedly, the presentation of anomalies seen in patients harbouring loss of function mutations in MID1 highlights a critical role for this microtubule-associated

protein in the development of the craniofacial complex and other organ systems. Although these cellular localisation data of MID1 protein have provided clues as to a potential function of this protein, the precise mechanism that leads to the highly specific OS phenotype remains to be elucidated.

Detailed developmental studies of *MID1* have been carried out in human, mouse and chick and shown that spatial and temporal *MID1/Mid1* expression is consistent with the developmental defects seen in OS patients. *Mid1* developmental expression analysis presented in Chapter Three using an inserted *LacZ* reporter and *in situ* hybridisation studies in chick embryos (Richman *et al.*, 2002) revealed localised *Mid1* expression in the facial epithelia and to some extent in the facial mesenchyme during the morphogenesis of the lip and primary palate. In fact, developmental expression analysis reported in this study has provided some of the first suggestions that *Mid1* may regulate the epithelial-mediate fusion process of facial primordia.

Malformations that characterise OS such as the specific craniofacial defects (i.e. cleft lip with or without cleft palate), urogenital anomalies (hypospadias) and congenital heart defects (primarily defects in cardiac septation and vascular remodelling) also occur with high incidence as isolated birth defects. Thus, MID1 may be involved in a commonly used developmental mechanism involved in epithelial function and/or tissue fusion. As formation of the lip/palate, male external genitalia and cardiac septa require fusion of epithelial-lined tissue and epithelial to mesenchymal transition (EMT) to subsequently remove the bi-layered epithelial seam, perturbation of MID1 could impact on one of any number of cellular events that co-ordinate these tissue fusions. Strikingly, the morphogenetic processes suggested to underlying tissue fusion such as cell migration, cell death and EMT are known to be dependent on microtubule dynamics and influenced by the activity of PP2A, the

phosphatase turned over by MID1 through its interaction with the α4 protein (Liu *et al.*, 2001; Short *et al.*, 2002; Trockenbacher *et al.*, 2001). Hypothetical models to explain the regulatory mechanism involving MID1 and PP2A and how their disruptions in OS might be affecting microtubule dynamics have also been suggested (Liu *et al.*, 2001; Short *et al.*, 2002; Trockenbacher *et al.*, 2001). However, characterisation of the cellular and developmental processes controlled by MID1 and how disruption of this protein affects the morphogenesis of the organs defective in OS has not yet performed.

With evidence suggesting a role for MID1 in morphogenetic processes during mammalian embryonic development, particularly during craniofacial morphogenesis, this chapter reports the development of stable Madin-Darby canine kidney (MDCK) (epithelial) and Cos-1 (mesenchymal) cell lines that express either wild-type GFP-MID1 or one of a number of different mutant GFP-MID1 fusion proteins in the presence of tetracycline or similar analogue. The development of these stable cell lines was based on the "Tet-On" system, which requires doxycycline (a tetracycline derivative) for binding to the tetracycline-responsive promoter and subsequent activation of the downstream genes (Gossen *et al.*, 1995). These cell lines were used to elucidate the role of MID1 in cellular processes such as cell migration, proliferation and cell death and can be used to test the ability of cells to undergo epithelial-mesenchymal transitions (EMT), a key event in the fusion of epithelial-lined tissue such as the facial prominences.

5.2 Results

5.2.1 Construction of inducible gene-specific expression plasmids

In order to establish a tetracycline-inducible stable MID1 expressing cell lines, gene-specific expression plasmids were constructed that would express either wild-type or one of a number of different mutant GFP-MID1 fusion proteins under the control of tetracycline-response element, TRE (Figure 5.1). The tetracycline-responsive promoter, phCMV*-1 (Mosser *et al.*, 1997) employed in this construction contained a TRE located just upstream of the minimal CMV promoter (P_{minCMV}). This phCMV*-1 promoter was amplified using the vector pTR5-DC/GFP (a gift from Dr D. Mosser, Biotechnology Research Institute, Montreal, Canada) as template and the following primers: (CMVTET-F) – CAC**ATTAAT**TTTACCACTCCCTATCAGTG-ATAGAG and (CMVTET-R) – CAC**GCTAGC**GTTTAAACTTGGACCTGGGA-GTGGA. A 5' *Ase*I site and a 3' *Nhe*I site (bolded sequences in the primers) were incorporated in the primer designs to facilitate directional cloning of the PCR product. The resultant PCR fragment contained the phCMV*-1 promoter region and an adenovirus tripartite leader sequence, TPL. The TPL was located downstream of the promoter to increase the expression of inserted transgenes by enhancing translation, without modifying the specificity of the promoter. The digested PCR fragment was subcloned into the enhanced green fluorescent protein vector, pEGFP-C2 (Clontech), to replace the original human cytomegalovirus immediate early promoter (pCMV IE) that has been excised out by double digestion with *Ase*I and *Nhe*I. pEGFP-C2 vectors containing various GFP-MID1 fusion constructs (full-length *MID1* (Cox *et al.*, 2000) and the *MID1* domain-specific deletion constructs: GFP-MID1ΔBB and GFP-MID1ΔCTD (Short *et al.*, 2002)) had previously been developed by our laboratory and successfully used in immunofluorescence analyses. The integrity of each inserts

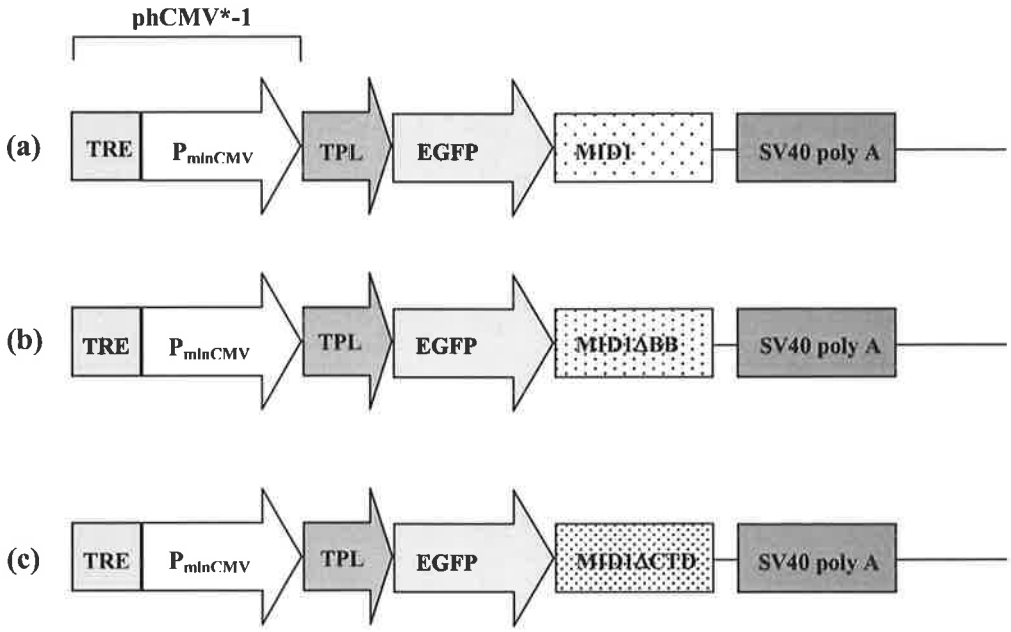

Figure 5.1 Schematic representation of inducible gene-specific expression plasmids

Maps of the tetracycline-responsive gene-specific expression vectors expressing either (a) wild-type GFP-MID1 fusion protein (pCMVTRE-GFPMID1), (b) GFP-MID1ΔBB fusion protein (pCMVTRE-GFPMID1ΔBB) and (c) GFP-MID1ΔCTD fusion protein (pCMVTRE-GFPMID1ΔCTD) that were constructed and used for the establishment of stable cell lines reported in this thesis.

(both promoter and GFP-fusion construct) was determined by restriction digestion and direct sequencing (data not shown).

5.2.2 Establishment and characterisation of tetracycline-inducible cell lines

A standard protocol for selecting a tetracycline-inducible cell line starts with transfecting a cell line with a plasmid expressing the regulatory component for the "Tet-On" system i.e. reverse tetracycline-regulated transactivator (rtTA). Both MDCK and Cos-1 cells were first transfected with pTetON/IRES/NEO (generously given by Anthony Fedele, School of Molecular & Biomedical Science, University of Adelaide) using Lipofectamine™ 2000 (Life Technologies). Transfectants surviving selection for 14 days in 400μg/ml Geneticin (G418) were then isolated and expanded. Each clone was then transiently transfected with a luciferase reporter gene under the control of the tetracycline operator and screened for high and low luciferase expression in the presence and absence of the tetracycline derivative, doxycycline (Dox), respectively using the Dual-Luciferase™ Reporter Assay System (Promega). The selection of high expression and low basal level cells were based on fold induction of the luciferase activity (Table 5.1).

Following selection of a suitable cell line for future desired studies, stable cell lines expressing the gene of interest under the control of tetracycline-responsive promoter (Section 5.2.1) could then be established. Tetracycline-responsive gene-specific expression plasmids that either expressed wild-type GFP-MID1 (pCMVTRE-GFPMID1) or one of a number of different mutant GFP-MID1 fusion proteins (pCMVTRE-GFPMID1ΔBB and pCMVTRE-GFPMID1ΔCTD) were independently transfected into the selected high and low expression 'Tet-On' MDCK or 'Tet-On' Cos-1 cells (see Table 5.1). Following expansion, transfected cells were induced with

Clones	Luciferase activity (RLU)		Fold induction
	+ Dox	- Dox	
Cos-1/pTET-ON #1	1.2×10^4	3.9×10^2	30.77
Cos-1/pTET-ON #2	2.1×10^4	4.7×10^2	44.68*
Cos-1/pTET-ON #3	8.2×10^3	6.5×10^2	12.62
MDCK/pTET-ON #1	1.4×10^5	3.5×10^3	40.00*
MDCK/pTET-ON #2	5.3×10^4	4.9×10^3	10.82
MDCK/pTET-ON #3	3.0×10^4	1.4×10^3	21.43
MDCK/pTET-ON #4	8.1×10^4	2.2×10^3	36.82

Table 5.1 Inducibility of stable cell lines in a tetracycline-sensitive luciferase reporter gene assay

Levels of luciferase activity in a tetracycline-sensitive luciferase reporter gene assay were determined in the presence and absence of the tetracycline analogue, doxycycline (Dox). The analysis showed that all clones displayed considerably high-fold induction of luciferase activity. The clones with the highest-fold induction (asterisk) were selected for the establishment of stable cell lines. [RLU: relative light units].

2μg/ml of Dox and the cells were then subjected to fluorescence-activated cell sorting (FACS). GFP-expressing cells were subsequently sorted and expanded in the absence of Dox until enough cells had been grown for another round of positive selection. This strategy was very effective in enriching cells that had the characteristics of tetracycline-inducible expression of the GFP-fusion proteins (Figure 5.2).

In order to obtain uniformly high levels of Dox-inducible GFP-expressing cells, single cell cloning of cells within the top of the fluorescence intensity was performed, with cells sorted into 96-well plates using FACS. These cells were expanded as individual clones and the clonal lines were then reanalysed again by FACS for green fluorescence in the presence or absence of Dox to identify clones with non-leaky expression. The Cos-1 and MDCK clones that expressed wild-type MID1, MID1ΔBB or MID1ΔCTD GFP-fusion proteins with no detectable leakiness and produced uniform and very high GFP positivity after Dox treatment were then selected for further investigation (Figure 5.3). Subcellular localisation of the various MID1 proteins in these selected Cos-1 and MDCK stable cell lines was then examined after Dox treatment to confirm the integrity of the expression constructs (Figure 5.4). Fluorescence detection of both Cos-1 and MDCK stable cell lines expressing wild-type MID1-GFP fusion proteins displayed a microtubular distribution throughout the cell cycle. In contrast, GFP fluorescence in cell lines expressing MID1ΔCTD showed cytoplasmic clumps or speckles while cytoplasmic aggregates in cells expressing MID1ΔBB appeared to have a variable cellular distribution. All intracellular localisations observed with these stable lines are in accordance with the previous reports (Cox *et al.*, 2000; Short *et al.*, 2002).

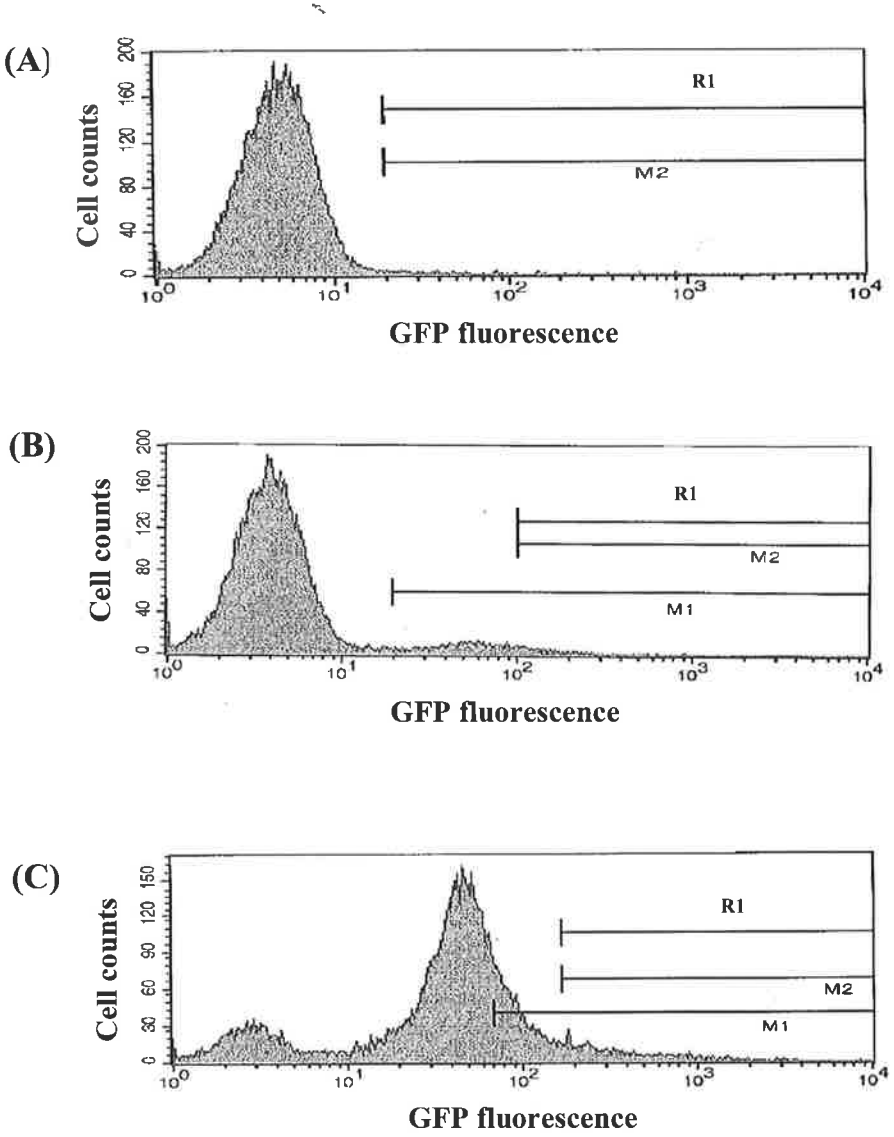

Figure 5.2 Sequential enrichment of fluorescence profiles after each round of fluorescence-activated cell sorting (FACS) selection

Fluorescence profiles of candidate stable cell lines before and after each round of FACS selection. Cells transiently transfected with tetracycline-responsive plasmids were subjected to FACS and a portion of cells (R1 in A) were sorted. These cells were expanded and sequentially enriched by another similar selection scheme (R1 in B). Cells from within the top of fluorescence intensity were then selected (R1 in C) for single cell cloning to produce uniformly high levels of Dox-inducible GFP-expressing cells. Results shown are representative of all separate experiments performed to produce different types of stable cell lines reported in this study. Gates M1 and M2 are for the FACS statistical data analyses.

Figure 5.3 Establishment of tetracycline-inducible stable cell lines

Fluorescence profiles of (A) Cos-1 and (B) MDCK stable cell lines expressing either wild-type GFP-MID1 or one of a number of different mutant GFP-MID1 fusion proteins. Cells were incubated in the presence or absence of doxycycline (Dox) for 12 hours before the cells were trypsinised and GFP fluorescence assessed using fluorescence-activated cell sorting (FACS). Approximately 20000 cells were analysed. Gates R2, M1 and M2 were for FACS statistical data analyses.

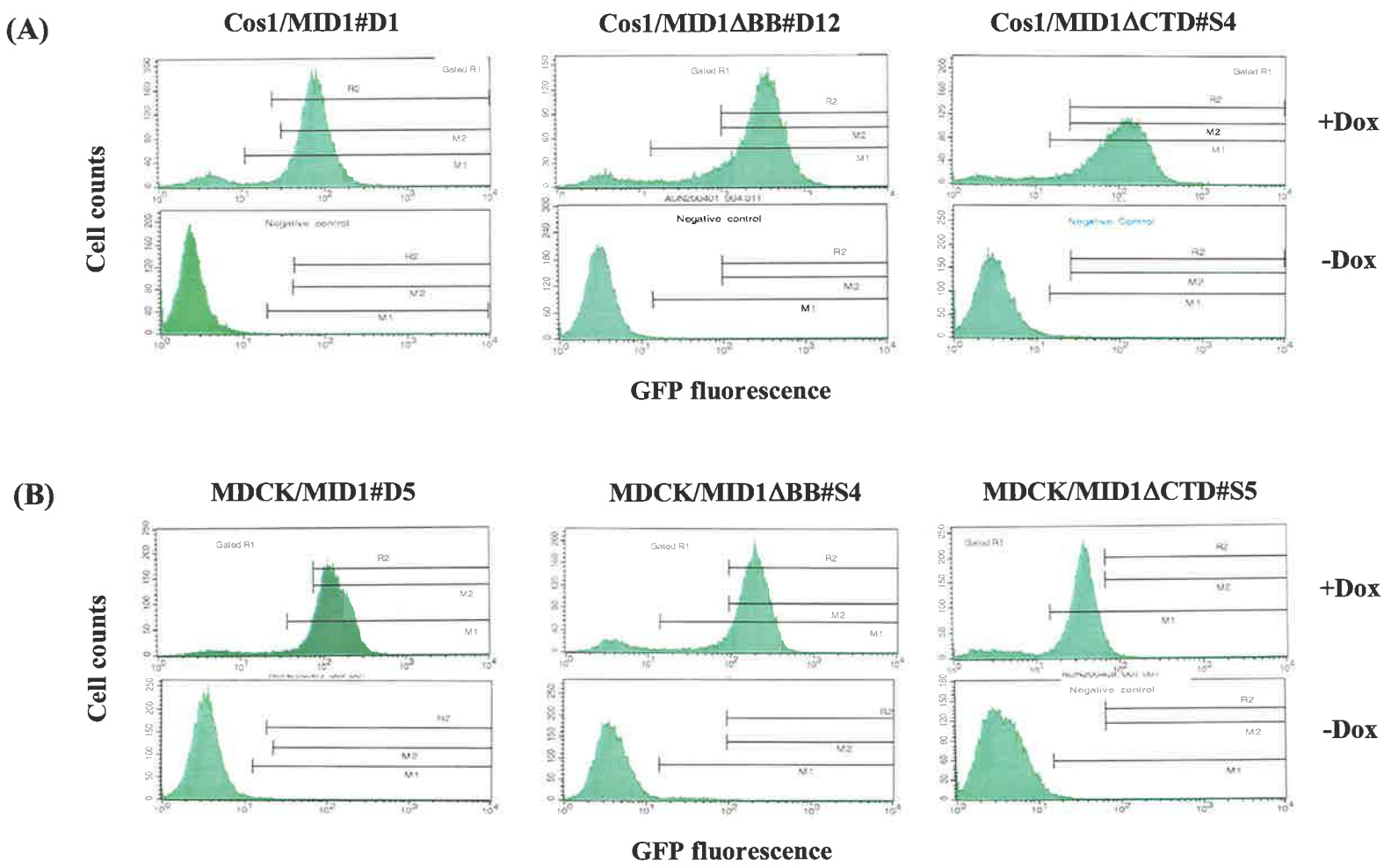
(A)
Cos1/MID1#D1
Cos1/MID1ΔBB#D12
Cos1/MID1ΔCTD#S4
Cell counts
+Dox
-Dox
Negative control
GFP fluorescence
(B)
MDCK/MID1#D5
MDCK/MID1ΔBB#S4
MDCK/MID1ΔCTD#S5
Cell counts
+Dox
-Dox
Negative control
GFP fluorescence

Figure 5.4 Expression of wild-type and mutant GFP-MID1 proteins in Cos-1 and MDCK stable cell lines

Fluorescence-based assay showing subcellular localisations of GFP-MID1 (A and B), GFP-MID1ΔBB (C and D) and GFP-MID1ΔCTD (E and F) in Cos-1 (A, C and E) and MDCK (B, D and F) stable cell lines respectively, following addition of Dox.

(A)

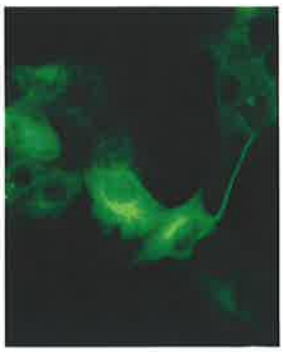

Cos1/MID1#D1

(B)

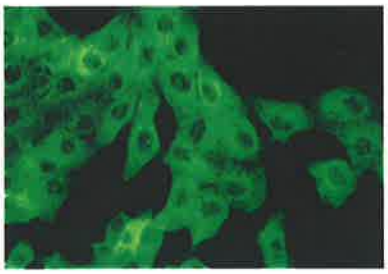

MDCK/MID1#D5

(C)

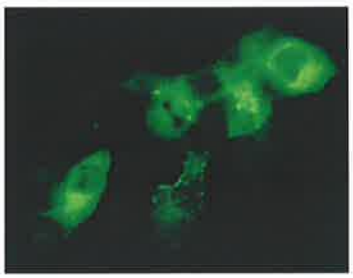

Cos1/MID1ΔBB#D12

(D)

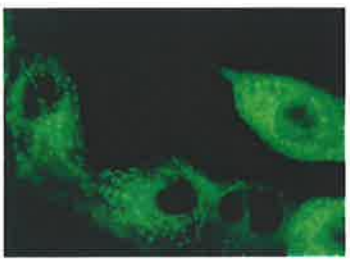

MDCK/MID1ΔBB#S4

(E)

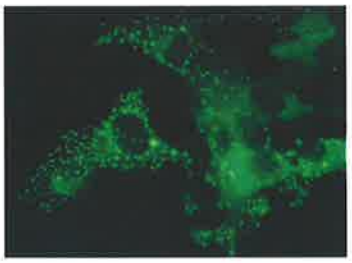

Cos1/MID1ΔCTD#S4

(F)

MDCK/MID1ΔCTD#S5

5.2.3 Investigating the cellular function(s) of MID1

5.2.3.1 Cell proliferation and apoptosis assays of cells stably expressing wild-type and mutant MID1 proteins

In order to analyse the effect of ectopically expressed wild-type and mutant MID1 proteins on two cell parameters; proliferation and programmed cell death, tetracycline-inducible Cos-1 and MDCK stable cell lines cultured in 96-well plates were induced for the expression of GFP-MID1, GFP-MID1ΔBB or GFP-MID1ΔCTD fusion proteins by adding Dox (2μg/ml) into the culture medium. Non-induced cells for each line were also set up as an internal control. Cell proliferation was measured using CellTiter 96® Aqueous One Solution Cell Proliferation Assay (Promega) 24 and 48 hours post-induction as described in Chapter Two. Apoptosis was detected in the same setting using the Caspase-Glo™ 3/7 Assay (Promega) (see Chapter Two). Both assays were performed in triplicate and data presented as the mean +/- standard deviation (SD).

Collectively, the results showed no obvious effects on cell proliferation in both Cos-1 and MDCK stably overexpressed wild-type and mutant MID1 GFP-fusion proteins (Table 5.2). Similarly, stable expression of wild-type and mutant MID1 proteins for up to 48 hours in these cell lines appeared not to consistently alter the amount of cell death (Table 5.3). Some differences seen in the data between induced and non-induced cells for both proliferation and apoptosis assays were very small and could not be considered as having significant effects on the cellular analysis performed in this study.

5.2.3.2 The effects of ectopic wild-type and mutant MID1 on wound closure

In vitro wound healing assays were performed on the tetracycline-inducible MDCK and Cos-1 stable cell lines in order to determine whether MID1 played any

Cell lines	Doxycycline	Absorbance (+/-SD)	
		24 hours	48 hours
Cos1/MID1#D1	+	1.132 (+/-0.029)	1.336 (+/-0.036)
	-	1.072 (+/-0.037)	1.271 (+/-0.018)
Cos1/MID1ΔBB#D12	+	1.178 (+/-0.015)	1.333 (+/-0.062)
	-	1.121 (+/-0.037)	1.321 (+/-0.046)
Cos1/MID1ΔCTD#S4	+	1.599 (+/-0.025)	1.966 (+/-0.104)
	-	1.511 (+/-0.008)	1.932 (+/-0.092)
MDCK/MID1#D5	+	1.747 (+/-0.072)	2.276 (+/-0.056)
	-	1.727 (+/-0.130)	2.128 (+/-0.023)
MDCK/MID1ΔBB#S4	+	2.081 (+/-0.040)	2.315 (+/-0.111)
	-	2.203 (+/-0.136)	2.303 (+/-0.183)
MDCK/MID1ΔCTD#S5	+	2.130 (+/-0.065)	2.596 (+/-0.016)
	-	2.054 (+/-0.030)	2.513 (+/-0.017)

Table 5.2 Cell proliferation analysis of stable, inducible cell lines expressing wild-type and mutant MID1 fusion proteins

Cell proliferation of Cos-1 and MDCK cells stably expressing wild-type and mutant MID1 proteins as measured using CellTiter 96® Aqueous One Solution Cell Proliferation Assay following 24 and 48 hours induction with (and without) 2μg/ml of Dox. Absorbance was measured at 490 nm (absorbance range is 0.000 – 3.000) using a spectrophotometer. Experiments were performed in triplicate and data represented as means (+/-SD). [SD: standard deviation].

Cell lines	Doxycycline	Relative light units (RLU) (+/-SD)	
		24 hours	48 hours
Cos1/MID1#D1	+	28770 (+/-568.7)	37705 (+/-407.4)
	-	29530 (+/-983.2)	42239 (+/-940.8)
Cos1/MID1ΔBB#D12	+	24252 (+/-2001.9)	32024 (+/-351.0)
	-	23011 (+/-1117.3)	37044 (+/-541.3)
Cos1/MID1ΔCTD#S4	+	28288 (+/-643.3)	43839 (+/-360.7)
	-	29609 (+/-1013.3)	47972 (+/-212.7)
MDCK/MID1#D5	+	62955 (+/-1506.7)	40321 (+/-335.7)
	-	64813 (+/-628.0)	43899 (+/-484.4)
MDCK/MID1ΔBB#S4	+	12329 (+/-313.1)	11831 (+/-405.3)
	-	12291 (+/-533.2)	12406 (+/-222.1)
MDCK/MID1ΔCTD#S5	+	11846 (+/-585.0)	10821 (+/-221.2)
	-	13312 (+/-548.2)	12420 (+/-50.8)

Table 5.3 Cell death (apoptosis) analysis of stable, inducible cell lines expressing wild-type and mutant MID1 fusion proteins

Cell death (apoptosis) in Cos-1 and MDCK cells stably expressing wild-type and mutant MID1 proteins as measured using the Caspase-Glo™ 3/7 Assay 24 and 48 hours post-induction with 2μg/ml of Dox. Luminescence (RLU) was measured using a luminometer (luminescence range is 00000 – 65535). Experiments were performed in triplicate and data represented as means (+/-SD). [RLU: relative light units; SD: standard deviation].

role in the ability of cells to undergo EMT and/or cell migration. Monolayer wounds of MDCK stable cell lines were made using a yellow pipette tip in confluent cell cultures (Chapter Two). The cells were then grown for another 60 hours with or without Dox, which allowed for complete healing of the wounded areas. The rate of wound closure for MDCK cells expressing GFP-MID1, GFP-MID1ΔBB or GFP-MID1ΔCTD fusion proteins was observed and noticed (Figure 5.5). Wound healing assays performed in this study showed that the healing rates of the wounded monolayer of epithelial cells stably expressing wild-type MID1 were noticeably slower compared to their uninduced counterpart (Figure 5.5A). In contrast, cells overexpressing the MID1ΔCTD fusion protein displayed a quicker rate of closure (Figure 5.5C) whilst MDCK cells stably overexpressing MID1ΔBB showed no obvious differences between induced and uninduced cell lines (Figure 5.5B).

Similar monolayer wound healing assays were also carried out using Cos-1 stable cell lines to assess whether MID1 has any ability to promote cell migration (cell motility) (Figure 5.6). These monolayer wound healing migration assays showed that MID1ΔCTD significantly enhanced cell migration into the wounded area (Figure 5.6C), whereas both wild-type MID1 and MID1ΔBB fusion proteins were unable to promote cell migration (Figure 5.6A and 5.6B, respectively).

5.3 Discussion

A feasible way to perform functional studies of a gene product is through phenotypic observations after expression of the genes of interest in cell lines. However, uncontrolled expression of genes with pleiotropic effects can result in selecting cell lines with biased characteristics and if the genes of interest are potentially toxic while overexpressed, there can be tremendous difficulties in

Figure 5.5 Wound healing assay of monolayer epithelial cells stably expressing wild-type and mutant MID1 proteins

Figures show representative wound healing data of monolayer epithelial cell lines stably expressing (A) wild-type MID1, (B) MID1ΔBB and (C) MID1ΔCTD proteins. Photomicrographs of the scratch wounds were taken immediately after their formation (0 hour) and again at 12 hour intervals until healing of the wounded areas were completed. Each data represents five independent experiments.

Figure 5.5 (A)

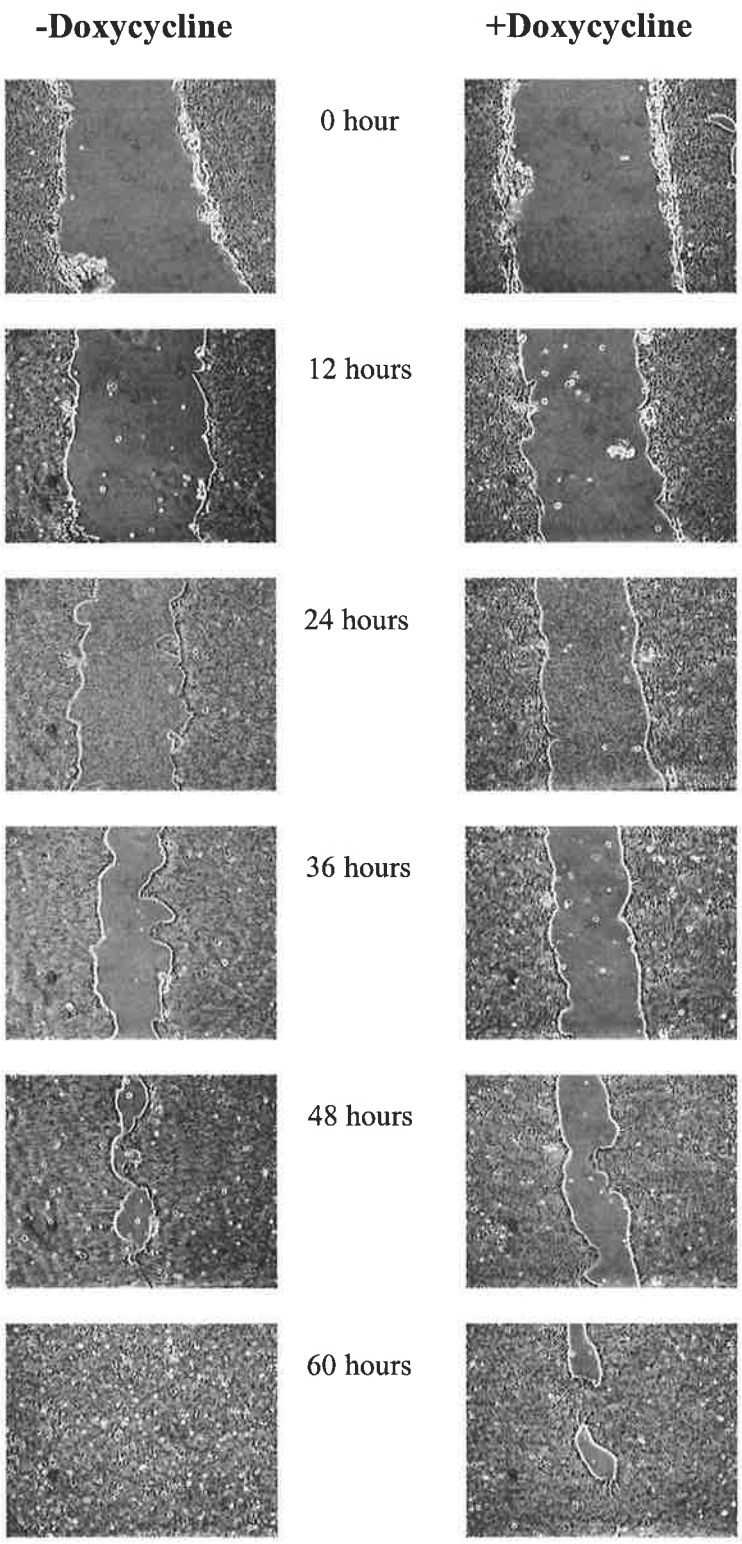
-Doxycycline
+Doxycycline
0 hour
12 hours
24 hours
36 hours
48 hours
60 hours

Figure 5.5 (B)

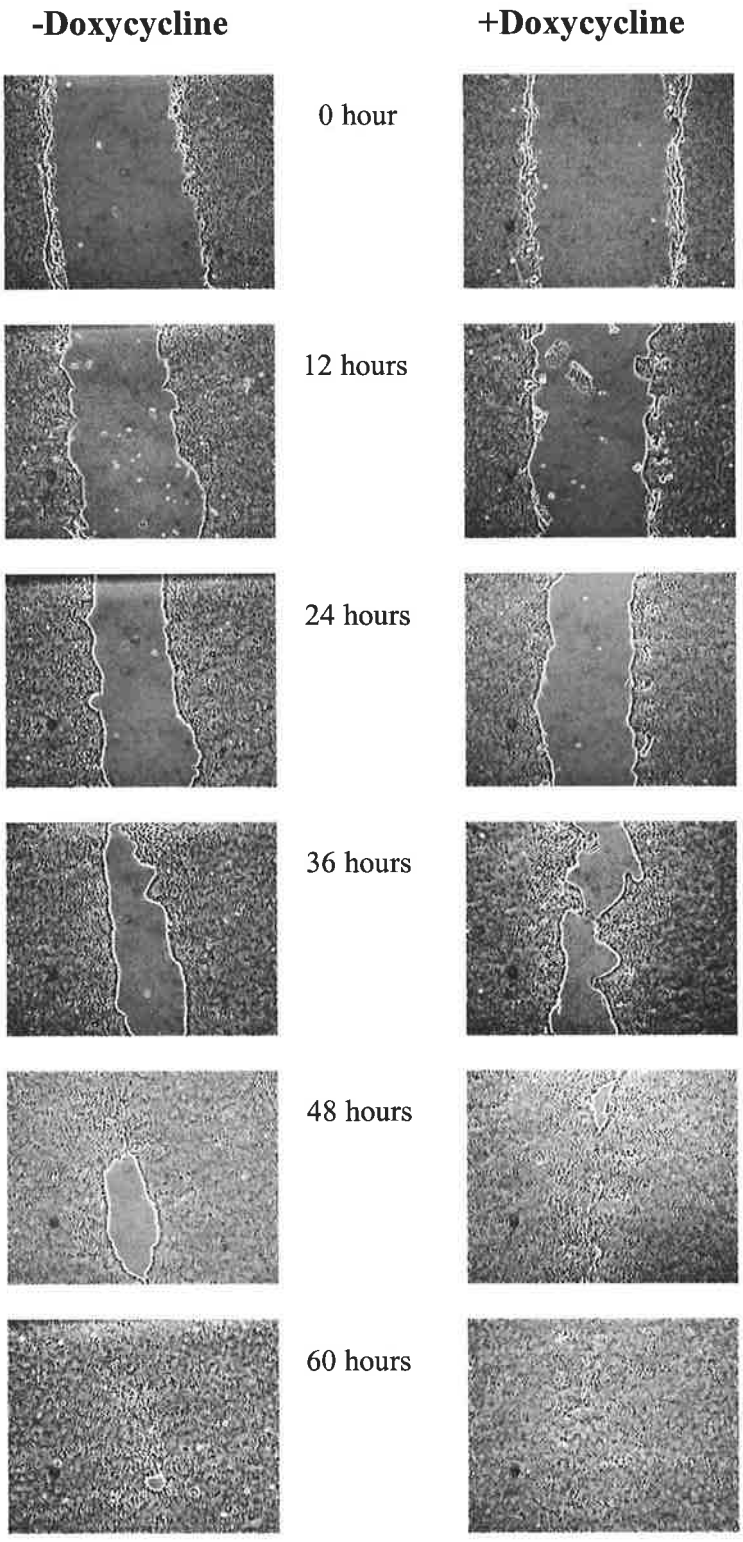
-Doxycycline
+Doxycycline
0 hour
12 hours
24 hours
36 hours
48 hours
60 hours

Figure 5.5 (C)

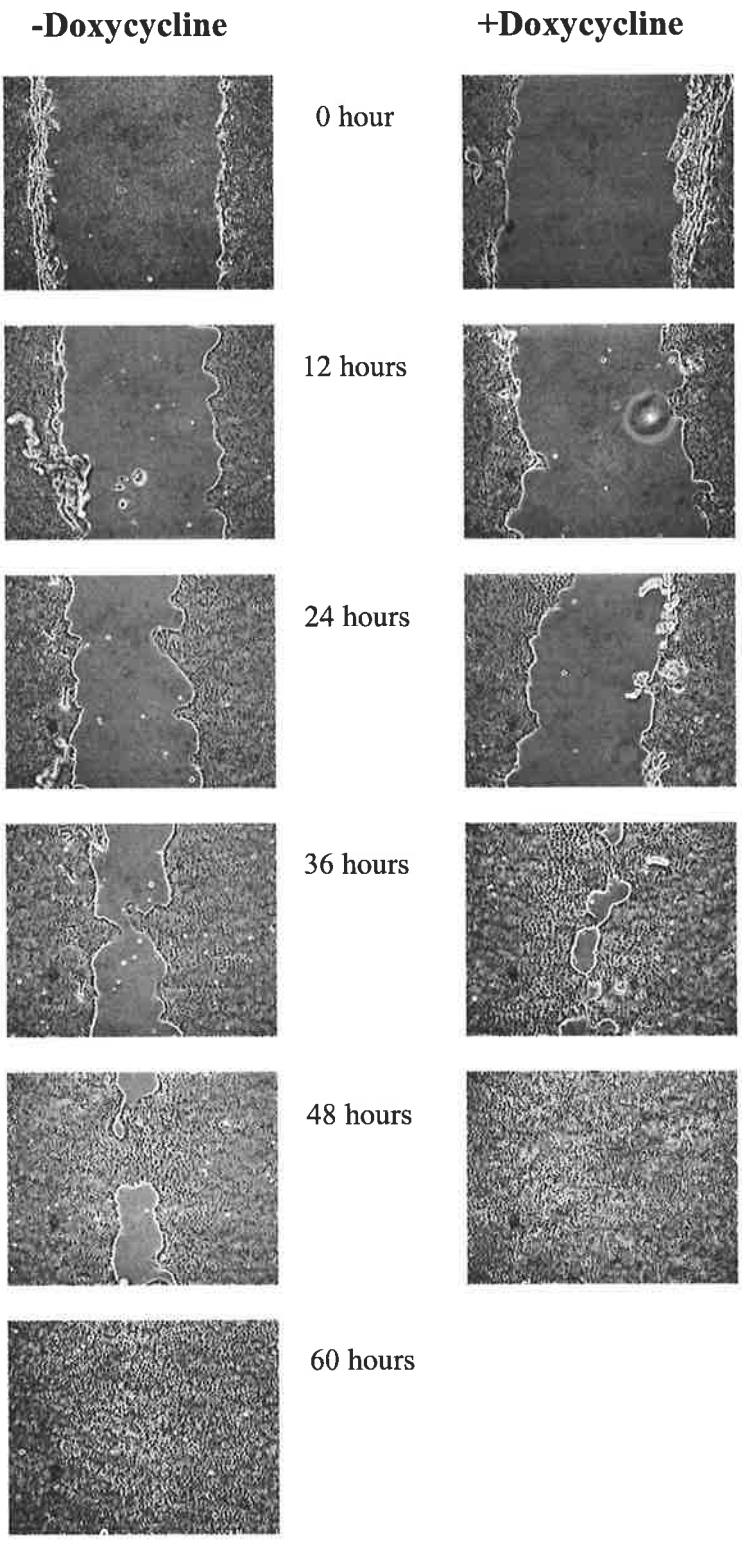
-Doxycycline
+Doxycycline
0 hour
12 hours
24 hours
36 hours
48 hours
60 hours

Figure 5.6 Monolayer wound healing migration assay of Cos-1 cells stably expressing wild-type and mutant MID1 proteins

Figures show representative wound healing data of monolayer Cos-1 (fibroblast) cells stably expressing (A) wild-type MID1, (B) MID1ΔBB and (C) MID1ΔCTD proteins. Photomicrographs of the scratch wounds were taken immediately after their formation (0 hour) and again at 12 hour intervals until healing of the wounded areas were completed. Each data represents five independent experiments.

Figure 5.6 (A)

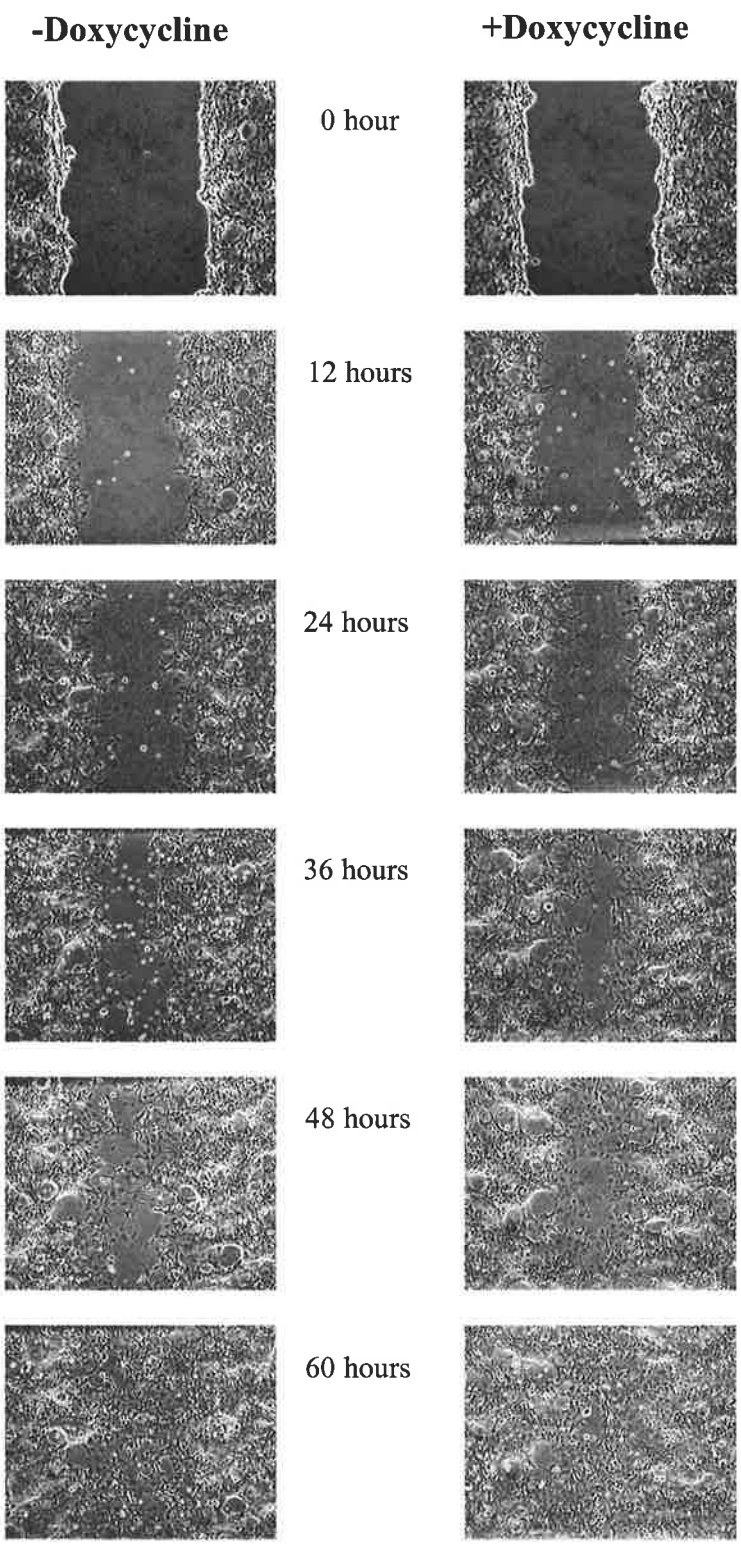
-Doxycycline
+Doxycycline
0 hour
12 hours
24 hours
36 hours
48 hours
60 hours

Figure 5.6 (B)

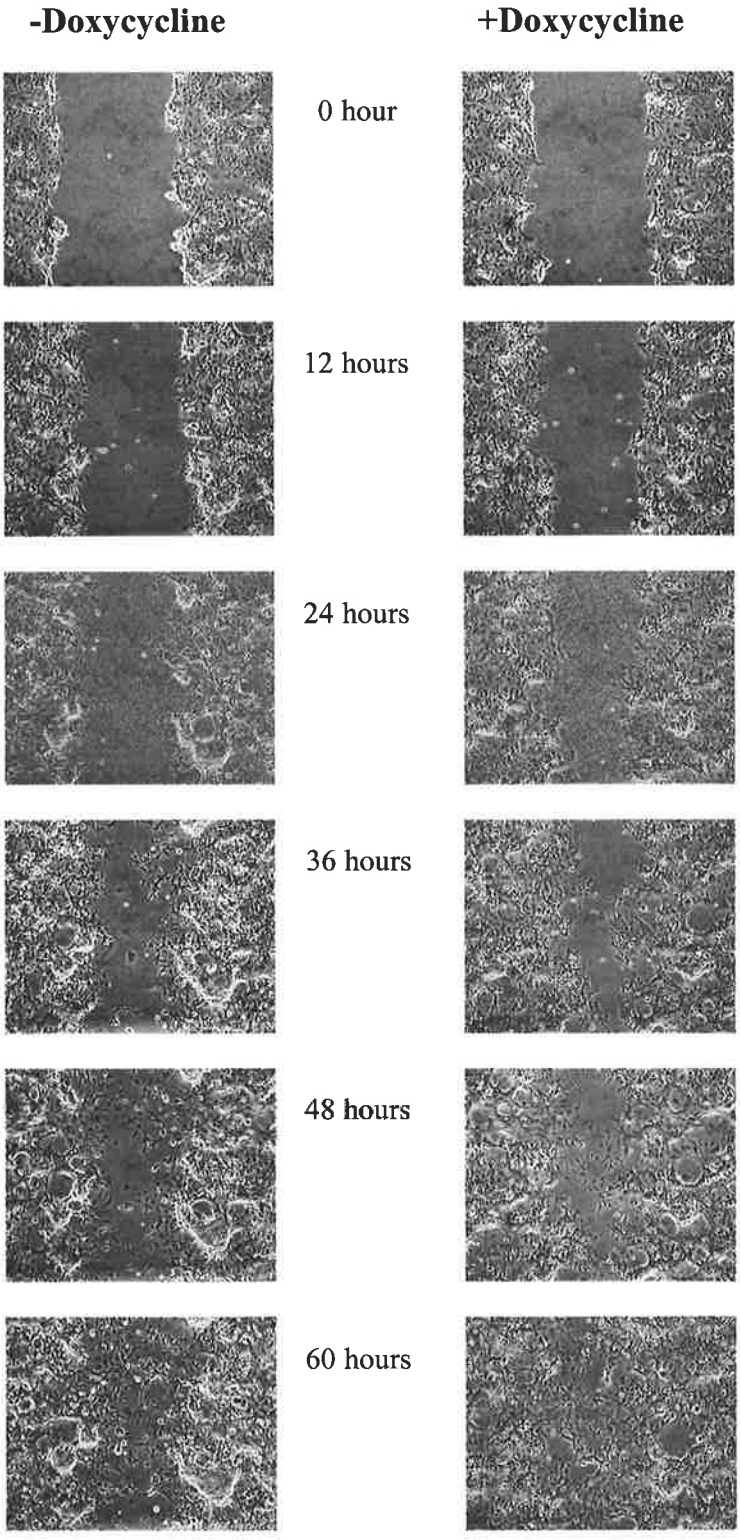
-Doxycycline
+Doxycycline
0 hour
12 hours
24 hours
36 hours
48 hours
60 hours

Figure 5.6 (C)

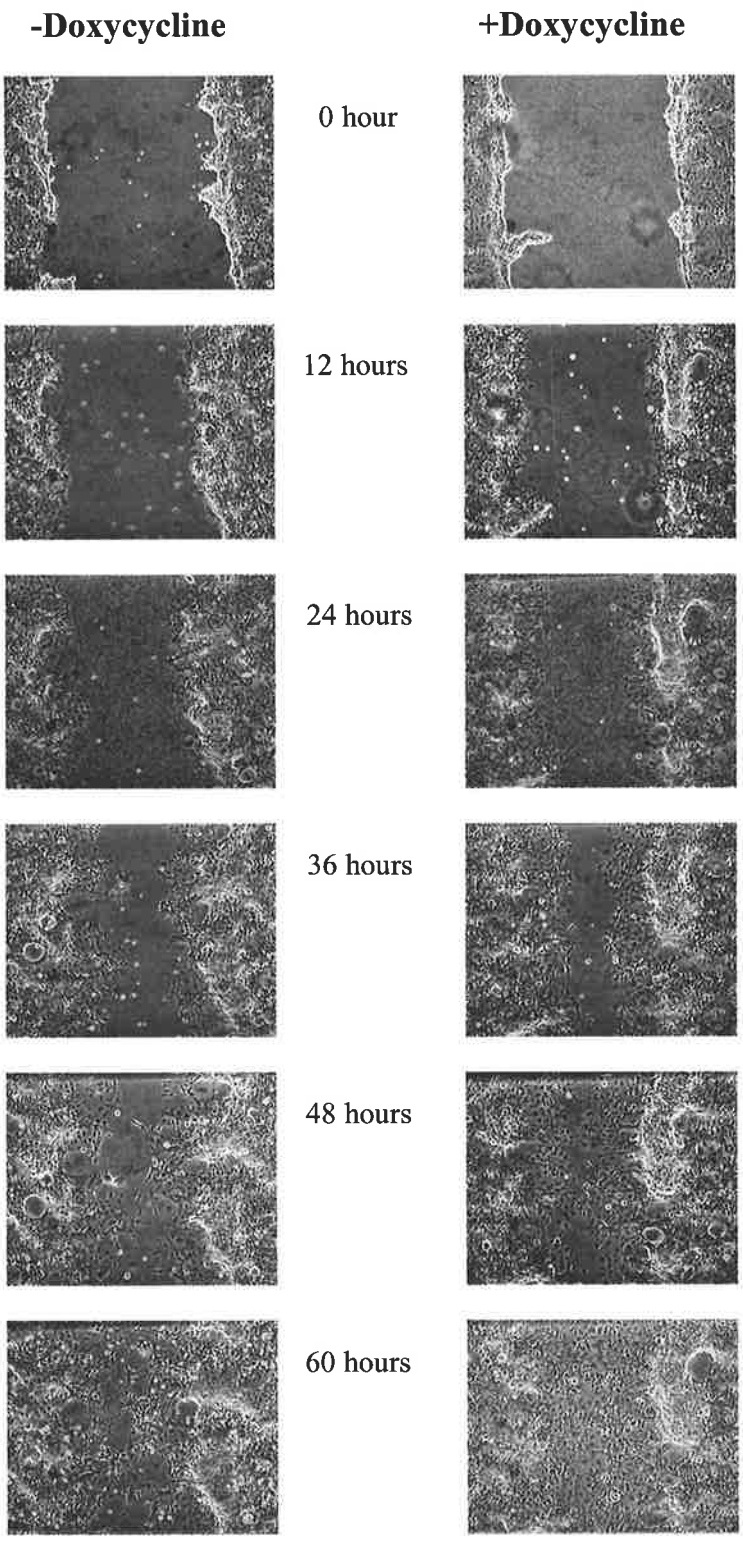
-Doxycycline
+Doxycycline
0 hour
12 hours
24 hours
36 hours
48 hours
60 hours

generating useful stable cell lines. In addressing these problems, several versions of tightly regulated gene expression systems have recently become available, including the tetracycline regulatory (Tet) system (Gossen & Bujard, 1992). This system is based on the repressor of the Tn*10* tetracycline (Tet) resistance operon of *Escherichia coli*. In this original Tet system known as the "Tet-Off" system, the Tet repressor (TetR) was fused to the C-terminal portion of a strong transcriptional activator, VP16 (from Herpes simplex virus) to generate the Tet-Off transactivator, tTA. Subsequently, a "reverse" Tet repressor (rTetR) was described which contained four amino acid substitutions in TetR to generate a reverse tet-transactivator, rtTA (also called the Tet-On transactivator) (Gossen *et al.*, 1995). In these tetracycline-controlled expression systems, TetR or rTetR bind with high affinity to tetracycline response elements (TREs), while the fused VP16 activates transcription from a minimal CMV promoter downstream of the TRE. Both Tet systems permit gene expression to be tightly regulated in response to varying concentration of the tetracycline analogue, doxycycline (Dox). Unlike the "Tet-Off" system, the "Tet-On" gene expression system is turned on in the presence of Dox in the culture medium. Thus, the "Tet-On" system was chosen in this study because it was more convenient to maintain the native/off state of the stable cell lines without the presence of doxycycline in culture medium (as the half-life of Dox is only 24 hours) and also because transient expression of MID1 for extended periods (up to 72 hours) led to deterioration of the cells appearance and motility.

Based on the "Tet-On" gene expression system described above, this chapter reports the development of tetracycline-inducible MDCK (epithelial) and Cos-1 (mesenchymal) cell lines that stably express either wild-type GFP-MID1 or one of a number of different mutant GFP-MID1 fusion proteins. Construction of the

tetracycline-responsive vectors expressing GFP-MID1, GFP-MID1ΔBB and GFP-MID1ΔCTD fusion proteins have allowed rapid selection of the GFP positive cells by fluorescence-activated cell sorting (FACS). This advantage has certainly enhanced the possibility of selecting tightly regulatable and highly inducible cells. In addition, stable expression of the GFP fusion proteins in these cell lines can easily be monitored either by FACS or visually by fluorescence microscopy.

The development of the tetracycline-inducible stable cell lines initiated in this study was done with the aim of investigating the cellular and developmental functions of MID1 that would provide clues as to its role during embryonic development. Several lines of evidence including data presented in the previous chapter of this thesis showed that *MID1* was mainly expressed in epithelial and endothelial (or mesenchymal) of the craniofacial complex and in the region of the developing external genitalia and anus, suggest that MID1 may have an important role in regulating specific processes critical for morphogenesis of a variety of organ system.

Microtubules and their associated proteins are known to be involved in many cellular processes including the regulation of cell proliferation, cell morphology and motility, cell division as well as intracellular protein trafficking (Mayer & Jurgens, 2002). A role for MID1 in one or more such processes is consistent with the conclusion that complete microtubule coverage by MID1 is important for its proper cellular function. Supporting this conclusion are the observations that all OS-related MID1 mutations and nearly all domain-specific deletions of MID1, including MID1ΔBB and MID1ΔCTD, are altered in their ability to decorate the microtubule network. In fact, most mutant MID1 proteins form cytoplasmic clumps/aggregates although in some cases these aggregates still appear to be tethered to microtubules (Short *et al.*, 2002). The use of GFP fusion proteins to investigate the role of wild-

type and mutant MID1 proteins is thought to be valid since overexpressed GFP-MID1 and GFP-MID1ΔCTD fusion proteins display microtubule association and cytoplasmic clumping, respectively, similar to that of endogenous wild-type MID1 and C-terminally truncated mutant MID1 in primary skin fibroblasts from an OS patient (Y. Zou, PhD Thesis, The University of Adelaide).

As previously mentioned that the development of the lip/palate, male external genitalia and cardiac septa undergoing the same cell programming and/or fusion of epithelial-lined tissue to form a mesenchymal confluence of these organs. Therefore, by homogenously expressing wild-type (normal functional protein) and mutant MID1 (represent loss of function) fusion proteins in both epithelial and mesenchymal stable cell lines to investigate the role of MID1 in cell migration and proliferation, cell death and the ability of cells to undergo EMT, should provide some insight into precise mechanism that leads to the highly specific OS phenotype, such as defective tissue fusion causing CLP, hypospadias as well as cardiac septation defects.

Assay systems that measure the number of viable and apoptotic cells showed there was no consistent influence of wild-type or mutant MID1 on proliferation and apoptosis of both Cos-1 and MDCK stable cell lines after 24 and 48 hours of induction making solid conclusions difficult to make. Well characterised cell lines which cellular proliferation and apoptosis have been documented using the same detection systems can be used as a positive control in the future experiments to resolve this ambiguity.

Classic *in vitro* wound healing assays were then performed using both MDCK and Cos-1 stable cell lines to monitor the timing and behaviour of wound-edge cells overexpressing wild-type and mutant MID1. When a confluent monolayer of cells were mechanically disrupted, these cells react via a transient repair process of

coordinated cellular movements until confluency is reached again. In the assays performed in this study, the healing process of wounded monolayer epithelial cells stably overexpressing wild-type MID1 was delayed, in contrast to that seen with MID1ΔCTD expressing cells where wound closure of the MDCK cells was more rapid. However at this stage, we could not confirm whether the mechanism that account for wound closure in epithelial cell sheets observed here involved EMT. The induction of the EMT can be qualitatively assessed by the expression of the epithelial marker, E-cadherin, as well as the mesenchymal markers, β-catenin and vimentin, in these wounding cells. Concurrently, Cos-1 stable cell lines were used to perform similar monolayer wound healing migration assays. Although no obvious effects were seen in Cos-1 cells stably overexpressing MID1, cells stably overexpressing MID1ΔCTD again showed significant migration of cells into the wounded area. The migrational behaviour of Cos-1 cell stably overexpressing MID1ΔCTD observed in this preliminary investigation, however, needs to be confirmed by performing the same wound healing migration assays in cell cultures grown on a special-coated (such as fibronectin-coated) tissue culture dish that is often used for this type of experiment. It was also noticed in these wound healing assays that cells overexpressing MID1ΔBB reacted differently to the cells overexpressing MID1ΔCTD. This observation in line with our studies showing that MID1ΔCTD acts as a dominant negative when overexpressed i.e. able to pull wild-type MID1 off microtubule and still bind to Alpha 4 protein, the ability not shared by the MID1ΔBB (Short *et al.*, 2002). Of interest however, promotion of wound closure by MID1ΔCTD reported in this chapter supports recent data obtained from our laboratories collaboration with Professor Ray Runyan (Arizona, USA) where treatment of endocardial cushion explants with anti-sense oligonucleotides to either *cMID1* or *cMID2* increases endothelial cell activation

(i.e. disruption of cell-cell adhesion) and mesenchymal invasion into a collagen matrix (i.e. a migratory cellular phenotype). These changes are consistent with an early step in the promotion of EMT, although the mechanism of EMT in the studies performed as part of this thesis is yet to be confirmed. Nevertheless, these preliminary data further supported the notion that complete microtubule coverage by a normal functioning MID1 is crucial for proper cellular function and any perturbation in this association during early embryogenesis give rise to the defective tissue fusion in the development of many organ systems such as lip/palate, male external genitalia and cardiac septa.

Chapter Six: Final discussion and future directions

6.1 Final discussion

Normal development of the craniofacial structures in vertebrates involves a multi-step process starting with the formation and migration of neural crest cells, followed by correct outgrowth and fusion of facial prominences in the ventral midline. Morphogenesis and differentiation of the craniofacial bones, cartilages, nerves and muscles will then transform the head and face into a characteristic functional organ system. Perturbations in any step of these complex morphogenetic events can result in an array of craniofacial defects. Many factors have been implicated in causing these dysmorphologies, including single-gene disorders, chromosome aberrations, teratogenic insults, as well as sporadic conditions of unknown origin. As a consequence, it has been reported that one third of all major birth defects involve the craniofacial region (Trainor, 2003), indicating the sensitivity of these developing structures to a range of influences. In fact, approximately 1 million (1%) infants born worldwide each year have craniofacial defects (Murray & Schutte, 2004). These congenital disorders impose an enormous healthcare burden not only to the affected individuals and their families, but also to the communities.

The work in this thesis was focussed on one such congenital disorder, Opitz GBBB syndrome (OS), which is characterised by defects in ventral midline structures. The lengthy argument over the clinical and genetic definition of OS was finally resolved with the demonstration of genetic heterogeneity, with both X-linked and autosomal loci confirmed by linkage analysis and cytogenetic anomalies (Robin *et al.*, 1995). Although both forms of OS appear to be clinically indistinguishable, higher penetrance of craniofacial defects, laryngotracheo-oesophageal (LTE) anomalies,

genital anomalies and developmental delay has been found in X-linked cases, while structural heart defects appear more common in the major autosomal form (De Falco *et al.*, 2003; So *et al.*, 2005).

Although the autosomal locus of OS remains unknown, a number of studies independently identified *MID1* as the gene responsible for the X-linked form (Perry *et al.*, 1998; Quaderi *et al.*, 1997; Van den Veyver *et al.*, 1998). Since then, different *MID1* mutations have been identified in around 40% of all tested cases where a diagnosis of OS is considered (Cox *et al.*, 2000; De Falco *et al.*, 2003; Gaudenz *et al.*, 1998; So *et al.*, 2005; Winter *et al.*, 2003). Notably, the success in identifying the causative mutation is significantly higher in familial cases compared to isolated cases.

Opitz syndrome is noted for its intriguing clinical variability that is most apparent in the facial presentation in patients in which cleft lip with or without cleft palate (CLP) is a prominent feature. In fact, *MID1* represents one of only a few genes directly linked to the common craniofacial anomalies with CLP. Therefore, much of the effort in this thesis has centred on understanding the cellular and developmental functions of MID1 during craniofacial morphogenesis and particularly its specific role during the outgrowth and fusion of craniofacial primordia to form the lip and primary palate. As the various affected systems in OS patients appear to arise as a result of defective tissue fusion or remodelling during embryogenesis, it was believed that this investigation would not only shed light on our understanding of the developmental basis of CLP but also on the processes leading to other characteristic features of OS such as cardiac septal defects and hypospadias.

In order to obtain a more detailed understanding of the precise tissue regions that express *MID1*, this study and a few others reported the spatial and temporal expression pattern of this gene during early embryogenesis using RNA *in situ*

hybridisation studies. Across species, highly conserved *MID1/Mid1* mRNA transcripts were shown to be widely expressed throughout embryogenesis, although at varying levels depending on the tissue and cell type. The *in situ* hybridisation data presented in this thesis further emphasise the importance of *Mid1* during craniofacial morphogenesis, as it was widely transcribed during outgrowth of facial prominences. The opportunity to further characterise the expression pattern of *Mid1* gene during early key morphogenetic time points in the development of the craniofacial tissues came with the availability of the *Mid1* knockout mouse, developed in collaboration with Professor Alan Ashworth (ICR, London). Modifications in the construction of the targeted DNA construct facilitated the insertion of a *LacZ* reporter gene into the *MID1* locus in the generation of this knockout line. This reporter was therefore placed under the control of the *Mid1* regulatory sequences such that detection of β-galactosidase activity would most likely mirror the endogenous *Mid1* pattern of expression. Interpretation of the spatial and temporal expression pattern of β-galactosidase activity presented in this study must therefore take into consideration any differences in half-life and stability of β-galactosidase compared to the *Mid1* mRNA. Nevertheless, the expression data obtained using whole-mount X-gal staining and subsequent tissue sectioning demonstrated that murine *Mid1,* like its orthologue in chicks and humans, was expressed in specific cell population during craniofacial morphogenesis and in relevant tissues/cell types of other organs affected in OS patients i.e. the heart and external genitalia. With respect to the craniofacial tissues, prominent levels of β-galactosidase activity were found in epithelia of the craniofacial primordia prior to and around the time of fusion of the lip and primary palate (as highlighted in Chapter Three), suggesting a likely role for this gene in regulating epithelial behaviour during the fusion event. This intriguing expression pattern can be

seen more clearly in frontal sections of 11.5 dpc *Mid1* knockout embryos (arrows in figure below) with curious absence of the expression in some neighbouring epithelia (asterisks). Meanwhile, the finding of dynamic *Mid1* expression in cardiac tissue throughout morphogenesis of the heart was consistent with the timing of cushion and outflow tract development and represents the first time cardiac expression has been shown for the murine *Mid1* gene. A close assessment of cardiac structures in *Mid1* knockout mice is currently being initiated based on these findings.

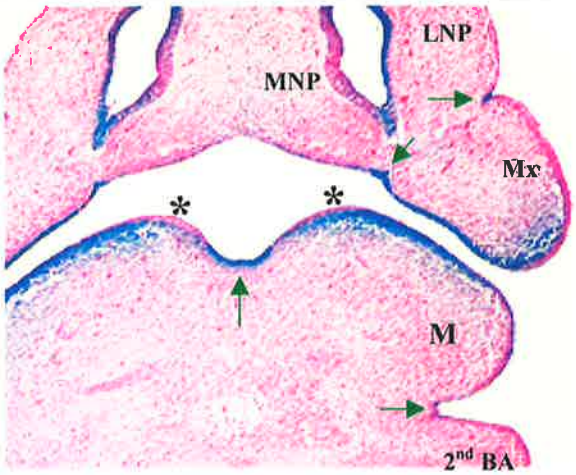

Figure shows detection of β-galactosidase activity in a frontal section of a 11.5 dpc *Mid1* knockout embryo. Expression in the epithelia at the site of fusion indicated by arrows [Mx: maxillary prominence; MNP: medial nasal prominence; LNP: lateral nasal prominence; M: mandibular process; BA: branchial arch]

Previous developmental studies in chicks have suggested the existence of a regulatory relationship between *Mid1, Shh* and *Bmp4* in the early events determining left/right asymmetry (Granata & Quaderi, 2003). Therefore, in this thesis, the expression patterns of both *Shh* and *Bmp4* were investigated in tissues lacking *Mid1* and compared to data from wild-type embryos. These studies, however, revealed no obvious differences in the expression patterns of either transcript. These results are consistent with the lack of gross phenotype in the *Mid1* knockout mice and the notion of redundant mechanisms substituting MID1 function in the majority of tissues by its protein homologue, MID2, although genetic background and/or epigenetic contributions could also account for this failure (these issues will be addressed in the next section). Of note, however, in preliminary analyses of embryos

from a cross between homozygous *Mid1* mice and heterozygous *Gli3* mice, weak ectopic expression of *Mid1* (β-galactosidase) was observed in the limb bud AER. *Gli3* encodes a transcription factor that can function as either an activator or repressor of Shh signalling (Villavicencio *et al.*, 2000). In fact, C-terminal processing of the activator form of Gli3 to the repressor form is inhibited by Shh. In the limb, this inhibition of processing by posteriorly restricted Shh sets up a counteractive antero-posterior gradient of Gli3 activator and repressor forms that help to pattern the limb mesoderm. The mutation in the *Gli3* locus in the *extra-toes* mutant is a 51.5kb deletion that results in the production of a C-terminally truncated protein, similar to that of the Gli3 repressor form (Maynard *et al.*, 2002). Thus in the heterozygous *extra-toes* mutant embryos, Shh is thought to be less able to induce its downstream targets, resulting in limb defects that include polydactyly (extra digits). However, it is well established that Shh not only patterns the limb mesoderm but also is necessary for maintenance of the AER (Ahn & Joyner, 2004). That *Mid1* expression in the AER is sensitive to changes in Gli3 levels (and hence Shh signalling strength) suggests an important regulatory relationship between the two factors despite the regulation being indirect (i.e. *Gli3* in the limb mesoderm; *Mid1* in the AER). Interestingly, in regard to the possible regulatory relationship between *Shh*, *Mid1* and *Bmp4* in the limbs, others have found that *Gli3* and *Bmp4* interact genetically to pattern the developing limb buds, although *Bmp4* expression in the AER and limb mesoderm does not appear to be affected in *Gli3* heterozygotes (Dunn *et al.*, 1997). A similar opposing relationship between *Shh* and *Bmp4* is known in many other tissues as well.

Considering the similarity of MID1 and MID2 in both their primary structure and cellular localisation, a level of functional redundancy between these two proteins has been considered feasible as one of the contributing factors to the variable severity

of the clinical features of different, or even related, OS patients (Cox *et al.*, 2000; So *et al.*, 2005). Investigation of the tissue-specific expression of both MID1 and MID2 is somewhat hampered by their high level of identity both at the nucleotide and protein levels resulting in the difficulty to reliably distinguishing between *MID1* and *MID2* based on their expression profile during early embryogenesis. Highlighting this is the fact that an antisense morpholino used to suppress *cMID1* expression was later found to also target *cMID2* (Granata *et al.*, 2005). Furthermore, a previously generated antibody against MID1 could not reliably differentiate between MID1 and MID2. Therefore, in this present study (Chapter Four), the production of MID1- and MID2-specific antibodies was initiated using synthetic peptides as antigens. Careful assessment during the selection of the MID1 and MID2 peptides was undertaken and the antibodies raised against them were predicted and subsequently confirmed to be specific to the peptides used. However, neither the MID1 polyclonal nor MID2 monoclonal antibodies were able to detect their native protein obtained from different sources under the conditions used in this study. The very poor recognition capabilities shown by these antibodies could be attributed to differences in conformation (i.e. functional state) of the MID proteins, since both are known to exist in higher order protein complexes. Due to unexpected limitation of these antibodies in addressing the issue of a possible redundant or compensatory mechanism between MID1 and MID2, this study (Chapter Four) utilised the available *Mid1* knockout mouse tissues to investigate whether such mechanism may involve changes to *Mid2* mRNA levels. However, reverse transcription-PCR (RT-PCR) analysis showed that there was no compensatory upregulation of *Mid2* in cells deficient in *Mid1*. This suggests that if *MID2* is compensating in any way then it does so at its normal endogenous levels.

Whether this phenomenon exists in all tissues or only in tissues expressing high levels of MID2 with low of MID1 could not be confirmed and need further investigation.

A growing body of evidence from both the *Mid1* expression profile (including data presented in this thesis) and understanding the etiology of the defects commonly seen in patients with OS provided some clues as to the cell types affected by loss of MID1 function. Each of the affected tissues i.e. lip and primary palate (CLP), male external genitalia (hypospadias) and the heart (cardiac septation defects) can be explained by disrupted or perturbed epithelial morphogenesis, such as a failure in the activation of epithelia/endothelia that initiates the sequence of changes in the epithelial sheet as individual epithelia convert to mesenchyme (the process known as EMT). Consistent with this notion, and as further highlighted in this study, *Mid1* is expressed most prominently in the relevant epithelial/endothelial populations. During primary palatogenesis, this expression is notable in the pre-fusion epithelia and persists until the epithelial seam forms but disappears by the time the epithelia have dispersed through EMT or cell death/migration to complete the fusion process of facial primordia. These observations suggest a role for MID1 in maintaining the epithelial state.

In Chapter Five, stable Madin-Darby canine kidney (MDCK) (epithelial) and Cos-1 (mesenchymal) cell lines that expressed either wild-type or one of a number of different mutant GFP-MID1 fusion proteins in Tet-inducible fashion were successfully developed. These stable and inducible cell lines were developed with the specific aim of elucidating the role of MID1 in various epithelial cellular processes akin to those reported during the fusion of epithelial-lined facial prominences. In the preliminary investigations using these inducible epithelial and mesenchymal cell lines, stably overexpressed MID1 in both cell lines did not effect either proliferation

or apoptosis levels. However, in wound healing assays, MDCK cells stably overexpressing wild-type MID1 displayed delayed closure of the wounding area (although this was not obvious in Cos-1 cell lines), in contrast to that seen with both MID1ΔCTD expressing cell lines where the rate of wound closure was notably more rapid. These early observations provide evidence that MID1 regulates the activation of epithelia, an early step in both EMT and migration. Notably, these results are in line with our laboratory's collaborative studies undertaken with Professor Ray Runyan (Arizona, USA) focusing on the role of MID proteins in the formation of cardiac septa, defects in which are common in patients with loss of function mutations in MID1. As mentioned earlier in this thesis, this collaborative study has provided direct evidence in support of a role for the MID proteins in remodelling epithelia using an *ex-ovo* chick atrioventricular (AV) canal culture system, a reliable means to assess endothelial cells undergoing EMT. Together, both results are consistent with the expected elevation in PP2Ac levels predicted to result from a deficiency of MID1 (e.g. ΔCTD mutant). The accumulation of PP2Ac results in the hypophosphorylation of microtubule-associated proteins (MAPs) and could then increase nuclear import of beta-catenin causing the destabilisation of cell adherens junctions initiating the transition of epithelium to mesenchyme. The link to fluctuating levels is also supported by the lack of effect seen for the ΔBB mutant that has been shown can no longer bind Alpha 4 and PP2Ac. This early breakage of the epithelial sheet and mesenchyme conversion may therefore disrupt proper fusion of many organs. Ongoing investigations are focussing in this possibility in order to further understand the role of *MID1* and how disruptions in this gene give rise to the various features seen in OS patients.

6.2 Future directions

Craniofacial abnormalities reflect a global health issue with both genetic and environmental factors recognised as contributing to the etiology of isolated facial clefts as well as the variability within syndromal forms. Recent investigations by many research groups including our laboratory have focussed on the identification protein factors that are functional partners of MID1, understanding similarities in cellular function of related protein family members, and dissecting the developmental function in model organisms. With regards to the latter, our laboratory has collaborated to produce genetically manipulated mouse models in order to assist our understanding of the development of OS. Although the generated *Mid1* knockout mouse model does not show any gross phenotype in the current 129SvJ/MF1 genetic background like that seen in OS patients. This knockout line will underpin future efforts aimed at understanding the developmental basis of CLP. As part of this ongoing research in the laboratory, crosses of these *Mid1* deficient mice onto different genetics background e.g. A/J and A/WySn to introduce the *Mid1* null allele onto these cleft susceptible backgrounds are currently being undertaken. Given the X chromosome location of *Mid1*, any changes in susceptibility of A/J or A/WySn strains to CLP will be assessed by comparing the frequency of the CLP phenotype in male mice with or without the inactivated *Mid1* allele. Another area of investigation is the production of a *Mid1/Mid2* double knockout mouse line where the issue of *Mid1* and *Mid2* redundancy will be specifically addressed by verification of any phenotypic differences between the double and single gene knockout mouse lines. It is planned to then attempt to rescue the phenotype by independently reintroducing *Mid1* and *Mid2* as weakly, but ubiquitously expressed transgenes. Further crossing of the *Mid1* knockout mice with *extra-toes* $Gli3^{XtJ}$ mutant mice to place *Mid1* in a homozygous

Gli3^{XtJ} background may extend this initial linkage also to morphogenesis of the craniofacial primordia.

Previous studies by a number of investigators, including our laboratory were aimed at identification of the protein factors that are functional partners of MID1. Perhaps, the most significant outcome was the identification of the PP2Ac binding protein, Alpha 4 (α4) where it was shown that MID1 recruits the α4-PP2Ac complex to microtubules and facilitates the ubiquitylation of PP2Ac, thus marking it for subsequent proteasomal degradation (Liu *et al.*, 2001; Short *et al.*, 2002; Trockenbacher *et al.*, 2001). Consistent with the notion of a level of functional redundancy between MID1 and MID2, α4-PP2Ac can also be recruited to the microtubules by MID2, which is also likely to mediate PP2Ac turnover (Short *et al.*, 2002; Trockenbacher *et al.*, 2001). It is of particular interest to understand how mutations in MID1 alter the levels of PP2Ac and thus perturb the regulation of one or more of their dependent cellular and developmental processes e.g. epithelial cell death, migration and/or EMT, that may be compromised in OS patients. Results presented in this thesis (Chapter Five) support the hypothesis that loss-of-function of MID1 (represented by ectopic expression of the dominant negative acting MID1ΔCTD) promoting an early epithelial sheet destabilisation/activation (and possible mesenchyme conversion), likely as a consequence of the elevation in PP2Ac levels. These preliminary findings have provided a springboard for a range of further investigations including:

1) Further investigation and confirmation of the role of MID1 in the ability of cells to undergo EMT and/or cell migration by performing *in vitro* wound healing assays of MDCK stable cell lines expressing wild-type and mutant MID1 in the presence of certain EMT-promoting growth factors e.g.

Hepatocyte Growth Factor (HGF). The effects of MID1 will be visible as the HGF-stimulated MDCK cells lose cell:cell contacts taking on a more fibroblastic-like morphology. This study can then be extended to monitor the spatial and temporal expression of the epithelial markers (e.g. E-cadherin) and mesechymal markers (e.g. β-catenin and vimentin) during wound closure. Morphological changes and morphogenetic movements of these MDCK cells can also be monitored using collagen gels where this system provides three-dimensional environment for the cells under investigation.

2) As a complementary approach, Cos-1 stable cell lines expressing the same proteins can be used to perform wound healing migration assays using a fibronectin-coated tissue culture dishes which provide support for motility of cells.

Information generated from this study and subsequent investigations will slowly elucidate complex function of *MID1*, a significant 'syndromal' CLP gene, and position it within one or more developmental pathway(s) that may not have previously been investigated for its role in primary palatal development or more specifically, susceptibility of the CLP.

References

Acampora D., Merlo G. R., Paleari L., Zerega B., Postiglione M. P., Mantero S., Bober E., Barbieri O., Simeone A., and Levi G. (1999). Craniofacial, vestibular and bone defects in mice lacking the Distal-less-related gene Dlx5. *Development* 126: 3811-3821.

Ahn S., and Joyner A. L. (2004). Dynamic changes in the response of cells to positive Hedgehog signaling during mouse limb patterning. *Cell* 118: 505-516.

Allanson J. E. (1988). G syndrome: an unusual family. *American Journal of Medical Genetics* 31: 637-642.

Ashique A. M., Fu K., and Richman J. M. (2002). Endogenous bone morphogenetic proteins regulate outgrowth and epithelial survival during avian lip fusion. *Development* 129: 4647-4660.

Barlow A. J., and Francis-West P. H. (1997). Ectopic application of recombinant BMP-2 and BMP-4 can change patterning of developing chick facial primordia. *Development* 124: 391-398.

Berti C., Fontanella B., Ferrentino R., and Meroni G. (2004). Mig12, a novel Opitz syndrome gene product partner, is expressed in the embryonic ventral midline and co-operates with Mid1 to bundle and stabilize microtubules. *BMC Cell Biology* 5: 1-12.

Beverdam A., Merlo G. R., Paleari L., Mantero S., Genova F., Barbieri O., Janvier P., and Levi G. (2002). Jaw transformation with gain or symmetry after Dlx5/Dlx6 inactivation: mirror of the past. *Genesis* 34: 221-227.

Buchner G., Montini E., Andolfi G., Quaderi N., Cainarca S., Messali S., Bassi M. T., Ballabio A., Meroni G., and Franco B. (1999). MID2, a homologue of the Opitz syndrome gene MID1: similarities in subcellular localization and differences in expression during development. *Human Molecular Genetics* 8: 1397-1407.

Cainarca S., Messali S., Ballabio A., and Meroni G. (1999). Functional characterization of the Opitz syndrome gene product (midin): evidence for homodimerization and association with microtubules throughout the cell cycle. *Human Molecular Genetics* 8: 1387-1396.

Celli G., LaRochelle W. J., Mackem S., Sharp R., and Merlino G. (1998). Soluble dominant-negative receptor uncovers essential roles for fibroblast growth factors in multi-organ induction and patterning. *EMBO Journal* 17: 1642-1655.

Chiang C., Litingtung Y., Lee E., Young K. E., Corden J. L., Westphal H., and Beachy P. A. (1996). Cyclopia and defective axial patterning in mice lacking Sonic hedgehog gene function. *Nature* 383: 407-413.

Chun K., Teebi A. S., Azimi C., Steele L., and Ray P. N. (2003). Screening of patients with craniosynostosis: molecular strategy. *American Journal of Medical Genetics* 120A: 470-473.

Cobourne M. T., Hardcastle Z., and Sharpe P. T. (2001). Sonic hedgehog regulates epithelial proliferation and cell survival in the developing tooth germ. *Journal of Dental Research* 80: 1974-1979.

Couly G., Creuzet S., Bennaceur S., Vincent C., and Le Douarin N. M. (2002). Interactions between Hox-negative cephalic neural crest cells and the foregut endoderm in patterning the facial skeleton in the vertebrate head. *Development* 129: 1061-1073.

Cox T. C. (2004). Taking it to the max: the genetic and developmental mechanism coordinating midfacial development and dysmorphology. *Clinical Genetics* 65: 163-176.

Cox T. C., Allen L. R., Cox L. L., Hopwood B., Goodwin B., Haan E., and Suthers G. K. (2000). New mutations in MID1 provide support for loss of function as the cause of X-linked Opitz syndrome. *Human Molecular Genetics* 9: 2553-2562.

Cuervo R., and Covarrubias L. (2004). Death is the major fate of medial edge epithelial cells and the cause of basal lamina degradation during palatogenesis. *Development* 131: 15-24.

Cuervo R., Valencia C., Chandraratna R. A., and Covarrubias L. (2002). Programmed cell death is required for palate shelf fusion and is regulated by retinoic acid. *Developmental Biology* 245: 145-156.

Dal Zotto L., Quaderi N. A., Elliott R., Lingerfelter P. A., Carrel L., Valsecchi V., Montini E., Yen C. H., Chapman V., Kalcheva I., Arrigo G., Zuffardi O., Thomas S., Willard H. F., Ballabio A., Disteche C. M., and Rugarli E. I. (1998). The mouse Mid1 gene: implications for the pathogenesis of Opitz syndrome and the evolution of the mammalian pseudoautosomal region. *Human Molecular Genetics* 7: 489-499.

De Falco F., Cainarca S., Andolfi G., Ferrentino R., Berti C., Rodriguez-Criado G., Rittinger O., Dennis N., Odent S., Rastogi A., Liebelt J., Chitayat D., Winter R., Jawanda H., Ballabio A., Franco B., and Meroni G. (2003). X-linked Opitz syndrome: Novel mutations in the MID1 gene and redefinition of the clinical spectrum. *American Journal of Medical Genetics* 120A: 222-228.

Depew M. J., Lufkin T., and Rubenstein J. L. (2002). Specification of jaw subdivisions by Dlx genes. *Science* 298: 381-385.

Dunn N. R., Winnier G. E., Hargett L. K., Schrick J. J., Fogo A. B., and Hogan B. L. (1997). Haploinsufficient phenotypes in Bmp4 heterozygous null mice and modification by mutations in Gli3 and Alx4. *Developmental Biology* 188: 235-247.

Edwards S. J., Gladwin A. J., and Dixon M. J. (1997). The mutational spectrum in Treacher Collins syndrome reveals a predominance of mutations that create a premature-termination codon. *American Journal of Human Genetics* 60: 515-524.

Everett A. D., and Brautigan D. L. (2002). Developmental expression of alpha4 protein phosphatase regulatory subunit in tissues affected by Opitz syndrome. *Developmental Dynamics* 224: 461-464.

Francis-West P., Ladher R., Barlow A., and Graveson A. (1998). Signalling interactions during facial development. *Mechanisms of Development* 75: 3-28.

Francis-West P. H., Robson L., and Evans D. J. (2003). Craniofacial development: the tissue and molecular interactions that control development of the head. *Advances in Anatomy, Embryology, and Cell Biology* 169: III-VI, 1-138.

Fryburg J. S., Lin K. Y., and Golden W. L. (1996). Chromosome 22q11.2 deletion in a boy with Opitz (G/BBB) syndrome. *American Journal of Medical Genetics* 62: 274-275.

Gaudenz K., Roessler E., Quaderi N., Franco B., Feldman G., Gasser D. L., Wittwer B., Horst J., Montini E., Opitz J. M., Ballabio A., and Muenke M. (1998). Opitz G/BBB syndrome in Xp22: mutations in the MID1 gene cluster in the carboxy-terminal domain. *American Journal of Human Genetics* 63: 703-710.

Gong S. G., and Guo C. (2003). Bmp4 gene is expressed at the putative site of fusion in the midfacial region. *Differentiation* 71: 228-236.

Gorlin R., Cohen M., and Hennekam R. (2001a). Opitz oculo-genito-laryngeal syndrome (Opitz BBB/G compound syndrome). *In* "Syndromes of the head and neck", pp. 988-991, Oxford University Press, Oxford.

Gorlin R., Cohen M., and Hennekam R. (2001b). "Syndromes of the head and neck," Oxford University Press, Oxford.

Gossen M., and Bujard H. (1992). Tight control of gene expression in mammalian cells by tetracycline-responsive promoters. *Proceedings of the National Academy of Sciences of the United States of America* 89: 5547-5551.

Gossen M., Freundlieb S., Bender G., Muller G., Hillen W., and Bujard H. (1995). Transcriptional activation by tetracyclines in mammalian cells. *Science* 268: 1766-1769.

Graham J. M., Wheeler P., Tackels-Horne D., Lin A. E., Hall B. D., May M., Short K. M., Schwartz C. E., and Cox T. C. (2003). A new X-linked syndrome with

agenesis of the corpus callosum, mental retardation, coloboma, micrognathia, and a mutation in the Alpha 4 gene at Xq13. *American Journal of Medical Genetics* 123A: 37-44.

Granata A., and Quaderi N. A. (2003). The Opitz syndrome gene MID1 is essential for establishing asymmetric gene expression in Hensen's node. *Developmental Biology* 258: 397-405.

Granata A., Savery D., Hazan J., Cheung B. M., Lumsden A., and Quaderi N. A. (2005). Evidence of functional redundancy between MID proteins: implications for the presentation of Opitz syndrome. *Developmental Biology* 277: 417-424.

Greene R. M., and Pisano M. M. (2004). Perspectives on growth factors and orofacial development. *Current Pharmaceutical Design* 10: 2701-2717.

Harlow E., and Lane D. (1988). "Antibodies: A laboratory manual," Cold Spring Harbor Press, New York.

Harris D. M., Myrick T. L., and Rundle S. J. (1999). The Arabidopsis homolog of yeast TAP42 and mammalian alpha4 binds to the catalytic subunit of protein phosphatase 2A and is induced by chilling. *Plant Physiology* 121: 609-617.

Hunt P., Clarke J. D., Buxton P., Ferretti P., and Thorogood P. (1998). Segmentation, crest prespecification and the control of facial form. *European Journal of Oral Sciences* 106 Suppl 1: 12-18.

Johnston M. C., and Bronsky P. T. (1995). Prenatal craniofacial development: new insights on normal and abnormal mechanisms. *Critical Reviews in Oral Biology and Medicine* 6: 368-422.

Kalluri R., and Neilson E. G. (2003). Epithelial-mesenchymal transition and its implications for fibrosis. *The Journal of Clinical Investigation* 112: 1776-1784.

Kaufman M. H. (1998). "The atlas of mouse development," Academic Press, London.

Lacassie Y., and Arriaza M. I. (1996). Opitz GBBB syndrome and the 22q11.2 deletion. *American Journal of Medical Genetics* 62: 318.

Landry J. R., Rouhi A., Medstrand P., and Mager D. L. (2002). The Opitz syndrome gene Mid1 is transcribed from a human endogenous retroviral promoter. *Molecular Biology and Evolution* 19: 1934-1942.

Leichtman L. G., Werner A., Bass W. T., Smith D., and Brothman A. R. (1991). Apparent Opitz BBBG syndrome with a partial duplication of 5p. *American Journal of Medical Genetics* 40: 173-176.

Liu J., Prickett T. D., Elliott E., Meroni G., and Brautigan D. L. (2001). Phosphorylation and microtubule association of the Opitz syndrome protein

mid-1 is regulated by protein phosphatase 2A via binding to the regulatory subunit alpha 4. *Proceedings of the National Academy of Sciences of the United States of America* 98: 6650-6655.

Liu Y. H., Kundu R., Wu L., Luo W., Ignelzi M. A., Snead M. L., and Maxson R. E. (1995). Premature suture closure and ectopic cranial bone in mice expressing Msx2 transgenes in the developing skull. *Proceedings of the National Academy of Sciences of the United States of America* 92: 6137-6141.

Martinez-Alvarez C., Tudela C., Perez-Miguelsanz J., O-Kane S., Puerta J., and Ferguson M. W. (2000). Medial edge epithelial cell fate during palatal fusion. *Developmental Biology* 220: 343-357.

May M., Huston S., Wilroy R. S., and Schwartz C. (1997). Linkage analysis in a family with the Opitz GBBB syndrome refines the location of the gene in Xp22 to a 4 cM region. *American Journal of Medical Genetics* 68: 244-248.

Mayer U., and Jurgens G. (2002). Microtubule cytoskeleton: a track record. *Current Opinion in Plant Biology* 5: 494-501.

Maynard T. M., Jain M. D., Balmer C. W., and LaMantia A. S. (2002). High-resolution mapping of the Gli3 mutation Extra-toes^{J} reveals a 51.5-kb deletion. *Mammalian Genome* 13: 58-61.

McDonald-McGinn D. M., Emanuel B. S., and Zackai E. H. (1996). Autosomal dominant "Opitz" GBBB syndrome due to a 22q11.2 deletion. *American Journal of Medical Genetics* 64: 525-526.

McDonald-McGinn D. M., Tonnesen M. K., Laufer-Cahana A., Finucane B., Driscoll D. A., Emanuel B. S., and Zackai E. H. (2001). Phenotype of the 22q11.2 deletion in individuals identified through an affected relative: cast a wide FISHing net! *Genetics in Medicine* 3: 23-29.

McGonnell I. M., Clarke J. D., and Tickle C. (1998). Fate map of the developing chick face: analysis of expansion of facial primordia and establishment of the primary palate. *Developmental Dynamics* 212: 102-118.

Mina M. (2001). Regulation of mandibular growth and morphogenesis. *Critical Reviews in Oral Biology and Medicine* 12: 276-300.

Moore K. L. (1988). "The developing human," WB Saunders Company Publishers, Sydney.

Mosser D. D., Caron A. W., Bourget L., Jolicoeur P., and Massie B. (1997). Use of a dicistronic expression cassette encoding the green fluorescent protein for the screening and selection of cells expressing inducible gene products. *Biotechniques* 22: 150-154.

Murata K., Wu J., and Brautigan D. L. (1997). B cell receptor-associated protein alpha4 displays rapamycin-sensitive binding directly to the catalytic subunit of

protein phosphatase 2A. *Proceedings of the National Academy of Sciences of the United States of America* 94: 10624-10629.

Murray J. C., and Schutte B. C. (2004). Cleft palate: players, pathways, and pursuits. *Journal of Clinical Investigation* 113: 1676-1678.

Nanci A. (2003). "Ten Cate's Oral Histology: Development, Structure and Function," Mosby Inc., Missouri.

Nanni L., Ming J. E., Du Y., Hall R. K., Aldred M., Bankier A., and Muenke M. (2001). SHH mutation is associated with solitary median maxillary central incisor: a study of 13 patients and review of the literature. *American Journal of Medical Genetics* 102: 1-10.

Nawshad A., LaGamba D., and Hay E. D. (2004). Transforming growth factor beta (TGFbeta) signalling in palatal growth, apoptosis and epithelial mesenchymal transformation (EMT). *Archives of Oral Biology* 49: 675-689.

Opitz J. M. (1987). G syndrome (hypertelorism with esophageal abnormality and hypospadias, or hypospadias-dysphagia, or "Opitz-Frias" or "Opitz-G" syndrome)--perspective in 1987 and bibliography. *American Journal of Medical Genetics* 28: 275-285.

Opitz J. M., Frias J. L., Gutenberger J. E., and Pellet J. R. (1969a). The G syndrome of multiple congenital anomalies. *Birth Defects* 5: 95-101.

Opitz J. M., Summit R. L., and Smith D. W. (1969b). The BBB syndrome: familial telecanthus with associated congenital anomalies. *Birth Defects* 5: 86-94.

Panganiban G., and Rubenstein J. L. (2002). Developmental functions of the Distal-less/Dlx homeobox genes. *Development* 129: 4371-4386.

Perez-Pomares J. M., and Munoz-Chapuli R. (2002). Epithelial-mesenchymal transitions: a mesodermal cell strategy for evolutive innovation in Metazoans. *The Anatomical Record* 268: 343-351.

Perry J., Feather S., Smith A., Palmer S., and Ashworth A. (1998). The human FXY gene is located within Xp22.3: implications for evolution of the mammalian X chromosome. *Human Molecular Genetics* 7: 299-305.

Perry J., Short K. M., Romer J. T., Swift S., Cox T. C., and Ashworth A. (1999). FXY2/MID2, a gene related to the X-linked Opitz syndrome gene FXY/MID1, maps to Xq22 and encodes a FNIII domain-containing protein that associates with microtubules. *Genomics* 62: 385-394.

Pinson L., Auge J., Audollent S., Mattei G., Etchevers H., Gigarel N., Razavi F., Lacombe D., Odent S., Le Merrer M., Amiel J., Munnich A., Meroni G., Lyonnet S., Vekemans M., and Attie-Bitach T. (2004). Embryonic expression of the human MID1 gene and its mutations in Opitz syndrome. *Journal of Medical Genetics* 41: 381-386.

Quaderi N. A., Schweiger S., Gaudenz K., Franco B., Rugarli E. I., Berger W., Feldman G. J., Volta M., Andolfi G., Gilgenkrantz S., Marion R. W., Hennekam R. C., Opitz J. M., Muenke M., Ropers H. H., and Ballabio A. (1997). Opitz G/BBB syndrome, a defect of midline development, is due to mutations in a new RING finger gene on Xp22. *Nature Genetics* 17: 285-291.

Raught B., Gingras A. C., and Sonenberg N. (2001). The target of rapamycin (TOR) proteins. *Proceedings of the National Academy of Sciences of the United States of America* 98: 7037-7044.

Reymond A., Meroni G., Fantozzi A., Merla G., Cairo S., Luzi L., Riganelli D., Zanaria E., Messali S., Cainarca S., Guffanti A., Minucci S., Pelicci P. G., and Ballabio A. (2001). The tripartite motif family identifies cell compartments. *EMBO Journal* 20: 2140-2151.

Rice R., Spencer-Dene B., Connor E. C., Gritli-Linde A., McMahon A. P., Dickson C., Thesleff I., and Rice D. P. (2004). Disruption of Fgf10/Fgfr2b-coordinated epithelial-mesenchymal interactions causes cleft palate. *Journal of Clinical Investigation* 113: 1692-1700.

Richman J. M., Fu K. K., Cox L. L., Sibbons J. P., and Cox T. C. (2002). Isolation and characterisation of the chick orthologue of the Opitz syndrome gene, Mid1, supports a conserved role in vertebrate development. *The International Journal of Developmental Biology* 46: 441-448.

Richman J. M., and Lee S. H. (2003). About face: signals and genes controlling jaw patterning and identity in vertebrates. *Bioessays* 25: 554-568.

Robin N. H., Feldman G. J., Aronson A. L., Mitchell H. F., Weksberg R., Leonard C. O., Burton B. K., Josephson K. D., Laxova R., and Aleck K. A. (1995). Opitz syndrome is genetically heterogeneous, with one locus on Xp22, and a second locus on 22q11.2. *Nature Genetics* 11: 459-461.

Robin N. H., Opitz J. M., and Muenke M. (1996). Opitz G/BBB syndrome: clinical comparisons of families linked to Xp22 and 22q, and a review of the literature. *American Journal of Medical Genetics* 62: 305-317.

Robledo R. F., Rajan L., Li X., and Lufkin T. (2002). The Dlx5 and Dlx6 homeobox genes are essential for craniofacial, axial and appendicular skeletal development. *Genes & Development* 16: 1089-1101.

Sambrock J., Fritsch E., and Maniatis T. (1989). "Molecular cloning: A laboratory manual," Laboratory Press, New York.

Santagati F., and Rijli F. M. (2003). Cranial neural crest and the building of the vertebrate head. *Nature Reviews Neuroscience* 4: 806-818.

Savagner P. (2001). Leaving the neighborhood: molecular mechanisms involved during epithelial-mesenchymal transition. *Bioessays* 23: 912-923.

Scambler P. J. (2000). The 22q11 deletion syndromes. *Human Molecular Genetics* 9: 2421-2426.

Schweiger S., Foerster J., Lehmann T., Suckow V., Muller Y. A., Walter G., Davies T., Porter H., van Bokhoven H., Lunt P. W., Traub P., and Ropers H. H. (1999). The Opitz syndrome gene product, MID1, associates with microtubules. *Proceedings of the National Academy of Sciences of the United States of America* 96: 2794-2799.

Schweiger S., and Schneider R. (2003). The MID1/PP2A complex: a key to the pathogenesis of Opitz BBB/G syndrome. *Bioessays* 25: 356-366.

Schweitzer R., Vogan K. J., and Tabin C. J. (2000). Similar expression and regulation of Gli2 and Gli3 in the chick limb bud. *Mechanisms of Development* 98: 171-174.

Shimamura K., Hartigan D. J., Martinez S., Puelles L., and Rubenstein J. L. (1995). Longitudinal organization of the anterior neural plate and neural tube. *Development* 121: 3923-3933.

Shook D., and Keller R. (2003). Mechanisms, mechanics and function of epithelial-mesenchymal transitions in early development. *Mechanisms of Development* 120: 1351-1383.

Short K. M., Hopwood B., Yi Z., and Cox T. C. (2002). MID1 and MID2 homo- and heterodimerise to tether the rapamycin-sensitive PP2A regulatory subunit, alpha 4, to microtubules: implications for the clinical variability of X-linked Opitz GBBB syndrome and other developmental disorders. *BMC Cell Biology* 3: 1-14.

Shuler C. F. (1995). Programmed cell death and cell transformation in craniofacial development. *Critical Reviews in Oral Biology and Medicine* 6: 202-217.

Shuler C. F., Guo Y., Majumder A., and Luo R. Y. (1991). Molecular and morphologic changes during the epithelial-mesenchymal transformation of palatal shelf medial edge epithelium in vitro. *The International Journal of Developmental Biology* 35: 463-472.

So J., Suckow V., Kijas Z., Kalscheuer V., Moser B., Winter J., Baars M., Firth H., Lunt P., Hamel B., Meinecke P., Moraine C., Odent S., Schinzel A., van der Smagt J. J., Devriendt K., Albrecht B., Gillessen-Kaesbach G., van der Burgt I., Petrij F., Faivre L., McGaughran J., McKenzie F., Opitz J. M., Cox T., and Schweiger S. (2005). Mild phenotypes in a series of patients with Opitz GBBB

syndrome with MID1 mutations. *American Journal of Medical Genetics* 132A: 1-7.

Sperber G. H. (2001). "Craniofacial development," BC Decker Inc., Hamilton.

Stanier P., and Moore G. E. (2004). Genetics of cleft lip and palate: syndromic genes contribute to the incidence of non-syndromic clefts. *Human Molecular Genetics* 13: 73-81.

Sun D., Baur S., and Hay E. D. (2000). Epithelial-mesenchymal transformation is the mechanism for fusion of the craniofacial primordia involved in morphogenesis of the chicken lip. *Developmental Biology* 228: 337-349.

Takigawa T., and Shiota K. (2004). Terminal differentiation of palatal medial edge epithelial cells in vitro is not necessarily dependent on palatal shelf contact and midline epithelial seam formation. *The International Journal of Developmental Biology* 48: 307-317.

Taya Y., O-Kane S., and Ferguson M. W. (1999). Pathogenesis of cleft palate in TGF-beta3 knockout mice. *Development* 126: 3869-3879.

Thyagarajan T., Totey S., Danton M. J., and Kulkarni A. B. (2003). Genetically altered mouse models: the good, the bad, and the ugly. *Critical Reviews in Oral Biology and Medicine* 14: 154-174.

Trainor P. A. (2003). Making headway: the roles of hox genes and neural crest cells in craniofacial development. *ScientificWorldJournal* 3: 240-264.

Trockenbacher A., Suckow V., Foerster J., Winter J., Krauss S., Ropers H. H., Schneider R., and Schweiger S. (2001). MID1, mutated in Opitz syndrome, encodes an ubiquitin ligase that targets phosphatase 2A for degradation. *Nature Genetics* 29: 287-294.

Trumpp A., Depew M. J., Rubenstein J. L., Bishop J. M., and Martin G. R. (1999). Cre-mediated gene inactivation demonstrates that FGF8 is required for cell survival and patterning of the first branchial arch. *Genes & Development* 13: 3136-3148.

Urioste M., Arroyo I., Villa A., Lorda-Sanchez I., Barrio R., Lopez-Cuesta M. J., and Rueda J. (1995). Distal deletion of chromosome 13 in a child with the "opitz" GBBB syndrome. *American Journal of Medical Genetics* 59: 114-122.

Van den Veyver I. B., Cormier T. A., Jurecic V., Baldini A., and Zoghbi H. Y. (1998). Characterization and physical mapping in human and mouse of a novel RING finger gene in Xp22. *Genomics* 51: 251-261.

Verloes A., David A., Odent S., Toutain A., Andre M. J., Lucas J., and Le Marec B. (1995). Opitz GBBB syndrome: chromosomal evidence of an X-linked form. *American Journal of Medical Genetics* 59: 123-128.

Verloes A., Le Merrer M., and Briard M. L. (1989). BBBG syndrome or Opitz syndrome: new family. *American Journal of Medical Genetics* 34: 313-316.

Villavicencio E. H., Walterhouse D. O., and Iannaccone P. M. (2000). The Sonic Hedgehog-Patched-Gli pathway in human development and disease. *American Journal of Human Genetics* 67: 1047-1054.

Walter G. (1986). Production and use of antibodies against synthetic peptides. *Journal of Immunological Methods* 88: 149-61.

Wilkie A. O., and Morriss-Kay G. M. (2001). Genetics of craniofacial development and malformation. *Nature Reviews Genetics* 2: 458-468.

Winter J., Lehmann T., Suckow V., Kijas Z., Kulozik A., Kalscheuer V., Hamel B., Devriendt K., Opitz J., Lenzner S., Ropers H. H., and Schweiger S. (2003). Duplication of the MID1 first exon in a patient with Opitz G/BBB syndrome. *Human Genetics* 112: 249-254.

Yamada G., Satoh Y., Baskin L. S., and Cunha G. R. (2003). Cellular and molecular mechanisms of development of the external genitalia. *Differentiation* 71: 445-460.

Yee G. W., and Abbott U. K. (1978). Facial development in normal and mutant chick embryos. I. Scanning electron microscopy of primary palate formation. *The Journal of Experimental Zoology* 206: 307-321.

Zhang Z., Song Y., Zhao X., Zhang X., Fermin C., and Chen Y. (2002). Rescue of cleft palate in Msx1-deficient mice by transgenic Bmp4 reveals a network of BMP and Shh signaling in the regulation of mammalian palatogenesis. *Development* 129: 4135-4146.